Systematic Simulation Method to Quantify and Control Pedestrian Comfort and Exposure during Urban Heat Island

Parham Mirazaei Ahranjani

A Thesis

in

The Department

of

Building, Civil and Environmental Engineering

Presented in Partial Fulfillment of the Requirements

For the Degree of Doctor of Philosophy at

Concordia University

Montreal, Quebec, Canada

November 2010

CONCORDIA UNIVERSITY

SCHOOL OF GRADUATE STUDIES

This is to certify that the thesis prepared

By: Parham Mirzaei Ahranjani

Entitled: Systematic Simulation Method to Quantify and Control Pedestrian

Comfort and Exposure during Urban Heat Island

and submitted in partial fulfillment of the requirements for the degree of

DOCTOR OF PHILOSOPHY (Building Engineering)

complies with the regulations of the University and meets the accepted standards with

respect to originality and quality.

Signed by the final examining committee:

Dr. R. Dssouli	Chair
Dr. J.S. Zhang	External Examiner
Dr. G. Vatistas	External to Program
Dr. Z. Chen	Examiner
Dr. R. Zmeureanu	Examiner
Dr. F. Haghighat	Thesis Supervisor

Approved by

Dr. K. Ha-Huy	Graduate Program Director
Dr. Robin A.L. Drew	Dean of Faculty

January 7, 2011

Abstract

Systematic Simulation Method to Quantify and Control Pedestrian Comfort and Exposure during Urban Heat Island

Parham Mirzaei Ahranjani
Concordia University, 2010

An urban heat island (UHI) originates with the increase of energy consumption and deforestation within urban areas. In addition to heat related illness and energy consumption increase, the UHI also has a mutual effect on pollution dispersion, mostly emitted from vehicular and industrial sources.

Many cities recently started to apply mitigation protocols by increasing tree planting and vegetation inside urban areas. A few cities also promoted higher-albedo materials for urban surfaces. Moreover, guidelines are developed to design an appropriate street canyon and building layout to naturally ventilate urban areas. However, the UHI intensity varies in different street canyons and climates. Thus, the aforementioned mitigation technologies are not always practical or economical to reduce energy consumption and keep pedestrian comfort and exposure (PCE) in the desired range.

The main goal of this research is to propose a systematic approach, PCE-algorithm, to quantify the level of PCE inside a street canyon before and after its construction. This approach is also capable of evaluating the possible advantages of passive mitigation strategies using a frequency of occurrence concept. This concept assesses the probability

of having acceptable comfort indices within the street canyon. For this purpose, a computational fluid dynamics (CFD) model is defined around the investigated street canyon. This model simulates the significant contributing parameters on UHI formation, including solar radiation, storage heat, latent heat, and sensible heat.

Moreover, an adaptive novel strategy, pedestrian ventilation system (PVS), is proposed in this research to control PCE of the target street canyon. Similar to the function of a building mechanical ventilation system, the PVS interactively controls PCE in outdoor spaces. The PVS employs exhausting and/or supplying fans installed in adjacent buildings of the street canyon in order to achieve an acceptable PCE, especially when passive strategies fail to have a considerable effect.

A case study of a street canyon, located in Montreal, is also considered to investigate the performance of the proposed algorithm. After an evaluation of PCE, the effect of the passive mitigation strategies is investigated. Furthermore, it is shown that the PVS can control and improve PCE, especially where severe UHI occurs.

Keywords: urban heat island, street canyon, pedestrian comfort, CFD

Acknowledgment

First and foremost, I would like to express my deepest gratitude to my supervisor, Dr. Fariborz Haghighat, for his continuous guidance, wisdom, and cordial demeanour. I am, and will always be, grateful for the invaluable advices, knowledge and time he devoted during this research.

Also, special thanks to the other members of my dissertation committee, Dr. Zhi Chen, Dr. Radu Zmeureanu, and Dr. Georgios Vatistas, for generously giving their time and expertise. I wish to also extend thanks to Dr. Akashi Mochida for his knowledgeable advices, valuable discussions and great cooperation in my research.

I wish to also extend thanks to my friends and colleagues in our research group, with whom I spent countless hours in the office. I appreciate their help, stimulating exchange of idea, and most importantly, their friendship.

Second to the last, I wish to express my warmest appreciation and love to my family. I would like to thank the two people who have contributed the most to my life, my parents – Hassan Mirzaei Ahranjani and Mansoureh Vilataj. Without them, none of this would have been possible. Also, I am thankful to my kindhearted sisters, Anousheh and Katayoon, and my trustworthy brother and friend, Arash, for their continuous inspiration and support.

Last, but the most, I owe my loving thanks to my wonderful wife Sanam Akhavannasab, her patience, continuous encouragement and kindness have always upheld me. I am indebted to her unconditional love.

Table of Contents

List of Figures

List of Tables

List of Symbols

English Symbols

d	zero plane displacement for velocity [m]
d_t	zero plane displacement for temperature [m]
f	roughness function [-]
g	gravitational acceleration [m^2/s]
h_f	fluid heat transfer coefficient [$W/(m^2.K)$]
I_z	turbulent intensity [-]
k	turbulent kinetic energy [m^2/s^2]
k_p	turbulence kinetic energy at point p [m^2/s^2]
k_t	turbulent thermal diffusivity [m^2/s]
$\bar{p}$	mean pressure [Pa]
$q_{conduction}$	conducted heat through the surface [W/m^2]
$q_{radiation}$	solar radiation [W/m^2]
q'	wall heat flux [W/m^2]
u, v, w	mean parts of the velocity in x, y, and z directions [m/s]
$ú, v́, ẃ$	fluctuation parts of the velocity in x, y, and z directions [m/s]
u_*	friction velocity [m/s]
x, y, z	cartesian coordinates [m]
y_p	distance of point p to the wall [m]
z_{BLH}	boundary layer height [m]
z_0	roughness length for air velocity [m]
z_{0t}	roughness length for temperature [m]
z_{Ref}	reference height [m]
A	apparent solar irradiation [W/m^2]
B	atmospheric extinction coefficient [-]
C_p	heat capacity [$J/(kg.K)$
D_t	pollutant eddy diffusivity [m^2/s]
G_b	generation of TKE due to the buoyancy [$1/m.s^3$]
G_k	generation of TKE due to the mean velocity gradients [$1/m.s^3$]
H	height of building [m]
K	thermal conductivity [$W/(m.K)$]

K_s	physical roughness height [m]
L	length of building [m]
L_1, L_2, L_3, L_4, L_5	domain dimensions [m]
L_r	long-wave radiation [W/m^2]
P_{k_z}	production term for k equation [m^2/s^3]
Pr_t	turbulent Prandtl number [-]
Q	source strength [m^3/s]
Q$_E$	latent heat flux [W/m^2]
Q$_F$	anthropogenic heat flux [W/m^2]
Q$_G$	conductive heat flux [W/m^2]
Q_{Gen}	heat source or sink [W/m^2]
Q$_H$	sensible heat flux [W/m^2]
Q*	net radiation [W/m^2]
$\dot{Q}$	mass flow rate [kg/s]
RH	relative humidity [%]
S	modulus of the mean rate-of-strain tensor [1/s]
Sc_t	turbulent Schmidt number [-]
S$_k$, S_ε	source terms [1/m.s^3]
S_r	short-wave radiation [W/m^2]
T	ambient air temperature [C]
T$_a$	inflow temperature [K]
T$_{air}$	ambient air temperature [K]
T$_f$	ground temperature [K]
T$_H$	temperature at the top of the street canyon [K]
T$_m$	mean temperature [K]
T_p	temperature at the point p [K]
T$_{surface}$	soil, pavement, or road temperature [K]
T_w	wall temperature [K]
T_*	temperature scale [K]
$\hat{U}$	gust wind velocity [m/s]
$\overline{U}$	mean wind velocity [m/s]
U	wind velocity [m/s]
U$_H$	mean wind speed at the top of the street canyon [m/s]
U_p	mean velocity at point p [m/s]
U_{Ref}	reference wind speed at z_{Ref} [m/s]
U$_z$	mean vertical velocity at height z [m/s]

U_∞	prevailing wind velocity [m/s]
W	width of street [m]
Y	ratio of vertical to horizontal sky diffuse radiation [-]
Y_M	fluctuating dilatation in to the overall dissipation rate [$1/m.s^3$]

Greek Symbols

α	prevailing wind angle [degree]
α	albedo [-]
α_{ground}	ground reflectivity [-]
β	thermal expansion coefficient [1/K]
δ_{ij}	Kronecker delta [-]
ε	turbulent rate of dissipation [m^2/s^3]
ϵ	angle of the surface related to the horizontal plane [rad]
θ_{air}	air temperature [K]
θ_{globe}	globe temperature [K]
θ_G	ground surface temperature [K]
θ_{MRT}	MRT temperature [K]
θ_z	air temperature at height z [K]
κ	von Karman constant [-]
λ	average time period [s]
μ	dynamic viscosity [s.Pa]
μ_t	turbulent viscosity [s.Pa]
$\hat{v}$	modified turbulent kinematic viscosity [m^2/s]
ξ	solar altitude [rad]
ρ	density [kg/m^3]
σ, σ_{u_z}	root-mean-square of velocity fluctuations [m/s]
σ_k	turbulent Prandtl number [-]
v_t	eddy viscosity [m^2/s]
φ, φ_t	universal functions for atmospheric stability [-]
ϕ	power-law exponent [-]
Γ	top-canyon surface [m^2]
ΔB	surface roughness [m]
ΔQ_A	net advection [W/m^2]
ΔQ_S	storage heat flux [W/m^2]

Abbreviations

ACH	Air Exchange Rate
AQI	Air Quality Index
AR	Aspect Ratio
ASHRAE	American Society of Heating, Refrigerating and Air-Conditioning Engineers
CFD	Computational Fluid Dynamics
DISC	Thermal Discomfort Index
IRF	Isolated Roughness Flow
LEED	Leadership in Energy and Environmental Design
LULC	Land-Use Land-Cover
MRT	Mean Radiation Temperature
NS	Navier-Stokes
OAQ	Outdoor Air Quality
PBL	Planetary Boundary Layer
PCE	Pedestrian Comfort and Exposure
PCH	Pollution Exchange Rate
PET	Physiologically Equivalent Temperature
PFR	Purging Flow Rate
PMV	Predicted Mean Vote Index
PVS	Pedestrian Ventilation System
PVZ	Pedestrian Ventilation Zone
RANS	Reynolds-averaged Navier-Stokes
RNG	Renormalization Group Theory
RTE	Radiative Transfer Equation
SET	Standard Effective Temperature
SF	Skimming Flow
THI	Temperature-humidity Index
TKE	Turbulent Kinetic Energy
TP	Pollutant Residence Time
TSENS	Thermal Sensation Index
UCM	Urban Canopy Model
UHI	Urban Heat Island
VF	Visitation Frequently

VR	Vegetation Ratio
WCH	Wind Chill Index
WCI	Wind Comfort Index
WIF	Wake Interference Flow

Dimensionless Numbers

Pr	Prandtl
Rb	Bulk-Richardson
Re	Reynolds
Ro	Rossby

1. Chapter One: Introduction

1.1. Background on Urban Heat Island

Urban area is considerably warmer than the surrounding rural area; this phenomenon is known as urban heat island (UHI). Characteristics of the UHI include a consistent air temperature increase, sometimes relative humidity decrease, and air pollution increase compared to the neighboring rural areas (Figure 1.1). In most cities, the UHI is a nocturnal phenomenon and is more significant during winter and on windless days (Arnfield, 2003). Alteration of the natural land, increase of the anthropogenic heat release, and lack of evapotranspiration caused by urbanization are the main sources of the UHI.
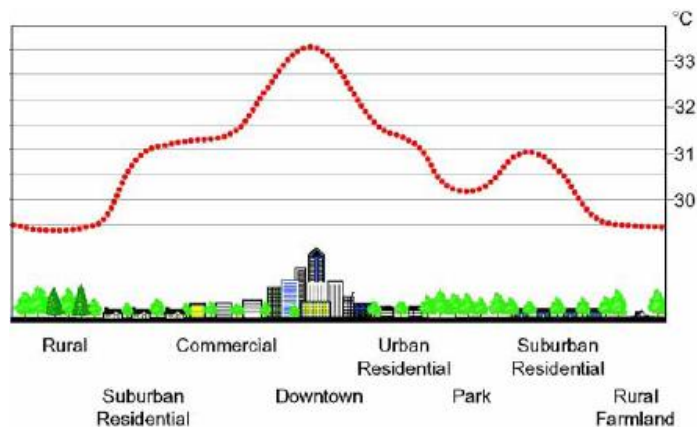
Figure 1.1 Urban Heat Island (UHI)

Replacement of original land with artificial materials causes modification in the thermal properties for urban texture, including heat capacity, thermal conductivity, emissivity and albedo for short and long-wave radiation. Also, constructed buildings hinder the flow of the wind in urban areas and cause an increase in both temperature and pollution concentration level.

The heat island phenomena also results in an increase of mean and peak building energy consumption during cooling seasons. Widespread power outages are attributed to the UHI. In addition, the UHI causes physical, psychological and sociological stress for pedestrians and dwellers (Patz et al., 2005). One should also consider the indirect effect of the UHI on pollution exposure since the UHI intensifies the pollution concentration within the street canyons.

Increasing the albedo of materials, vegetation, planting trees, reducing released anthropogenic heat, and designing efficient street canyons and buildings to facilitate air movement are common techniques to mitigate the UHI. However, the implementation of these techniques is not always practical or economical. Furthermore, the outcome of these strategies significantly varies according to climate and characteristics of the city. One can therefore refer to these mitigation strategies as passive technologies because after their

implementation, further control of them is either very expensive or impossible. For example, widespread tree planting is an effective strategy against the UHI, but it could inversely elevate the pollution concentration in some places.

1.2.   Outdoor Air Quality and Pedestrian Comfort

In order to evaluate the pedestrian comfort and exposure (PCE) in a certain location of a city, the first step is the definition of proper indices based on human comfort and health criteria. Despite of the efforts to develop indoor comfort indices, only limited research has been conducted to define outdoor comfort indices. Air temperature, moisture, and pollution exposure are parameters that have been mostly addressed with regards to indoor comfort. However, the effect of solar radiation, air velocity, and precipitation are not negligible on PCE in outdoor environment.

The relation between airflow regime and characteristics of street canyons, where pedestrian activities mostly happen, is widely studied in literature. Therefore, PCE can be investigated by combining human activity indices with the characteristics of the street canyons. These characteristics include aspect ratio (the ratio of the windward building's height to the canyon breadth), roof slope and shape, street layout, and the adjacent building's configuration and type (step-up/down).

Experimental and analytical approaches have been employed to find the relationship between PCE and street canyon characteristics. Even though experimental approaches are the most reliable techniques, a continuous and urban-scale implementation of them is not practical or economical. Alternatively, dynamic numerical models have been extensively used due to the recent advancement made in the computer technology. However, modeling of PCE within all street canyons of a city still has limitations due to the computational time and cost.

1.3.   Research Objectives

The UHI phenomena increase the vulnerability of street canyons for pedestrian health and comfort. Thus, it is important to identify street canyons with a high risk of vulnerability and to quantify whether the passive UHI mitigation strategies are effective in these areas. This implies that there is always concern about the effectiveness of the mitigation strategies on PCE.

The main aim of this research is to develop a systematic procedure, PCE-algorithm, to quantify and control PCE around a constructed or planned building. For this purpose, three stages are included inside the PCE-algorithm:

1. Collection of information regarding the street canyon and annual weather:

   A methodology to adapt weather data to the simulation model is proposed using a frequency of occurrence concept. Heat storage effect is also included within this model, performing a pre-simulation approach.

2. Evaluation of the effect of passive strategies on PCE:

   First, a Computational Fluid Dynamics (CFD) model integrated with a solar radiation model is developed to simulate physical interactions around and inside the target street canyon. Second, a procedure to select the proper domain and mesh size for the target street canyon is proposed. In addition, it is shown how the CFD model can simulate and predict the effect of possible mitigation strategies before and after the construction of a building. Temperature-humidity index (THI) is integrated with a wind comfort index (WCI) to quantify pedestrian comfort. Air quality index (AQI) is also employed to determine the concentration level of pollutants. Finally, air and pollution exchange rate (ACH and PCH) indices are considered in order to justify the air movement and pollution exposure inside the street canyon.

3. Evaluation of the effect of the pedestrian ventilation system (PVS) on PCE:

A pedestrian ventilation system (PVS) is proposed to control the PCE indices within the street canyon when applied strategies fail to considerably improve them. The feasibility of this system is also discussed in this study. Eventually, performance of the PCE-algorithm is investigated using a case study street canyon within the Montreal city.

2. Chapter Two: Literature Review

2.1. Introduction

The present chapter aims to prepare a solid background of the existing efforts to quantify

and enhance pedestrian comfort and exposure around buildings. The maximum level of

pedestrian discomfort is usually reported during heat waves when the UHI is more

intensified. Therefore first in section 2.2, the formation of the UHI and its impact on

outdoor comfort and air quality are discussed. Current studies that propose mitigation

strategies in order to enhance PCE are briefly presented in this section. Furthermore, the

existing indices necessary to evaluate PCE are addressed in section 2.3. Most pedestrian

activities occur inside street canyons. Therefore, section 2.4 discusses the structure and

characteristics of these locations. Eventually, existing experimental and simulation

approaches to model the physical processes within the street canyon are classified in

section 2.5.

2.2. Urban Heat Island

The growth of world urbanization has been extensively accelerated since the Second

World War. According to the Population Reference Bureau (2005), 50% of the world

population (3.4 billion) is settled in urban areas. Also, it is predicted that the inhabitation of cities will reach 60% (5.0 billion) by 2030, which means approximately two billion more people will reside in cities by this year. In addition, the number of cities with a population of over one million is expected to increase by approximately 100 from 2005 to 2015 (Population Reference Bureau, 2005). Massive building construction is underway to respond to this overwhelming demand for dwellings. This excessive and unplanned growth of urbanization has caused an undesired rise in the temperature of cities. The behavior of artificial urban texture in terms of absorption of short-wave and long-wave radiation, transpiration, releasing of anthropogenic heat, and blocking prevalent wind is significantly different from that of the original nature. This phenomenon, urban heat island, considerably decreases human health and comfort and increases the buildings cooling load within a city during warm seasons. This means that a "vicious circle" is formed within the urban areas by extra released heat from air conditioners.

Several power outages are reported due to the increase in air conditioning usage (CBCNews, 2006; ScienceDaily, 2006). For example, thousands of homes and businesses went without power in California for a period of five days in 2006.

Furthermore, thousands of deaths are annually reported due to heat related illnesses. The most recent example is the severe heat wave that contributed to the death of nearly 50,000 people in Europe, in August 2003. Many of the victims were elderly people who lived in poorly designed buildings without air-conditioning when the urban air temperature reached 40°C.

Furthermore, UHI impacts the local meteorology by altering local wind patterns, forming cloud and fog, impacting humidity, and changing the precipitation rate (Taha, 1997). Apart from the above mentioned effects, the UHI mutually intensifies pollutant concentration in urban areas (Sarrat et al., 2006). Increased air temperature accelerates the rate of chemical reaction. Additionally, the high level of pollution in urban areas intensifies the UHI by trapping short-wave and long-wave radiation (Arnfield, 2003).

2.2.1. Effect of the UHI on Pedestrian Comfort and Exposure

As discussed earlier, air temperature drastically increases during the UHI which lessens the level of pedestrian comfort within street canyons. This should be separated into direct and indirect impact of the UHI on outdoor air quality (OAQ). The UHI directly elevates the chemical reaction rate of the pollution in street canyons. At the same time, the intensified temperature difference between urban surfaces changes the airflow regime

through street canyons (Murena et al., 2009). This alteration of airflow regime, addressed as an indirect effect of the UHI, can inversely increase the pollution concentration level and produce a vulnerable air pollution situation.

Moreover, lack of evapotranspiration and vegetation reduces moisture and consequently the level of pedestrian comfort. In addition, construction of street canyons results in the blocking of the prevailing wind breakthrough. Reduction of this infiltrated air through street canyons impacts pedestrian comfort in two ways. First, it reduces the pollution removal by urban-ventilation. Second, it decreases the convective heat transfer between pedestrian bodies and outdoor air.

2.2.2. Urban Heat Island Mitigation Techniques

Demonstrated in Table 2.1, the most effective approaches to mitigate UHI include increasing the surface albedo of materials in a city, increasing vegetation, trees, and ponds within urban areas, reducing the release of anthropogenic heat within canopies, and designing efficient canopies and buildings in order to improve natural ventilation.

These mitigation strategies have both a direct and indirect effect on the energy consumption and OAQ of a city (Akbari et al., 2001; Mochida et al., 1997; Murakami,

2006; Oke, 1988). The direct effect is related to the reduction of the heat release by a particular building when the UHI is mitigated. The indirect effect is also attributed to the surrounding buildings when they contribute less to intensifying the UHI due to the reduction in the particular building thermal load. The direct effect provides immediate benefits for a building, but indirect effect could only be achieved by widespread employment of the mitigation strategies.

Table 2.1 Urban heat island reduction technologies

Urban Heat Island Mitigation Strategy	Reduction of the environmental load on buildings and improvement of outdoor air quality and pedestrian thermal comfort
Urban Ventilation	▪ Improving air movement within street canyons ▪ Adjusting buildings arrangement ▪ Adjusting the aspect ratio of street canyons ▪ Adjusting the geometry and layout of the building ▪ Increasing green spaces and ponds
Shading	▪ Using trees, piloti, eaves and pergola inside the buildings or above the pedestrian sidewalks
Urban Materials Alteration	▪ Using green elements ▪ Reducing the asphalt-paved area ▪ Greening exterior walls and rooftops of buildings ▪ Using higher solar reflectance (albedo) materials
Anthropogenic Heat Release Reduction	▪ Optimizing the position of air-conditioning and combustion equipments ▪ Changing the type of air conditioning systems ▪ Improving the efficiency of equipment systems ▪ Using natural ventilation and day lighting ▪ Utilizing the unused energy of the building, sewage system, environmental sources, and heat storage system

It is not always economically practical to apply the mitigation strategies to the existing unplanned urban area. This is the main limitation of the mitigation strategies. Moreover,

the UHI intensity is a function of city location and characteristics. Therefore, it can be concluded that the energy balance inside a city is altered when contributing parameters in formation of the UHI varies. This means that UHI intensity is not spatially and temporally similar in different cities. For instance, radiation absorption can be a dominant factor for diurnal UHI in an equatorial climate, especially when the sky is calm and cloudless. However, anthropogenic heat release can be the main cause of a nocturnal UHI in high-rise and dense metropolitan areas when the sky is cloudy. Therefore, it is necessary to adapt proper mitigation strategies for different cities. Even after the adaption, the outcome could vary from one region of a city to another and makes the mitigation strategies ineffective. Therefore, presented strategies in Table 2.1 can be called passive techniques. This implies that there is not an in-situ control on these strategies after their implementation.

2.3.   Pedestrian Comfort and Exposure within Street Canyons

Despite a lot of research that have been carried out to study the air quality and thermal comfort, only limited work has been done in the area of pedestrian comfort and exposure. The existing efforts, however, are mostly adapted from indoor studies. Appendix A

though C represent number of the developed thermal and wind comfort indices which are

applied to the outdoor environment studies.

2.4. Effect of Street Canyon Characteristics on Airflow Regime and Pollution Concentration

Airflow regime directly influences pedestrian's thermal sensation and indirectly affects

the pedestrian health by changing the pollution concentration and dispersion inside the

street canyon. Additionally, the airflow regime itself is affected by street canyon

geometry. In addition, the street canyon geometry has a direct impact on the shading

factor which influences human comfort. One can, therefore, develop the relation among

the shading effect, street canyon parameters, and the airflow pattern.

Calculation of the shading effect is a straightforward procedure if the location of the

street canyon and cloud cover are known. This is possible through resolving the

obstructed solar beam by the street canyon during the day. To calculate long-wave

radiation, it is necessary to find the sky and surface view factors. Again, these view

factors are a function of the street canyon geometry (Kondo et al., 2001; Kusaka et al.,

2001; Masson, 2000).

As shown in Figure 2.1, street canyons are mostly categorized by their aspect ratio (the ratio of the height of the adjacent building to the street's width, H/W). The street canyon is called avenue, regular or deep when the aspect ratio is half, one, or greater than two, respectively. Also, a canyon is symmetric when the height of the adjacent buildings is equal. An asymmetric street canyon is called step-down/step-up when the upwind/downwind building is taller than the downwind/upwind one.
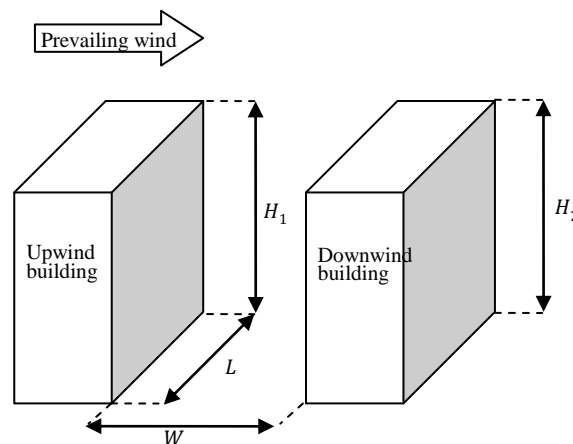
Figure 2.1 Street canyon characteristic; Step-down $(H_1 > H_2)$ - Step-up $(H_2 > H_1)$ - Symmetric $(H_1 = H_2)$

Moreover, the length of a street canyon (L) is expressed by the distance of two associated lateral intersections. The street canyon can again be characterized by its length as short,

medium, or long when the ratio of L/H is respectively around three, five, or seven (Li et al., 2006).

As illustrated in Figure 2.2, Oke (1988) reported that the airflow pattern depends on the street canyon aspect ratio, and categorized three airflow regimes when the perpendicular wind speed over a long street canyon is above 1.5m/s: (a) isolated roughness flow (IRF), (b) wake interference flow (WIF), and (c) skimming flow (SF). In isolated roughness flow (H/W<0.3), buildings are considered as aerodynamic roughness, since in this regime, the airflow travels a sufficient distance downwind of the first building before encountering the subsequent building. Conversely, in WIF, the wake region after the building encounters the next building as an obstacle in higher aspect ratios (H/W<0.7). In the third regime, a single circulation is produced inside the street canyon because of the skimming flow passing over the buildings where 0.7<H/W. The strength of this circulation depends on the prevailing wind speed. A minimum of air exchange rate and pollution removal from the street canyon is reported in skimming flow (Hunter et al., 1992).

Pollutant exchange in street canyons is a function of vertical and horizontal air exchange from top-canopy and lateral surfaces. Many studies have been carried out to find the

effect of the street canyon's character on the number, strength, circulation direction, and form of the circulation(s); street canyon aspect ratio (Murena et al., 2009); roof slope and shape (Rafailidis, 1997); street layout (Xie et al., 2006); atmospheric stability by heating ground and walls (Sini et al., 1996); street canyon configuration and type (step-up/down) (Chan et al., 2001) surface material's characteristic (Oliveira Panao et al., 2009); and vegetation and tree planting (Gromke et al., 2008).

(A)

(B)   (C)
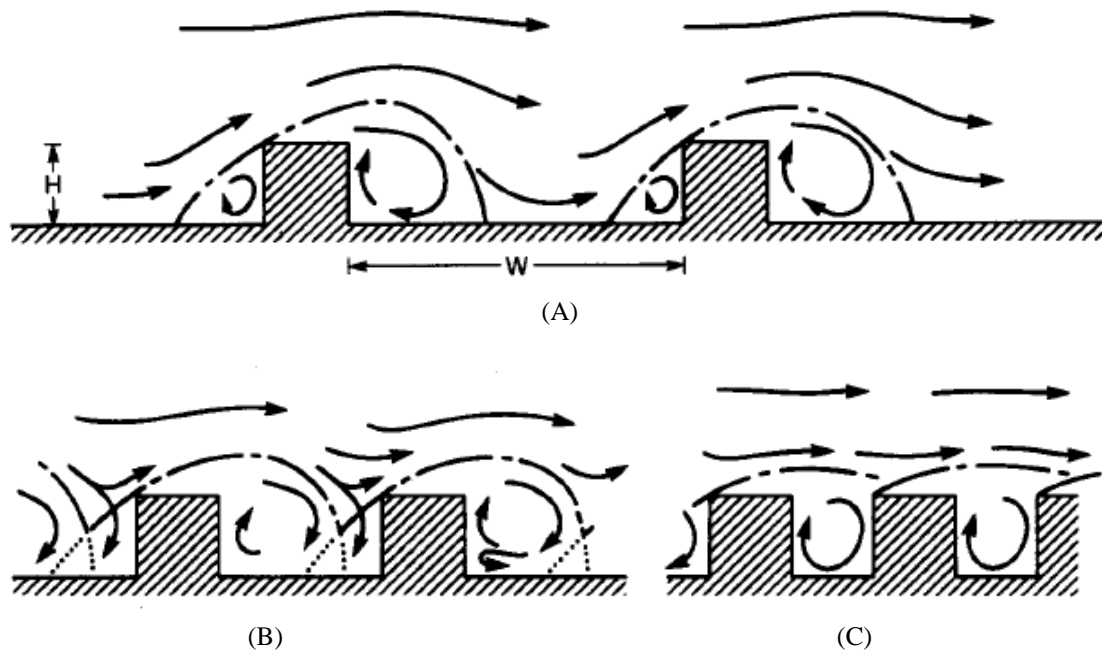
Figure 2.2 The airflow over long street canyons (A) isolated roughness flow (B) wake interference flow (C) skimming flow (Oke, 1988)

For example, a threshold aspect ratio of 1.6<H/W<2.67 is suggested for increasing from a one-circulation regime to a two counter-rotating circulation regime (Jeong and Andrews,

2002), where the main circulation is generally moved to the upper part of the street canyon, and a secondary weak circulation is observed in the bottom part. This threshold is reported to be H/W=3.4-3.6 for the evolution of the airflow to a three-circulation regime in the street canyon (Kim and Baik, 2001).

Above mentioned investigations show the significance of street canyon characteristics on airflow regime and pollution dispersion. However, there is still an urgent need for a comprehensive and reliable design guideline for pedestrian air quality (Tominaga et al., 2008). This means that implementation of various simplifications and limitations within the street canyon studies provide only preliminarily information for the urban planner and building designer to enhance pedestrian comfort and exposure.

These limitations include non-homogeneity in the shape and the material of buildings, discrepancy in providing boundary conditions, and ignoring details of stationary and mobile objects inside the street canyons (Mirzaei and Haghighat, 2010c). In addition to these limitations, the landscape of cities is mostly developed and applying the outcomes of such studies on existing street canyons is economically impractical. Moreover, even after applying these strategies such as the use of vegetation and higher-albedo materials, achieving appropriate pedestrian comfort is not guaranteed. For example, it is assumed

that tree planting always has a beneficial effect on outdoor air quality. However, it can improperly influence the natural airflow regime of the street canyon; directly by creating a drag effect and indirectly by the alteration of surface temperatures. Moreover, the possibility of obtaining improper air circulation due to changing the facade temperature is expected inside the street canyon when higher-albedo materials are used.

In general, the existing limitation of pollution removal from street canyons can be summarized by the weakness of these strategies in having active control on pedestrian's comfort, including air velocity, temperature, humidity, radiation, and pollution concentration.

2.5. Modeling Approaches

Different scales are required to model all physical processes occurring inside the street canyons, including small-scale processes like human metabolism or meso-scale interactions like planetary forces. However, integration of all scales together is not a straightforward procedure due to complexities in providing a comprehensive database as well as the limitations of existing theories. Because of these limitations a number of assumptions are made to simplify the investigation.

2.5.1. Observational Approaches

In recent years, observation techniques have been made in accordance with the geographic scope of heat island and OAQ studies, including field measurement, thermal remote sensing, and small-scale modeling.

2.5.1.1.   Field Measurement

The field measurement campaign of the street canyons, air temperature, velocity, moisture, turbulence fluctuations and pollution concentration is a simple approach to monitor PCE (Murena and Favale, 2007; Nikolopoulou and Lykoudis, 2006). Nonetheless, one should note that field measurement, as an independent approach, has several limitations; only a limited number of parameters are simultaneously measured. This implies that it is not possible to demonstrate all three-dimensional spatial distributions of the quantities inside a street canyon at the same time. Instead, approximations are frequently made to estimate these quantities for inaccessible points. In addition to these shortcomings, it is necessary to carry out the measurements for a long period of time to filter the effect of unpredictable errors. Even after collecting sufficient data, consistent generalizations cannot be made with simple correlations because of the abundance of parameters that could influence the results.

Some field measured data were collected for the validation of models or defining boundary condition (Tominaga et al., 2008), Nunez and Oke 1977).

2.5.1.2. Thermal Remote Sensing

With the advancement of sensor technology, thermal remote observation became possible through the use of satellite, airborne and aircraft platforms. However, it is not possible to observe the other above mentioned PCE parameters in this approach. Also, the resolution of this approach is not fine enough to monitor pedestrian-scale activities. Thus, this approach only helps to locate the thermally vulnerable street canyons "hot zone".

It should be noted that remote sensing is a very expensive approach, and it is not possible to have steady images from the urban surface. This is partly related to the capability of the used apparatuses and partly due to the atmospheric interactions. For example, satellites, which revolve around the earth, spend a limited time over one specific region, and there is always the probability of a cloudy sky. The main technical concern in this approach is nonetheless that the surface temperature measured by sensors only relates to the spatial patterns of upward thermal radiance received by the remote sensor (Voogt and Oke, 2003). However, the surface temperature is different from the ambient temperature. This means that the observed surface temperature can be significantly different from the

ambient air temperature inside a street canyon. Therefore, in order to fully utilize the measured data, it is necessary to first predict the actual temperature from the surface by developing sensor-view models. Even though various sensor-view models have been adapted (Hafner and Kidder, 1999), a considerable gap still exists between the estimated and the actual ambient air temperatures, in addition to cosmic noises, long distance between urban surface and satellite effects on the performance of these sensors. It is therefore necessary to develop a reliable filtration and conversion model between the radiation received by satellite sensors and the actual surface temperatures (Voogt and Oke, 2003).

Another limitation of this approach is that a significant portion of street canyon surfaces cannot be viewed due to the three dimensional structure. This means that the vertical field of the study domain cannot be captured in this scheme. Therefore, the vertical temperature distribution once again has to be extracted from thermal data observed from a birds-eye point of view, using sensor-view models. The performance of current models has to be improved in order to correlate temperature of unseen vertical surfaces with the satellite-view. Improvement in spectral and spatial satellite-sensors is also expected to provide more detailed information about the urban surfaces at lower cost and higher

resolution. Similar to the field measurement, thermal remote sensing can also be used to provide a boundary condition for models (Goldreich, 2006; Kato and Yamaguchi, 2005; Kolev et al., 2000).

2.5.1.3. Small-scale Modeling

In this approach, the street canyons are mostly replaced with a prototype which obeys the Similarity Theory between the real case and small-scale model (Cermak, 1984). The prototypes are tested either using wind tunnels (Uehara et al., 2000) or outdoor spaces (Flor and Domınguez, 2004; Kanda et al., 2005). It is difficult and sometimes unfeasible to ensure similarity between the real case and the small-scale model. For example, implementing solar radiation similarity is complicated in wind tunnel modeling, while radiation is evidently one of the most significant factors on pedestrian comfort. Small-scale modeling is mostly used to validate, calibrate and improve the mathematical models (e.g. turbulence, stratification). However, similarity between model and prototype is a necessary condition for achieving accurate results.

Small-scale modeling can help to study the impact of a limited number of parameters of a building on its environment (e.g. dimension, pollution dispersion) or over the small region of a city (Cermak, 1996; Poreh, 1996). Although it is not easy to model complex

dynamics of atmosphere interactions in this approach, this can be compensated by selecting appropriate boundary conditions (Cermak, 1984). Accuracy of a small-scale model in the problem depends on the ability to identify the most significant dimensionless numbers, to reduce the number of unmatched dimensionless numbers, and to develop criteria that reduces their impact (Poreh, 1996).

The main drawback of small-scale modeling is the cost. Also, it is very challenging to experimentally generate thermal stratification in order to investigate the impact of stratification on airflow patterns and on pollution distribution (Uehara et al., 2000). Furthermore, a complete adjustment is required to obtain the similarity between boundary conditions of a small-scale experiment and a real problem (e.g. producing inflow, geostrophic or free-surface boundary conditions in a wind tunnel).

2.5.2. Simulation Approaches

Besides the observation approaches, mathematical models have been developed to solve urban climate problems including outdoor air quality and pedestrian comfort. Among these models, energy balance and dynamical numerical approaches showed the most reliable and satisfactory outcomes.

2.5.2.1.   Energy Balance Model (Simplified Model)

The energy balance budget for a street canyon was first suggested by (Nunez and Oke, 1977) as follows:

$$Q^* + Q_F = Q_H + Q_E + \Delta Q_S + \Delta Q_A \qquad (2.1)$$

where Q^* is the net radiation, Q_H and Q_E are the fluxes of the sensible and latent heat, respectively, Q_F represents the anthropogenic energy release within the control volume, ΔQ_A is the net advection through the lateral sides of the control volume, and ΔQ_S is the storage heat flux and represents all energy storage mechanisms within elements of the control volume, including air, trees, building fabrics, and soil. Also, the energy balance for each facet of this control volume was expressed as below:

$$Q^* = Q_H + Q_E + Q_G \qquad (2.2)$$

where Q_G is the conductive heat flux.

This method uses the law of conservation energy for a given control volume, and considers the atmospheric phenomena, turbulence fluctuations and velocity field as heat fluxes. These fluxes are generally defined by analytical or empirical equations.

The urban canopy model (UCM) is derived from the energy balance equation for a control volume which contains two adjacent buildings. The model considers the energy exchanges with surfaces and ambient air in the urban canopy. The UCM predicts the ambient temperature and the surface temperature of buildings, pavements, and streets. However, the airflow is decoupled from the temperature field, and has to be defined as a particular input into the control volume. Logarithmic-law and power-law are widely assumed in the UCMs.

In the UCM approach, all surfaces and control volumes are connected to each other like electrical network. Equation (2.1) is then applied to each node, and the matrix of temperature and humidity of the surfaces are formed. By solving these matrices, the temperature and relative humidity of the domain are attained. Single-layer (Kusaka et al., 2001) and multi-layer (Kondo et al., 2005) schemes are related to the number of nodes on the buildings' walls. Models can be also developed in one, two, or three dimensions. This approach is generally very quick as it only approximates building canopies with limited nodes. It also provides acceptable accuracy for large-scale energy consumption studies (Table 2.2).

Absence of the air velocity field serves as the major weakness of the energy balance models; the velocity field information is necessary in order to study the effect of airflow pattern (e.g. eddy circulation, wake region and turbulence), to study formation of the atmospheric phenomena (e.g. precipitation and stratification), and to determine the sensible and latent heat fluxes. The assumption of these fluxes with empirical correlations does not therefore appropriately represent the interaction between velocity and temperature fields. Modeling transient effect is also an inherently challenging issue with this approach, since different uncoupled terms contribute to equation (2.1) varying in different time-steps. For example, thermal storage of building materials may have a large time step compared to convective heat fluxes. Therefore to ensure reliable results, it is either necessary to select very small time-steps which increases the calculation time but neutralizes the major advantage of using this approach, or to clarify all terms based on one specific term (e.g. radiation) which physically weakens the modeling.

The geometry and complexity of buildings are also approximated with limited grids on the ground, roof, and walls. Apparently, this makes the spatial resolution of the energy conservation technique very weak, especially when it is required to study the thermal comfort and pollution dispersion at the pedestrian level.

2.5.2.2.　　　Computational Fluid Dynamics (CFD)

Unlike the energy balance models in which velocity and temperature fields are separated, CFD simultaneously solves all the governing equations of fluid inside the street canyons: conservation of mass, potential temperature, momentum, and species (water vapor and chemical reaction). As a result, CFD is capable of obtaining more accurate information about the pedestrian level of street canyons than UCM. Consideration of complex details in addition to complicated atmospheric interactions is nonetheless a computationally and theoretically challenging problem. The computational problem is due to the number of control volumes or required nodes to simulate the street canyon environment. On the other hand, the theoretical problem is related to the unmatched temporal and spatial resolution of the phenomena which occur inside a city. For example, atmospheric and canopy-scale turbulence cannot be modeled in the same scale of time and length. Therefore, CFD simulations are mostly separated into different scales. This means that the simplification of Navier-Stokes is significantly different due to the scale of the study. Two scales are generally used: meso-scale and micro-scale (urban-scale).

2.5.2.2.1.   Meso-scale Model

Meso-scale models are smaller than synoptic-scale and larger than micro-scale systems. The horizontal resolution of these models ranges approximately from one to several-hundred kilometers. Also, these models vary vertically with the depth of Planetary Boundary Layer (PBL) between 200m-2km. This layer exists between the earth surface and geostrophic wind. In meso-scale models, large-scale interactions under the PBL are resolved, including atmospheric stratification and surface layer treatment. In this approach, the Navier-Stokes equations are either based on a hydrostatic or non-hydrostatic hypothesis to include the atmospheric stratification effect. In hydrostatic models, the equation of motion in the vertical direction is simplified into a balanced equation between the buoyancy and the pressure terms. In non-hydrostatic models the equation of motion in the vertical direction is expressed with a full Navier-Stokes equation.

Meteorological schemes usually use Monin-Obukhov or other similarity schemes to model surface sub-layer (Anthes et al., 1978; Yamada and Bunker, 1987). This means that street canyons are assumed to be like aerodynamic roughness. This implies that in meso-scale models the whole urban canopy layer with its complex details is replaced

with a roughness number. Thus, information about the quantities within the canopy layer is not available, and PCE cannot be directly obtained using this approach. However, coupling meso-scale and micro-scale models is extremely useful to provide more accurate upper boundary conditions for micro-scale models (Murakami, 2006).

The accuracy of a meso-scale model prediction strongly depends on the database provided for the Land-Use Land-Cover (LULC). Detailed information of micro-scale surfaces (e.g. thermal properties, geometry, radiative characteristics) is rarely available for the entire urban region, and even if it is, applying these details to a meso-scale model is very CPU-intensive. Since the spatial resolution is in magnitude of a few kilometers, it is also necessary to assume a meso-scale zone as a homogeneous area, and estimate the surface properties with bulk values (e.g. albedo, emissivity, roughness).

Appropriate assumption of the PBL is another important issue in meso-scale methods. In addition, many moisture schemes (Reisner et al., 1998; Schultz, 1995; Tao and Simpson, 1993) and soil models (Chen and Dudhia, 2001; Xiu and Pleim, 2001) have been developed for integration with PBL models. The interaction between cumulus and radiation is also required for meso-scale modeling. It is noteworthy to mention that cumulus, soil, radiation and PBL models are coupled in meso-scale models and

development of these interactions therefore is a wide topic of research. Furthermore, the accuracy of meso-scale models is a function of proper wind and surface temperature boundary condition that is generally provided by observational techniques (Saitoh et al., 1996; Tong et al., 2005).

2.5.2.2.2. Micro-scale Model

Unlike the meso-scale model, micro-scale CFD resolves the conservation equation inside the surface layer. This means that the horizontal spatial quantities are assumed with bulk values in a meso-scale model, where these are simulated with actual geometry and details with surface layer interactions in a micro-scale model. These interactions are generally assumed with Monin-Obukhov similarity inside the PBL in meso-scale models. In this approach, the simulations are horizontally limited to a small domain in magnitude of some blocks of buildings (a few hundred meters) due to the high computational cost. On the other hand, the treatment of the PBL in a micro-scale model is not as comprehensive as a meso-scale model. It implies that the micro-scale model mostly does not include the atmospheric interactions like atmospheric vertical mixing or Coriolis effect. Generally, it can be concluded that the micro-scale model is an appropriate approach to study the high-Rossby number (Ro: the ratio of inertial to Coriolis forces) problems.

Observational schemes can significantly improve the mentioned limitations of boundary conditions (Mochida et al., 2006). However, providing boundary conditions for the micro-scale is even more complicated than meso-scale models. In this model more measurements are necessary due to high fluctuation of quantities at the surface layer. Although assumptions (e.g. log-law, power-law, and outflow) are usually made for the boundary conditions, these approximations are physically weak due to the stochastic nature of airflow velocity, and the different geometry and height of buildings. Similar to the meso-scale model, the treatment of turbulent closure and radiation has a significant effect on the accuracy of the micro-scale model prediction.

2.6.   Simulation Tools

As pointed out, the complexity and quantity of urban details, the theoretical weakness and the high cost of simulation approaches, difficulties in providing high-resolution, continuous and real time boundary conditions, and the inconsistency of the observational method make the urban climate investigation a challenging one.

Table 2.2 Comparison of the urban heat island simulation approaches

Approach	Urban Canopy Models	CFD	
		Meso-scale	**Micro-scale**
Governing Equation	Energy balance equation (2.12) An input assumption for velocity equation of the canopy layer Heat conduction equation for surface	Navier-stokes equations (Including Coriolis term with hydrostatic or non-hydrostatic assumption) Monin-Obukhov for ground surface Heat conduction equation for soil	Navier-stokes equations Monin-Obukhov for surfaces of the urban structures (e.g. wall, ground) Heat conduction equation for surface
Major Limitations	**1.** Decoupled velocity field from temperature and moisture **2.** Assumption of a city with similar homogeneous array of buildings **3.** Limited resolution of urban geometry **4.** Only good for steady state solution **5.** Neglecting the atmospheric effect **6.** Empirical assumption for convective latent and sensible heat	**1.** Assumption of the urban canopy layer as roughness **2.** Difficult to provide Land-Use Land-Cover database **3.** Accuracy dependent on field measurement **4.** Modeling of the turbulence	**1.** Not including the atmospheric phenomena **2.** Difficult to create database for canopy details **3.** Providing boundary conditions **4.** Modeling of the turbulence
Maximum Domain Size	City	City	Building Block
Spatial Resolution	1m-10m	1-10km	10m-1km
Temporal Resolution	Hour	Minute	Second
CPU-Cost	Medium	Very High	Very High

Table 2.2 summarizes the developed study models based on the governing equations, major limitations, domain size, spatial and temporal resolution and CPU-cost. It is obvious from Table 2.2 that meso-scale tools are practical approaches when underlying surface details are not important (e.g. urban-scale energy conservation and pollution dispersion). Conversely, for cases with concern about canopy layer phenomena (e.g. pedestrian thermal comfort, building-scale energy conservation) micro-scale CFD and

UCM are more useful schemes. Nonetheless, because of the high computer cost, real-time and real-size simulation of a city is not possible and major assumptions have to be made.

It is noteworthy that the selection of the most appropriate models depends on objective of the application: decreasing urban temperature, improving the OAQ, reducing heat island related diseases, or energy conservation.

2.7.   Literature Review Conclusion

- Urban heat island increases energy consumption and peak electricity demands of a city. The UHI also reduces outdoor air quality and pedestrian comfort.

- The street canyon geometry and stratification are known as the most significant parameters in PCE. More vulnerable PCE is reported at skimming flow.

- Experimental and simulation approaches have been widely used in order to quantify pedestrian comfort. The observational models are reliable but not very practical or economical approaches. Dynamical numerical methods are widely used after intensive development of the computers.

- Before evaluation of the OAQ and pedestrian comfort, it is first necessary to adapt appropriate comfort indices. However, only limited studies have been done in order to develop an outdoor comfort index.

- Several passive UHI mitigation strategies have been proposed to enhance OAQ and pedestrian comfort, however, their effectiveness varies in different urban structures and climates. This implies that the studies should locally evaluate the impact of these passive strategies in different street canyons.

- It is also necessary to develop a systematic procedure to assess all parameters of PCE in micro-scale (building-scale) after employment of mitigation technologies.

3. Chapter Three: Assessment of Pedestrian Comfort and Exposure

3.1. Algorithm for Enhancement of Pedestrian Comfort and Exposure (PCE)

Figure 3.1 exhibits the proposed PCE-algorithm to quantify pedestrian comfort and exposure around a building before and after its construction. As shown in Figure 3.1, the PCE-algorithm includes three major steps:

1. Collecting street canyon and annual weather information

2. Evaluation of the effect of passive strategies on PCE

3. Evaluation of the effect of pedestrian ventilation system (an active mitigation technology) on PCE

The most important step is gathering information about the built environment around the target building. This contains the street canyon geometry, orientation, material properties (e.g. emissivity, albedo, and conductivity), green spaces, ponds, and the rate of pollution emission from vehicles. Evidently, weather information history measured by weather stations or monitoring devices is required to statistically provide initial and boundary condition.
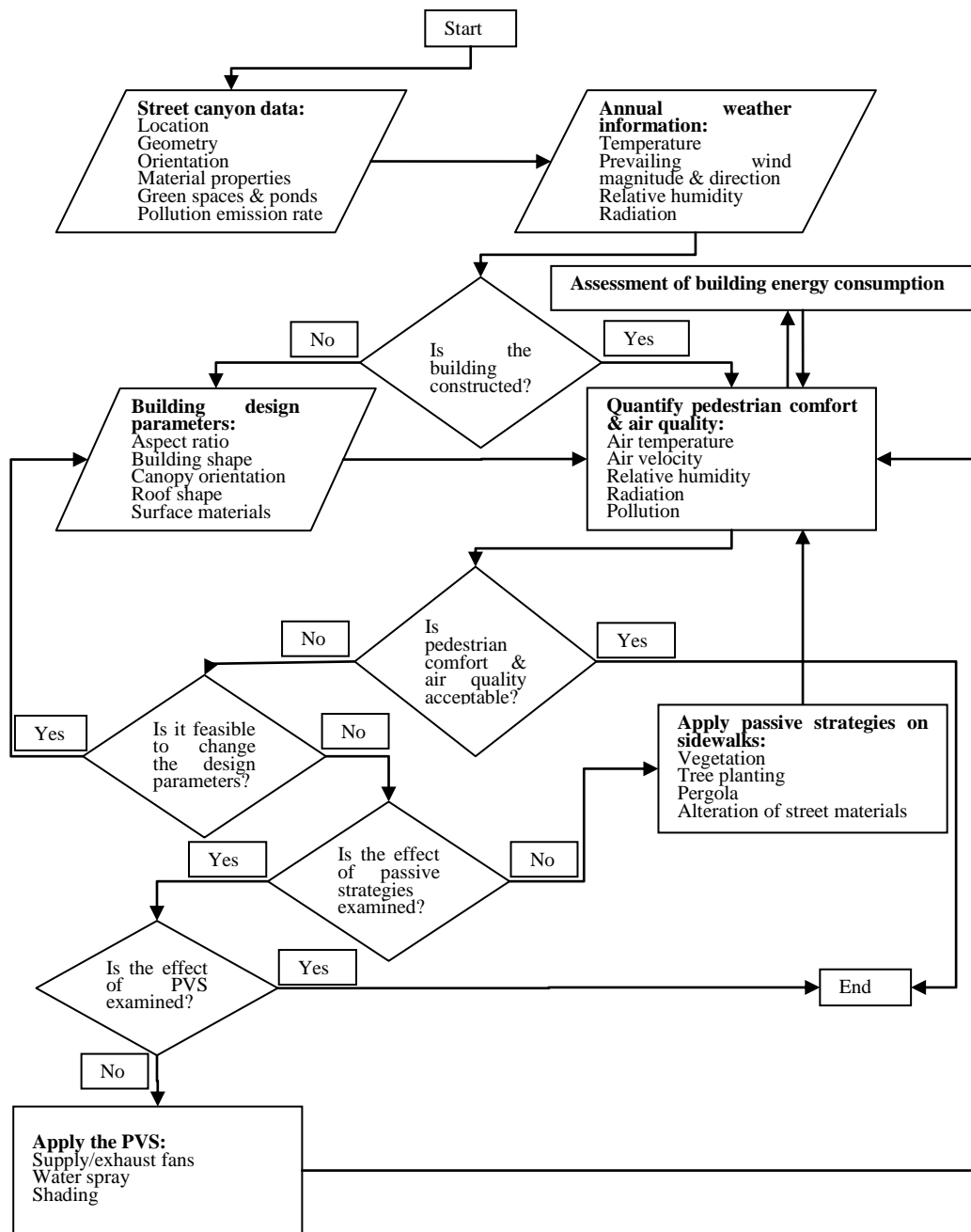
Figure 3.1 PCE-algorithm; a systematic model to evaluate and control PCE around the buildings

The passive strategies discussed in Table 2.1, can be applied either to buildings or to its built environment. The proposed algorithm first checks the construction status of the building. If the building is not constructed, the PCE-algorithm suggests practical and economical reconsideration of the building's design parameters, including selection of material's properties, aspect ratio, layout, roof shape, and place of anthropogenic heat release. If the building is already constructed or pedestrian comfort and exposure is not significantly enhanced after reconsideration of the design parameters, the PCE-algorithm recommends the implementation of other passive strategies, including tree planting, vegetation, pergola and lower albedo materials in roads and pavements. The quantification of PCE is obtained using a coupled CFD-radiation model. The output of the CFD-radiation model is air temperature, velocity and moisture in addition to radiation flux and pollution concentration at the pedestrian level. This data is required to evaluate pedestrian comfort and exposure by integrating associated indices.

Eventually, implementation of the PVS is suggested by the PCE-algorithm, especially during UHI episodes when PCE is not considerably changed by applying passive strategies. The PVS receives feedback measuring related parameters of PCE and attempts to control them. It is noteworthy to mention that an energy assessment block could be

integrated with the PCE quantification block (shown in Fig. 3.1) in order to minimize the energy consumption of the studied building.

3.2. Pedestrian Ventilation System (PVS)

To control the air quality and pollutant dispersion inside street canyons, it is feasible to modify the existing air movement created by turbulence and buoyancy by imposing a controlled air movement. This air movement is different from unpredictable and stochastic vortex/vortices created by the top-canopy prevailing wind. It is postulated that the required air movement is obtainable with an active control system in the form of a pedestrian ventilation system (PVS).

3.2.1. System Configuration

As shown in Figure 3.2, the PVS induces air movement in a region near the ground, the pedestrian ventilation zone (PVZ), using ventilation ducts. The PVZ volume is extended around the building up to three meters in height (sidewalks or regions where most pedestrian activity occurs). The mechanism for ventilation is based on guiding air through a designed vertical duct system from the roof of the building to the surrounding street level.

Contaminated/Fresh Air

Technique to Provide Pressure Gradient:
Natural Convection (Heating):
Exhaust from AC's Condenser
Solar Radiation
Electricity
Force Convection:
Intake/Blowing Fan

Responsible Buildings to Pedestrian Level

Pedestrian Walking Area

Water Spray

Pergola

Ventilation Ducts

Pedestrian Control Volume
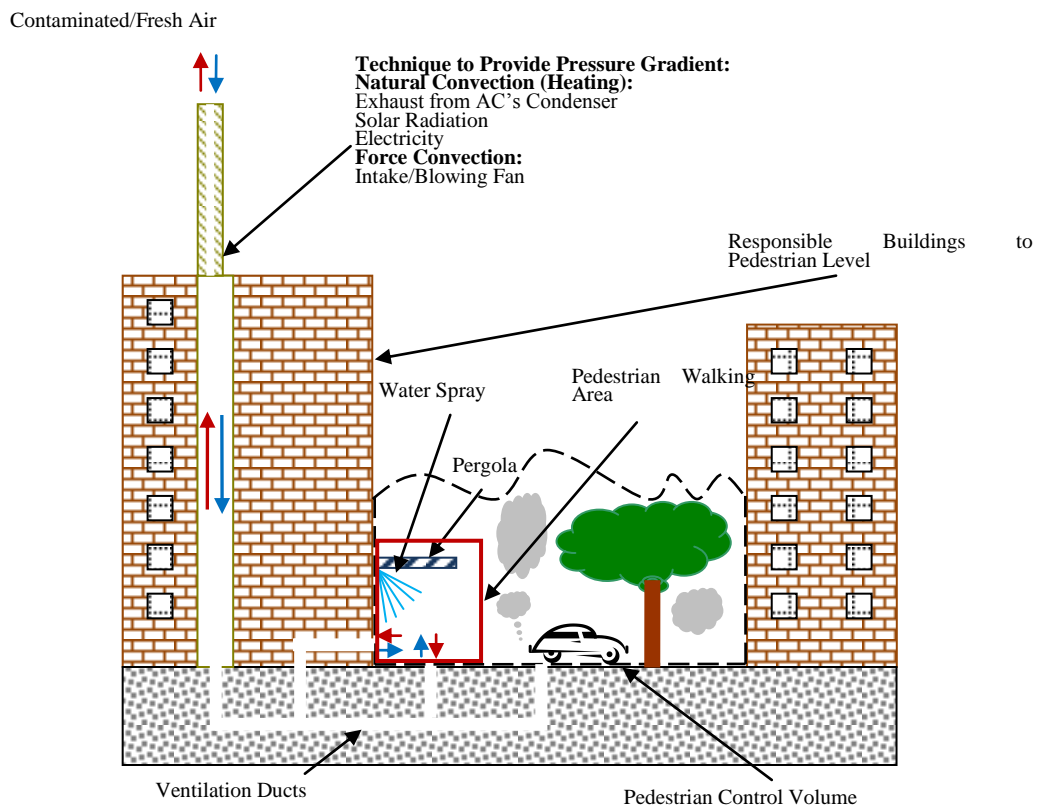
Figure 3.2 New design approach: Pedestrian Ventilation System (PVS)

When pollutant is accumulated in the PVZ, the PVS can replace the pedestrian level air with fresher air from the top-canopy level, specifically in a stratified situation (the street temperature is lower than the prevailing wind temperature). On the other hand, this system is useful to accelerate the movement of cooler air from the top-canopy to the PVZ where the weather is in an unstable condition (the prevailing wind temperature is colder than the canopy temperature). Therefore, the pedestrian air velocity, temperature and pollution concentration can be placed under control by changing the airflow rate within

the street canyon. To provide the required pressure gradient for the system, both natural

and force convection can be taken into account.

Heating the duct can provide the required air movement (stack flow). The required

energy for heating can be obtained from heat exhausted from the condenser of the air

conditioning systems, and/or solar energy. Alternately, force convection can be achieved

using a supply/exhaust fan.

When the ambient air relative humidity is not within the thermal comfort range, the

pedestrian ventilation system can humidify the PVZ with water spray system (Figure

3.2). Solar radiation can also be shaded by placing flexible pergolas (Figure 3.2). In this

research, however, only the capability of the PVS in enhancing PCE by removing

pollutants and improving air velocity and temperature within the canopy has been studied

using an electrical fan (force convection mechanism).

3.2.2. Combined Pedestrian Ventilation System

It is feasible to have various way of integrating the PVS inside a canopy by installing two

systems on the adjacent buildings (Figure 3.3). These systems strengthen or weaken the

vortex/vortices of the street canyon. Strategy (A) uses two exhaust fans to intensify a

downward flow. In strategy (B), an upward flow toward the top-canopy can be achieved

using two supply fans. Strategies (C) and (D) are capable of establishing a washing flow

through one sidewalk to another using a supply and an exhaust fan. It is noteworthy to

mention that the closest vortex to the ground is either clockwise or counterclockwise

depending on the aspect ratio and the number of vortices (see section 2.4). Thus, (C) or

(D) strategy is always strengthening the airflow while the other is weakening that.

Obviously, the required pedestrian comfort situation is an important factor to consider

when choosing the most effective strategy. This flexibility is investigated in the following

chapters for various aspect ratios and under different weather stabilities.
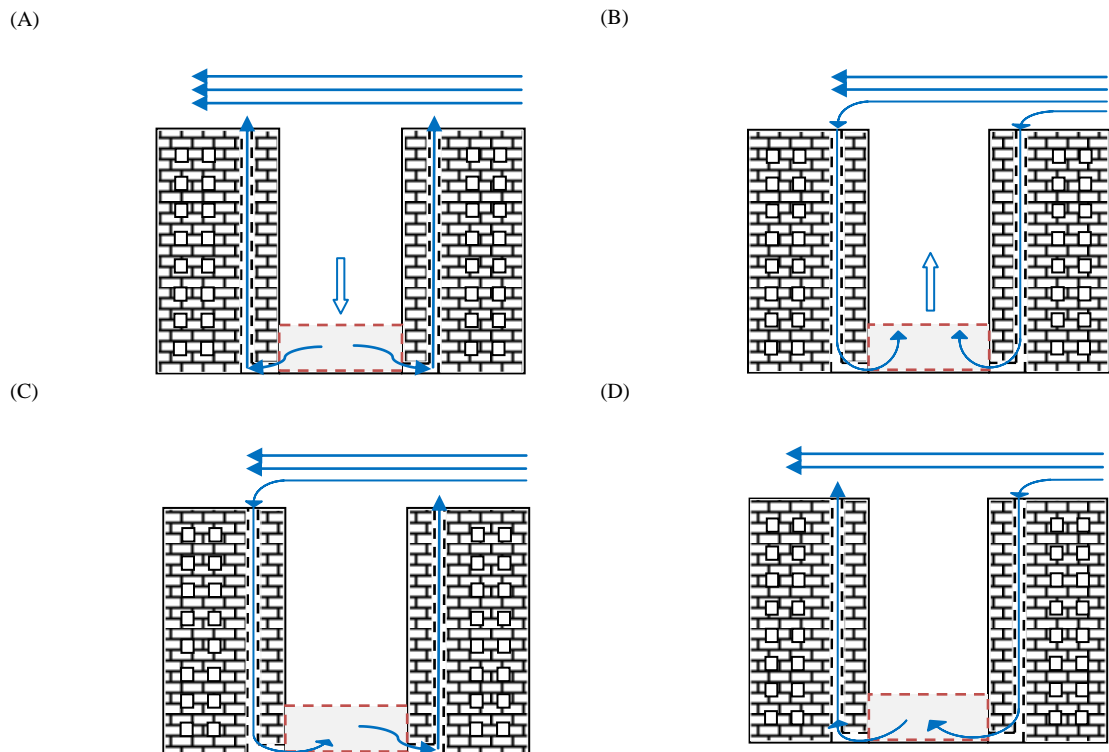
Figure 3.3 Different strategies of the PVS

3.3. Methodology

The following section presents the necessary models to study the performance of the PCE-algorithm. Airflow model, turbulence scheme, heat storage model, radiation model, and assigning proper boundary conditions are all discussed in this section.

3.3.1. Mathematical Model

Presented in Table 2.2, micro-scale simulation is selected as a simulation tool, since fine resolution and contribution of wind velocity are necessary to study PCE. This implies that Navier-Stokes (NS) equation is used as the governing equation to study the physical interactions within the street canyon. The Reynolds-averaged Navier-Stokes (RANS) model is also adapted as the turbulence model. In this model, the variables in the Navier-Stokes equation are decomposed into the mean and fluctuating components:

$$\varphi_i = \bar{\varphi}_i + \acute{\varphi}_i \qquad\qquad (3.1)$$

where $\bar{\varphi}_i$ and $\acute{\varphi}_i$ can be the mean and fluctuating components of velocity or other scalar quantities such as pressure, energy, or species concentration.

The ensemble-averaged continuity and momentum equations can be also derived by substituting mean and fluctuating components of the airflow variables into the Navier-Stokes equation:

$$\frac{\partial \rho}{\partial t} + \frac{\partial}{\partial x_i}(\rho \bar{u}_i) = 0 \tag{3.2}$$

$$\frac{\partial}{\partial t}(\rho \bar{u}_i) + \frac{\partial}{\partial x_j}(\rho \bar{u}_i \bar{u}_j) = -\frac{\partial \bar{p}}{\partial x_i} + \rho \bar{f}_i + \frac{\partial}{\partial x_j}\left[\mu\left(\frac{\partial \bar{u}_i}{\partial x_j} + \frac{\partial \bar{u}_j}{\partial x_i} - \delta_{ij}\frac{2}{3}\frac{\partial \bar{u}_k}{\partial x_k}\right)\right] + \frac{\partial}{\partial x_j}\left(-\rho\overline{\acute{u}_i\acute{u}_j}\right)$$

$$\tag{3.3}$$

where ρ is the density, μ is the dynamic viscosity, $\bar{f}$ is the body force ($\bar{f}_i = g\delta_{i3}$), δ_{ij} is the Kronecker delta, g is the gravitational acceleration, and $\bar{p}$ is the mean pressure. $\bar{u}_i$ and $\acute{u}_i$ are also mean and fluctuation parts of velocity.

Equations 3.2 and 3.3 are called RANS equations. The additional term at the end of the equation 3.3, $-\rho\overline{\acute{u}_i\acute{u}_j}$, is called Reynolds stress. This equation represents the turbulence closure. Many schemes are proposed to model Reynolds stress in order to enclose equation 3.3 and solve the closure problem.

3.3.2. Turbulent Scheme

The $k - \varepsilon$ is employed as a turbulent closure model (Launder and Spalding, 1972). $k - \varepsilon$ is a semi-empirical model and includes two transport equations to resolve turbulent

kinetic energy (k) and its rate of dissipation (ε). Standard, realizable, and renormalization group theory (RNG) are known as reliable $k - \varepsilon$ models. The major differences in these models are associated with calculation of turbulent viscosity, turbulent Prandtl number, and terms of ε equation. Standard $k - \varepsilon$ has been widely used in micro-scale studies due to its low computational cost, robustness, and reasonable accuracy (Chan et al., 2001; Gromke et al., 2008; Xie et al., 2006). This model is based on a fully-turbulent condition assumption when molecular viscosity is negligible.

The RNG $k - \varepsilon$ model (Yakhot et al., 1992) was also used in many outdoor environment problems specifically under lower-Reynolds-numbers (Cheng et al., 2009; Memon et al., 2009; Murena et al., 2009). The RNG $k - \varepsilon$ includes an additional term in its ε equation and the effect of swirl-turbulence. Unlike the standard form, RNG assumes an analytical formula for turbulent Prandtl numbers. In $k - \varepsilon$ models, the Reynolds stress tensor is defined as below:

$$\rho \overline{\acute{u}_i \acute{u}_j} = -\mu_t \left(\frac{\partial \bar{u}_i}{\partial x_j} + \frac{\partial \bar{u}_j}{\partial x_i} \right) + \frac{2}{3} \delta_{ij} k \tag{3.4}$$

where $\mu_t = \rho C_\mu \frac{k^2}{\varepsilon}$ ($C_\mu = 0.09$) is the turbulent viscosity in standard $k - \varepsilon$. The treatment of μ_t in RNG $k - \varepsilon$ is as below:

$$d\left(\frac{\rho^2 k}{\sqrt{\varepsilon\mu}}\right) = 1.72\frac{\hat{v}}{\sqrt{\hat{v}^3 - 1 + C_v}}d\hat{v} \tag{3.5}$$

where $\hat{v}$ is the modified turbulent kinematic viscosity and $C_v \approx 100$.

As presented before, k is the turbulent kinetic energy (TKE), and it can be obtained from the following transport equation:

$$\frac{\partial}{\partial t}(\rho k) + \frac{\partial}{\partial x_j}(\rho k \bar{u}_j) = \frac{\partial}{\partial x_j}\left(\left(\mu + \frac{\mu_t}{\sigma_k}\right)\frac{\partial k}{\partial x_j}\right) + G_k + G_b - \rho\varepsilon + Y_M + S_k \tag{3.6}$$

where σ_k is the turbulent Prandtl number for k. Y_M stands for the contribution of the fluctuating dilatation in compressible turbulence to the overall dissipation rate. S_k is the source terms. G_k and G_b are also the generation of TKE due to the mean velocity gradients and to buoyancy:

$$G_k = \mu_t\left(\frac{\partial\bar{u}_i}{\partial x_j} + \frac{\partial\bar{u}_j}{\partial x_i}\right)\frac{\partial\bar{u}_i}{\partial x_j} \tag{3.7}$$

$$G_b = \beta g\delta_{i3}\frac{\mu_t}{Pr_t}\frac{\partial\bar{\theta}}{\partial x_i} \tag{3.8}$$

where $Pr_t = 0.72$ is the turbulent Prandtl number for energy, $\bar{\theta}$ is the air temperature, and β is the thermal expansion coefficient:

$$\beta = \frac{1}{\rho}\left(\frac{\partial\rho}{\partial\bar{\theta}}\right)_p \tag{3.9}$$

The turbulence rate of dissipation ε for the standard form can be derived from the following equation:

$$\frac{\partial}{\partial t}(\rho\varepsilon) + \frac{\partial}{\partial x_j}(\rho\varepsilon\bar{u}_j) = \frac{\partial}{\partial x_j}\left(\left(\mu + \frac{\mu_t}{\sigma_\varepsilon}\right)\frac{\partial\varepsilon}{\partial x_j}\right) + C_{1\varepsilon}\frac{\varepsilon}{k}(G_k + C_{3\varepsilon}G_b) - \rho C_{2\varepsilon}\frac{\varepsilon^2}{k} - R_\varepsilon + S_\varepsilon$$

$$(3.10)$$

where σ_ε is the turbulent Prandtl number for ε. Table 3.1 represents the coefficient for standard and RNG form of the $k - \varepsilon$. $C_{3\varepsilon}$ can be assumed as $C_{3\varepsilon} = \tanh|w/v|$. where v and w are horizontal and vertical component of the airflow (Henkes et al., 1991). Also, R_ε is set to zero for standard $k - \varepsilon$ and for RNG is defined as below:

$$R_\varepsilon = \frac{\rho C_\mu \eta^3 (1-\eta/\eta_0)\varepsilon^2}{(1+\beta\eta^3)k} \qquad (3.11)$$

Where $\eta \equiv Sk/\varepsilon$, $\eta_0 = 4.38$ and $\beta = 0.012$. S is also the modulus of the mean rate-of-strain tensor:

$$S \equiv \sqrt{2S_{ij}S_{ij}} \qquad (3.12)$$

Table 3.1 Coefficient of standard and RNG $k - \varepsilon$ turbulence model

$k - \varepsilon$ model	$C_{1\varepsilon}$	$C_{2\varepsilon}$	σ_k	σ_ε
Standard	1.44	1.92	1	1.3
RNG	1.42	1.68	0.7194	0.7194

To consider the thermal effects, the energy conservation can be expressed by following equation:

$$\frac{\partial}{\partial t}(\bar{\theta}) + \bar{u}_j \frac{\partial}{\partial x_j}(\bar{\theta}) = \frac{\partial}{\partial x_j}\left(k_t \frac{\partial \bar{\theta}}{\partial x_j}\right) \tag{3.13}$$

where $k_t = \frac{v_t}{Pr_t}$ is the turbulent thermal diffusivity. The transport equation for pollution concentration ($\bar{c}$) is as follows:

$$\frac{\partial}{\partial t}(\bar{c}) + \bar{u}_j \frac{\partial}{\partial x_j}(\bar{c}) = \frac{\partial}{\partial x_j}\left(D_t \frac{\partial \bar{c}}{\partial x_j}\right) \tag{3.14}$$

3.3.3. Solution Method and Computational Domain

A CFD approach is selected to solve the discussed governing equations 3.1 through 3.14. Also, it is necessary to select a reasonable discretization scheme for momentum and energy equations, convergence criteria for residuals, and a solver algorithm.

As depicted in Figure 3.4, a cuboid domain is allocated around the studied building to investigate PCE. Appropriate mesh size will be first obtained by a mesh size test. In addition to this test, a geometry test will be applied to assign appropriate dimensions to the cuboid (L_1 to L_5). These tests help to include the physical phenomena inside the model and to reduce the cost of simulations. This means that these tests (discussed in

section 3.4) are necessary for each particular case which is investigated in PCE-algorithm.

Top boundary:
Meso-scale model
Symmetry
Zero-gradient

Lateral boundary:
Symmetry
Smooth wall function

Outflow boundary:
Zero-gradient

Wall and roof boundary:
Smooth wall function
Constant temperature
Conducting heat through building
Wall-enhanced Treatment

Inflow boundary:
Constant
Logarithmic
Power law

L_5

L_4

L_1

L_3

L_2

Ground boundary:
Smooth wall function
Rough wall function
Constant temperature
Conducting heat through soil
Wall-enhanced Treatment

Interior building boundary:
Constant temperature
Variable temperature
Calculated temperature from energy analysis mode

Bottom and lateral soil boundary:
Symmetry
Constant temperature

Figure 3.4 Domain of study and boundary condition options

3.3.4. Conductive Heat Flux and Storage Effect

Heat storage fluxes within urban areas contribute to the formation of air stratification within the street canyon. Part of radiation and convection heat is conducted through the

soil, pavements, roof and building material and part is stored within the soil and ambient air of the building canopies. In the solid surface, the energy balance equation is expressed as below:

$$q_{conduction} = h_f(T_{surface} - T_{air}) + q_{radiation} \tag{3.15}$$

Where h_f is the fluid heat transfer coefficient, $T_{surface}$ is the soil, pavement, or road temperature, T_{air} the air temperature, $q_{radiation}$ shows solar radiation, and $q_{conduction}$ denotes conducted heat through the surface.

Using the heat-diffusion equation, temperature distribution inside surfaces can be obtained through the numerical models as below:

$$\rho C_p \frac{\partial T}{\partial t} = Q_{Gen} + \frac{\partial}{\partial x_j}\left(K \frac{\partial T}{\partial x_j}\right) \tag{3.16}$$

where ρ is the surface density, C_p is the heat capacity of surface, K is the thermal conductivity, and Q_{Gen} is the heat source or sink. Usually, the sink or source term is omitted, and materials are assumed homogeneous (Kanda et al., 2005). The equation can also be used in the form of one, two, or three dimensions.

If wall thickness and air conditioning details of the building is known, it is also possible to assume the standard indoor air situation (e.g. SET*) as a boundary condition.

Moreover, it is feasible to integrate the calculation with a building energy calculation model (e.g. DOE2, TRANSYS) to improve the accuracy of simulations using temperature distribution within the building instead of one SET* temperature (Mochida et al., 2006).

Two approaches are mostly used to assign the bottom boundary condition for the soil. One approach is to assume that the conducting heat through the soil reaches a zero gradient surface a few meters below the ground. In another approach, mean seasonal temperature of a climate is assigned as constant temperature to the surface a few meters below the ground.

3.3.5. Radiation Model

The influence of radiation fluxes on street canyon studies is significant. Many models have been developed to define the radiation exchange mechanism inside urban areas. However, several limitations made radiation the weakest point of these studies. The radiative transfer equation (RTE) for an absorbing, emitting, and scattering medium was presented by Chandrasekhar (1960). Nonetheless, using this equation is CPU-intensive in urban studies. Therefore, surface-to-surface schemes are more popular in this field. A surface-to-surface radiation model, equation 3.17, is an appropriate technique for

modeling the enclosure radiative transfer without participating media. The net radiation

budget to surfaces within a street canyon is mostly simplified as follows:

$$Q^* = S_r \downarrow - S_r \uparrow + L_r \downarrow - L_r \uparrow \tag{3.17}$$

where S_r and L_r represent the short and long-wave radiation, respectively, and $\downarrow \uparrow$ are

for the downward and upward radiation. One of the main problems with radiation models

is determining the interaction of surfaces to each other and the sky. Therefore, the

radiative transfer equation cannot be properly developed in control volume of a city. For

example, it is not easy to trace the absorption ratio of diffuse part of solar radiation in

surfaces. Radiation models mostly use diffuse assumption for surfaces (Kondo et al.,

2005; Martilli et al., 2002; Masson, 2000). This implies that the reflection of incident

radiation at one surface is isotropic with respect to a solid angle.

Solar radiation contributes significantly to a diurnal heat island when the sky is mostly

clear and calm. Solar radiation is partly absorbed by urban surfaces, and partly reflected.

The incident solar radiation on surfaces is also composed of direct and diffuse fractions.

Assessment of the direct and diffuse portions is a function of cloud cover which is not

physically easy to find. Many atmospheric models have been developed to evaluate the

cloud cover (Dudhia and Bresch, 2002; Skamarock et al., 2005). Another important issue

in short-wave radiation models is how to trace the reflected portion of direct and diffuse parts of solar radiation, which is extremely CPU-intensive. This means that only limited reflections have to be simulated (Kondo et al., 2005; Kusaka et al., 2001). The main problem of radiation models is the calculation of the sky-view factor for each surface in addition to the view factor between a surface and other surfaces. The calculation of the view factor for all surfaces inside urban canopies is also very CPU-intensive and impractical.

In the current study, a simplified model is coupled with CFD simulation. This model only includes the solar radiation and simulates the sun's location in the sky for a given time of the day, date, and position. This model also contains a ray tracing algorithm that calculates the direct incident solar radiation. For this purpose, a solar beam impacting all surfaces is modeled using the sun position vector and intensity parameters, including global position (latitude, longitude, and time zone), starting date and time, grid orientation, and sunshine factor. Here, the sunshine factor is assumed as a constant number to account for the effect of cloud cover. The resulting solar beam on a certain surface, including the direct and diffuse parts, is assumed as a source term in the energy equation within CFD. Moreover, a shading algorithm checks whether a surface is blocked

by other surfaces. Thus, the studied surface is shaded if an opaque surface intersects the

solar beam in front of that surface.

The solar model computes the direct normal solar irradiation at the earth's surface, diffuse

solar irradiation at vertical and horizontal surfaces, and ground diffuse reflected solar

irradiation to vertical surfaces. The equation of the direct normal solar irradiation is given

by (American Society for Heating Ventilating and air conditioning engineers, 2001):

$$S_r \downarrow_{direct} = \frac{A}{e^{B/\sin \xi}}$$
(3.18)

where A, B and ξ are respectively the apparent solar irradiation, the atmospheric

extinction coefficient, and the solar altitude.

The diffuse solar irradiation at a vertical or oblique surface is calculated below

(American Society for Heating Ventilating and air conditioning engineers, 2001):

$$S_r \downarrow_{diffuse-vertical} = CYS_r \downarrow_{direct}$$
(3.19)

$$S_r \downarrow_{diffuse-oblique} = CS_r \downarrow_{direct} \frac{(1+\cos \epsilon)}{2}$$
(3.20)

where C is constant. Y is the ratio of vertical to horizontal sky diffuse radiation on a surface. Also, ϵ is the angle of the surface related to the horizontal plane. Eventually, ground reflected solar irradiation is given by:

$$S_r \uparrow_{diffuse\ -ground\ \rightarrow surfaces} = \alpha_{ground}\ S_r \downarrow_{direct}\ (C + \sin \xi)\frac{(1-\cos \epsilon)}{2} \qquad (3.21)$$

where α_{ground} is the ground reflectivity.

3.3.6. Boundary Condition

The use of observational schemes is the most reliable method to provide boundary conditions for OAQ studies. Since it is not spatially or temporally possible to always have observational data, assumptions are generally made in these studies for the inflow, outflow, ground, soil, building surfaces, top-canopy, and lateral boundary conditions.

3.3.6.1. Inflow Boundary Condition

Wind tunnel experiments and field measurements are reliable approaches for assigning the vertical distribution of turbulence energy to inflow boundary (Gromke et al., 2008; Takahashi et al., 2004). When observation data is not available, numerous methods have been conducted as turbulence boundary condition. For example, the following equation is proposed by the AIJ (Tominaga et al., 2008):

$$k_z \cong I_z{}^2 (U_z)^2 \tag{3.22}$$

where U_z is the mean vertical velocity at height z , and I_z is the turbulent intensity:

$$I_z = \frac{\sigma_{u_z}}{U_z} = 0.1 \left(\frac{z}{z_{BLH}}\right)^{(-\phi - 0.05)} \tag{3.23}$$

where ϕ is the power-law exponent, z_{BLH} the boundary layer height, and σ_{u_z} is the root-mean-square of the turbulent velocity fluctuations. ε_z is also proposed by the AIJ as follows:

$$\varepsilon_z \cong P_{k_z} \cong C_\mu^{0.5} k_z \frac{\partial U_z}{\partial z} \tag{3.24}$$

where P_{k_z} denotes the production term for k equation.

Another approach for the inflow turbulent kinetic energy and dissipation rate profile is represented below (Baik and Kim, 2002; Jeong and Andrews, 2002):

$$k_z = c(U_z)^2 \tag{3.25}$$

$$\varepsilon_z = \frac{C_\mu^{0.75} k_z{}^{1.5}}{\kappa \ z} \tag{3.26}$$

where c is a constant number and $\kappa = 0.41$ is the von Karman constant.

Furthermore, to provide boundary conditions for k_z and ε_z, the turbulent intensity can be set equal to 10% and the turbulent viscosity ratio (μ_t/μ) equal to 10 (Li et al., 2006).

Wind flow, temperature, and humidity profiles over the city terrain are affected by surface layer roughness. These profiles over urban canopies are inside the surface layer of the PBL. Different options have been implemented in micro-scale simulations, including field observation (Takahashi et al., 2004) and wind tunnel data (Kubota et al., 2008; Soulhac et al., 2009), constant or linear values (Cheng et al., 2008; Cheng et al., 2009; Memon et al., 2009), log-profile (Kang et al., 2008; Mirzaei and Haghighat, 2010a; Tominaga et al., 2008), and power law (Gromke et al., 2008; Kim and Baik, 2003; Murena et al., 2009).

A semi-empirical approach, the log-profile, is generally used to describe the vertical profile of horizontal distribution above the ground within the atmospheric surface layer. This layer is a function of weather stability, and is limited approximately to 10 percent of the PBL. The equation to estimate the log-profile is as follows:

$$U_z = \frac{u_*}{k}\left[\ln\frac{z-d}{z_0} + \varphi(z, z_0, L)\right] \tag{3.27}$$

$$\theta_z - \theta_G = \frac{Pr_t T_*}{k}\left[\ln\frac{z-d_t}{z_{0t}} + \ln\frac{z_0}{z_{0t}} + \varphi_t(z, z_0, z_{0t}, L)\right] \tag{3.28}$$

where θ_z is the air temperature at height z above the ground. θ_G denotes the ground surface temperature. u_* is the friction velocity and T_* is the temperature scale. z_0 and z_{0t} are the roughness length for air velocity and temperature. d and d_t are the zero plane displacement for velocity and temperature. φ and φ_t are the universal functions for atmospheric stability which has different values under stable and unstable weather conditions. Zero-plane displacement varies significantly as a result of airflow obstacles like trees or buildings. In street canyon studies however the height is generally approximated as 2/3 of the average height of the obstacles (Masson, 2000). For humidity profiles, the equation is almost the same as that of velocity (Mochida et al., 1997). When weather stability is under neutral condition, or the roughness information is not available, the inflow profile is assumed with the simple and reliable option of power-law:

$$U_z = U_{Ref} \left(z / z_{Ref} \right)^{\phi} \tag{3.29}$$

where U_{Ref} is the reference wind speed at reference height z_{Ref}.

3.3.6.2. Outflow Boundary Condition

Outflow condition is typically assumed as zero gradient condition (Cheng et al., 2008; Gromke et al., 2008; Huang et al., 2009; Xie et al., 2007). It has been proven that this

could be a reasonable assumption, if the distance from building roughness (tail or fetch

length) is appropriate for fluid to reach the fully-developed condition (Tominaga et al.,

2008).

3.3.6.3. Surface Boundary Conditions

To provide the surface boundary condition of temperature and humidity for building or

urban-scale problems, it is necessary to include conduction heat transfer through the

surfaces (see section 3.3.4). Also, treatment of humidity is generally demonstrated by

adding source term to the species equation in CFD. To model turbulent flow near the

ground and walls, the proposed model employs standard wall-function or wall-enhanced

treatment methods based on the characteristics of the airflow.

3.3.6.3.1. Standard wall-function

When the number of meshes is limited and the viscosity-affected region between the wall

and the fully-turbulent region does not substantially affect the airflow, a standard wall-

function provides reasonable results and reduces computational costs for modeling of

airflow through street canyons:

$$U_p = \frac{U_* \tau_w}{\rho C_\mu^{0.25} k_p^{0.5}}$$
(3.30)

$$U_* = \frac{1}{\kappa} \ln(E y^*) - \Delta B \qquad (3.31)$$

$$y^* = \frac{\rho\, C_\mu^{0.25} k_p^{0.5} y_p}{\mu} \qquad (3.32)$$

where U_p and k_p are respectively the mean velocity and turbulence kinetic energy at point p, y_p denotes the distance of point p to the wall, and $E = 9.793$ is empirical constant. In the presented model, mesh size should be set to $30 < y^* < 300$. Also, ΔB represents the roughness of a surface (zero for smooth surfaces) which depends on its type and size:

$$\Delta B = \frac{\ln f}{\kappa} \qquad (3.33)$$

where f is a roughness function. In current model, types of surfaces are classified based on a non-dimensional roughness height:

$$K_s^+ = \frac{\rho\, K_s C_\mu^{0.25} k^{0.5}}{\mu} \qquad (3.34)$$

where K_s is the physical roughness height. These surfaces are as follows (Cebeci and Bradshaw, 1977):

Hydro-dynamically smooth ($K_s^+ \leq 2.25$):

$$\Delta B = 0 \qquad (3.35)$$

Transitional ($2.25 < K_s^+ \leq 90$):

$$\Delta B = \frac{1}{\kappa} ln\left(\frac{K_s^+ - 2.25}{87.75} + C_s K_s^+\right) \times sin[0.4258(ln(K_s^+) - 0.811)] \tag{3.36}$$

Fully rough ($90 < K_s^+$):

$$\Delta B = \frac{1}{\kappa} ln(1 + C_s K_s^+) \tag{3.37}$$

The following equation is also implemented for treatment of the energy equation when effects of turbulence dominate conduction:

$$T_* \equiv \frac{\rho c_p C_\mu^{0.25} k_p^{0.5}(T_w - T_p)}{q'} =$$

$$\begin{cases} Pr y^* + \dfrac{\rho Pr\, c_\mu^{0.25} k_p^{0.5} U_p^2}{2q'} & (y^* < y_T^*) \\[2mm] Pr_t \left[\dfrac{1}{\kappa} ln(Ey^*) + P\right] + \dfrac{\rho c_\mu^{0.25} k_p^{0.5}}{2q'}\{Pr_t U_p^2 + (Pr - Pr_t)U_c^2\} & (y^* > y_T^*) \end{cases} \tag{3.38}$$

$$P = 9.24\left[\left(\frac{Pr}{Pr_t}\right)^{0.75} - 1\right]\left[1 + 0.28e^{\frac{-0.007\,Pr}{Pr_t}}\right] \tag{3.39}$$

Where c_p is the specific heat of fluid, q' is the wall heat flux, T_p is the temperature at point p, T_w is the wall temperature, Pr is the molecular Prandtl number, Pr_t is the turbulent Prandtl number (0.85 at the wall), and U_c is the mean velocity magnitude at $y^* = y_T^*$. y_T^* is also assumed equal to y^* computed from the intersection of the linear law (eq. 3.31) and logarithmic law (eq. 3.32). For a rough surface, the following equation (3.39) is modified as below:

$$P_{rough} = 3.15Pr^{0.695}\left(\frac{1}{E'}-\frac{1}{E}\right)^{0.359} + \left(\frac{E'}{E}\right)^{0.6} P \tag{3.40}$$

where E' is defined by $E' = E/f$.

3.3.6.3.2. Wall-enhanced Treatment

Wall-enhanced treatment is a combination of two-layer scheme and enhanced wall function in order to model both viscosity-affected and turbulence regions when the near-surface viscosity is important and computational cost is not high. The two-layer scheme calculate ε and the turbulent viscosity in the vicinity of wall cells. The enhance wall function links the above mentioned regions with a blending function Γ (Kader, 1981):

$$u^+ = e^\Gamma u_{lam}^+ + e^{\frac{1}{\Gamma}} u_{turb}^+ \tag{3.41}$$

$$\frac{\partial u^+}{\partial y^+} = e^\Gamma \frac{\partial u_{lam}^+}{\partial y^+} + e^{\frac{1}{\Gamma}} \frac{\partial u_{turb}^+}{\partial y^+} \tag{3.42}$$

$$y^+ = \frac{\rho u_* y}{\mu} \tag{3.43}$$

$$\Gamma = -\frac{a(y^+)^4}{1+by^+} \tag{3.44}$$

where u^+ denotes the mean velocity, u_* is the friction velocity, and $a = 0.01$ and $b = 5$. In the proposed model, acceptable y^+ lays below unity. Furthermore, turbulent and laminar velocities are given by (White and Christoph, 1971):

$$\frac{\partial u_{turb}^+}{\partial y^+} = \frac{1}{\kappa y^+}[S'(1 - \beta u^+ - \gamma(u^+)^2)]^{0.5} \tag{3.45}$$

$$\frac{\partial u_{lam}^+}{\partial y^+} = 1 + \alpha y^+ \tag{3.46}$$

$$S' = \begin{cases} 1 + \alpha y^+ & y^+ < y_s^+ \\ 1 + \alpha y_s^+ & y^+ \geq y_s^+ \end{cases} \tag{3.47}$$

where $y_s^+ = 60$. α represents the influence of pressure gradient while β, and γ represent thermal effect. The wall enhanced treatment for thermal effect is developed in a same manner as the velocity profile (Kader, 1981):

$$T^+ = \frac{\rho c_p C_\mu^{0.25} k^{0.5}(T_w - T_P)}{q'} = e^\Gamma T_{lam}^+ + e^{\frac{1}{\Gamma}} T_{turb}^+ \tag{3.48}$$

$$\Gamma = -\frac{a(\Pr y^+)^4}{1 + b(\Pr)^3 y^+} \tag{3.49}$$

$$T_{turb}^+ = \Pr_t\left\{u_{turb}^+ + P + \frac{\rho C_\mu^{0.25} k^{0.5}}{2q'}\left[u^{+2} - \left(\frac{\Pr}{\Pr_t} - 1\right)\left(u_c^+ C_\mu^{0.25} k^{0.5}\right)^2\right]\right\} \tag{3.50}$$

$$T_{lam}^+ = \Pr\left(u_{lam}^+ + \frac{\rho C_\mu^{0.25} k^{0.5} u^{+2}}{2q'}\right) \tag{3.51}$$

where u_c^+ is the same as value of u^+ at the intersection of laminar and turbulence region.

3.3.6.4. Top-canopy and Lateral Boundary Conditions

The integration of the surface layer with the atmospheric layer is an important parameter in selecting the suitable boundary conditions for top-canopy and lateral faces. Using

observational data over some section of the cities serves as the best option (Dudhia and Bresch, 2002). However, in the absence of the measurements, a nesting scheme can be used to provide an acceptable boundary condition through meso-scale models (Murakami, 2006; Sasaki et al., 2008; Yamada, 2004). In this case, unknown variables of the model at the lateral boundaries for the small area are interpolated from the corresponding computed values of meso-scale models.

If the height of the computational domain is higher than the height of the atmospheric boundary layer above an urban area (approximately 1-2 km above the ground surface.), it can be concluded that geostrophic wind serves as a good approximation. Therefore, turbulence, mean potential temperature, and water vapor mixing ratio can be set equal to constant values. Also, the free-slip condition can be used as top condition when the height of the domain is high enough to be assumed as a fully-developed situation (Cheng et al., 2008; Mirzaei and Haghighat, 2010b; Nazridoust and Ahmadi, 2006). In this case, the Neumann boundary condition can be also specified at the lateral boundaries. This indicates that there is no change in the physical variables of the horizontal directions at lateral boundaries and the selected domain is large enough to avoid any influence on the target building.

3.4. Model Validation

Prior to the final study of PCE, it is necessary to evaluate the performance of the CFD model based on obtained sizes for the study domain and mesh. Also, it is always necessary to validate the CFD model with at least one experimental benchmark. After reaching an acceptable discrepancy for the developed CFD model, simulation of the desired case is the next step. If the discrepancies of the results are not acceptable, more adjustments in the dimensions of the study domain, type and size of the meshes, or assigned boundary conditions are necessary.

3.4.1. Geometry Tests

Selecting the appropriate height, length, and width (see Figure 3.4; L_1 to L_5) results in more accurate prediction of the airflow pattern around the studied street canyon by the CFD model. Nonetheless, only few studies addressed specific protocols for these dimensions. For example, the distance of the studied building from lateral and outflow boundaries is respectively suggested to be 5H and 10H (Tominaga et al., 2008), while H is the height of the studied building. For top boundary, the required height should simulate the boundary layer height determined by the terrain category of the surroundings.

As discussed earlier, assigned boundary conditions are reasonable when fully-developed and zero-gradient conditions are vertically or horizontally satisfied. This implies that the effect of buildings and street canyons is negligible on the downstream/top-canopy airflow regime. Therefore, for each direction, several trial simulations with changing dimensions are required to minimize the interaction of buildings on airflow pattern.

3.4.2. Mesh Size Test

A mesh independency exam is a necessary test for CFD simulations. It is of utmost importance to show that the results are not a function of mesh size. Although applying finer mesh results in a lower discrepancy, it is not feasible to use an extremely fine mesh size due to the limitations of CPU and time cost. This means there is always a tradeoff between reducing the computational expenses and increasing the accuracy of the results (Hefny and Ooka, 2009). In building street canyon studies, however, it is important to choose appropriate mesh size in order to reproduce the separating flows near the roof and the walls. For this purpose, a minimum of 10 grids is recommended on each side of a target building (Tominaga et al., 2008).

3.5. Implemented PCE Index

In reality, prevailing wind exhibits stochastic behavior in magnitude and direction during the period of study. However, it is necessary to assume a limited velocity magnitude and direction for inflow boundary condition of the study domain in order to reduce the computational cost and the number of simulations. Evaluation of the PCE parameters (i.e. air velocity, air temperature, moisture, pollution concentration, and radiation) around the building is then feasible using the indices introduced in Appendix A through C.

3.6. Case study: Application of the PCE-algorithm

To demonstrate the performance of the proposed PCE-algorithm, a case study is introduced in this section. The purpose of this case study is to first evaluate PCE around an unconstructed array of buildings in Montreal. It then investigates the capability of passive and active strategies to enhance PCE. Thus, implementation of the PCE-algorithm is shown in three steps in the following section.

Montreal climate is classified as humid continental with muggy summers. The Montreal heat island is illustrated in Figure 3.5. This figure compares the last 40 years of mean temperature, mean minimum, and mean maximum temperature of two sites, one located

close to downtown and the other in a rural area. As depicted in Figure 3.6, an exponential

population growth is also monitored during these years. This implies that Montreal's heat

island intensity continues to grow and its side effects will impact PCE and energy

consumption in future years.
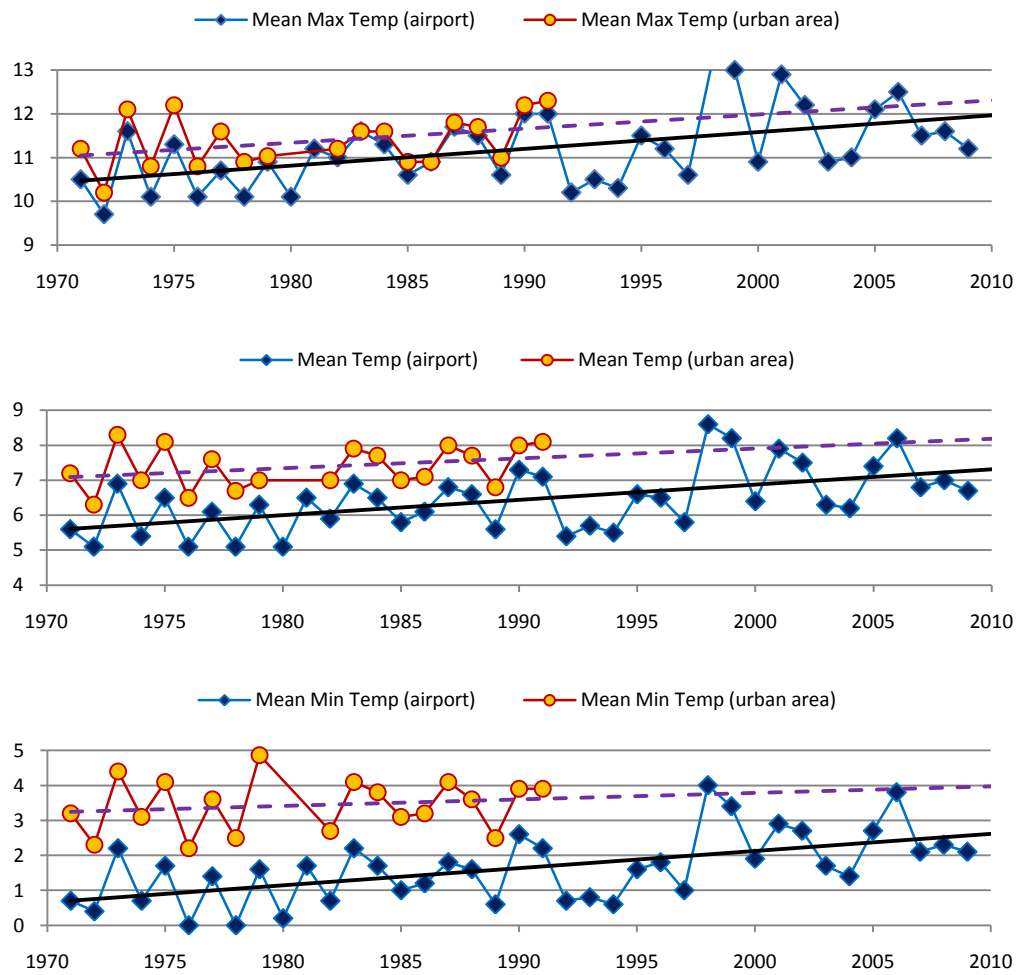
Figure 3.5 Comparison between mean maximum, mean, and mean minimum temperature $(°C)$ of urban and rural area of Montreal metropolitan
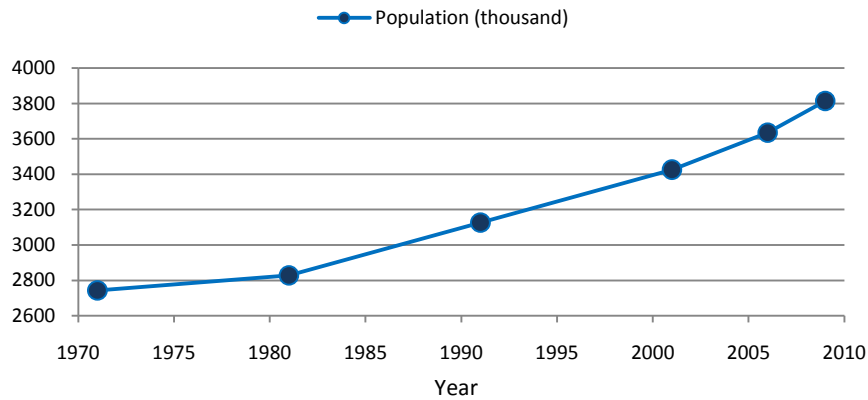
Figure 3.6 Population growth profile of Montreal metropolitan

3.6.1. Step 1-1: Collecting Street Canyon and Weather Data

The layout of a 3×3 array of homogeneous buildings (W=L=10m) is illustrated in Figure 3.7. The studied street canyon is also between marked buildings (A) and (B). The flexibility in design parameters of the street canyon is also presented in Table 3.2. Due to economical and architectural priorities, any kind of modification to the street canyon, shape of the buildings, or type of roof is not considered feasible. Thus, only albedo of the surface materials and aspect ratio of the street canyons can be varied as shown in Table 3.2. The building will also be in a commercial area without any vegetation (VR=0).

The Montreal heat island was intensified during a severe heat wave that occurred on August, 1 2006 (Environment-Canada, Date Accessed: November, 2010). According to Environment Canada, the temperature peaked at 5:00 PM reaching 306.6 (°K) which

hindered pedestrian activities. Therefore, this time episode is selected for the case study.

Weather data history is also depicted in Figure 3.8.

Prevailing Wind

A   B

H

L

W   W
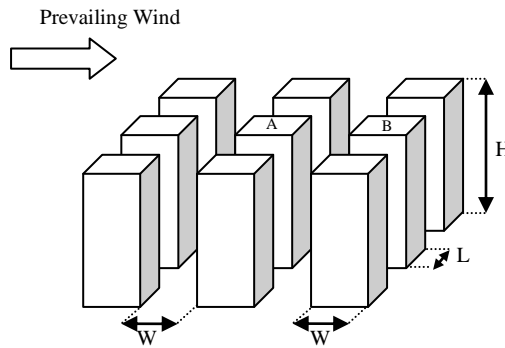
Figure 3.7 Layout of a 3×3 array of homogeneous buildings

Table 3.2 Street canyon characteristics

Buildings' Parameter	Flexibility
Street canyon orientation	No: north -south
Bulk-albedo of buildings' wall	Yes: $0.20 < \alpha < 0.40$
Bulk-albedo of buildings' roof	Yes: $0.20 < \alpha < 0.40$
Buildings aspect ratio	Yes: $1 < AR < 2$ (W=L=10m) (preference AR=2)
Building shape	No: Cuboid
Roof shape	No: Flat
Street canyon's parameter	**Flexibility**
Bulk-albedo of the asphlts	No: $\alpha = 0.10$
Bulk-albedo of the pavements	Yes: $0.20 < \alpha < 0.40$
Vegetation ratio	No: $VR = 0\%$

It can be concluded from Figure 3.8 that wind velocity is almost changing between

1(m/s) and 7(m/s). Moreover, the variation of wind angle is mostly between 0 (degrees)

and 90 (degrees). Thus, as discussed in section 3.5, the wind velocity magnitude is

interpolated into three velocities: 1, 3, and 7 m/s (Figure 3.10). As illustrated in Figure 3.8, wind directions are also approximated with three angles: 0, 45, and 90 degrees (Figure 3.10). Therefore, nine runs of simulation are necessary to show the stochastic airflow over the domain of study. A frequency of occurrence can be assigned to each prevailing wind in order to present its occurrence probability. Selected velocities clearly cover a wide range of airflow inside the pedestrian area from buoyancy-driven to fully-turbulent. Also, chosen angles represent different airflow directions from perpendicular to parallel. The accuracy of the proposed model will be improved by increasing the number of interpolated wind velocities and angles. However, this involves a considerable increase in the number of simulations.

3.6.2. Step 1-2: Simulation Setting

As mentioned earlier, validation of the proposed model and finding the appropriate geometry and mesh size for the study domain are the first steps. The procedure and results are shown in the next chapter. For the validation part, a steady scheme is used with the Realizable $k-\varepsilon$ model for turbulent closure. As shown below, an unsteady procedure with the Realizable $k-\varepsilon$ model has been conducted to show the performance of the PCE-algorithm:
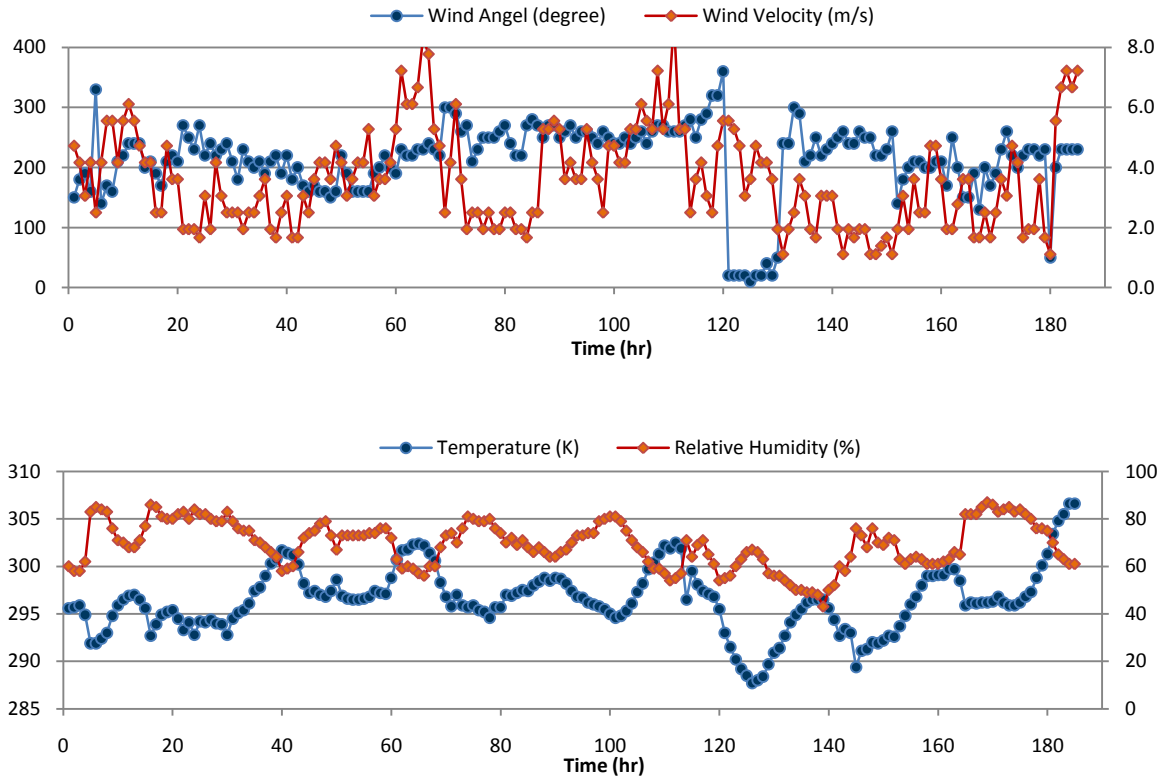
Figure 3.8 (Top) wind velocity (m/s) and direction (degree) - (Bottom) Temperature (°K) and relative humidity (%) for Montreal city from 25 July to 1 August 2006 (Environment Canada, 2006)

1. Domain creation: based on velocity directions (0, 45, and 90 degree), three domains are created and meshed as shown in Figure 3.9. Over one million meshes are generated for each domain.

2. Soil effect: seven days of unsteady pre-simulation (time-step=1 hour) without pollution release is applied to the domain of study. Radiation is also calculated by coupling the CFD and solar radiation model presented in section 3.3.5.

3. Velocity magnitude: one hour of unsteady simulation is performed to produce the prevailing wind (1, 3, and 7 m/s) over the studied street canyon (Figure 3.10).

4. Pollution release: 10-15 minutes of unsteady simulation (time-step=10 sec) is performed by releasing carbon-monoxide, the main pollutant emitted from vehicles, as a pollutant through the second street canyon beyond the inflow boundary (Figure 3.9). The exact time is selected based on reaching a consistent situation in carbon-monoxide concentration level within the sidewalks.

5. PVS effectiveness: unsteady simulation is again performed for 10 minutes after the release of the pollutant. Two PVSs are set on adjacent leeward and windward walls of the studied street canyon (Figure 3.9).

The boundary conditions, solution schemes, pollution release concentration, and soil properties are presented in Table 3.3. Also, second-order upwind is employed as discretization scheme for momentum to improve mass conservation. Residuals of less than 10^{-6} for energy, continuity and carbon-monoxide are applied as convergence criteria. This number was 10^{-4} for the remaining parameters. A SIMPLE algorithm is also performed as a numerical procedure to solve the NS equation.

Free slip wall Condition

Logarithmic Inflow

Outflow

6H

Studied street canyon

PVS

Wall

Ground

H

W

d=0.7H

2H

5H

4H

z

x

Left sidewalk

Right sidewalk
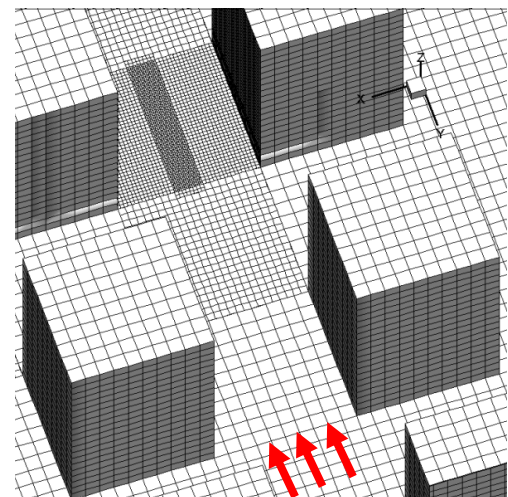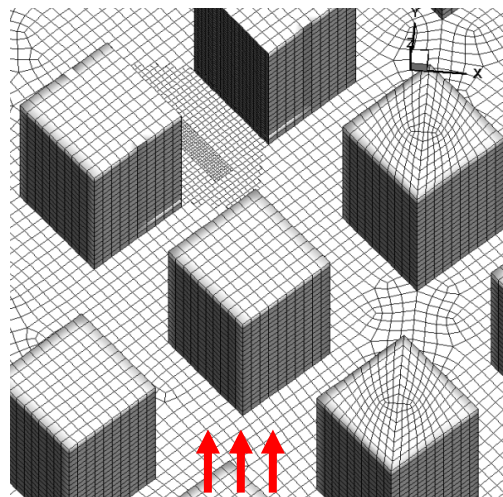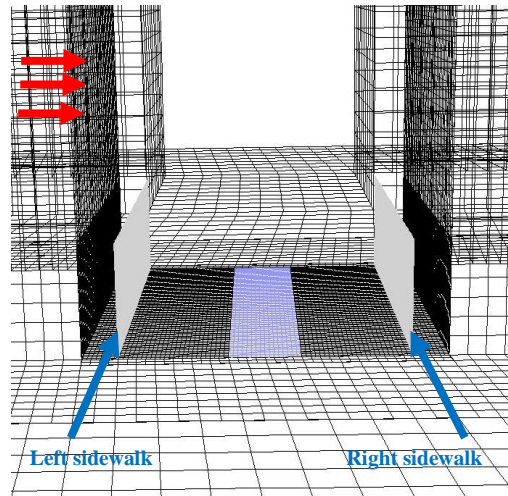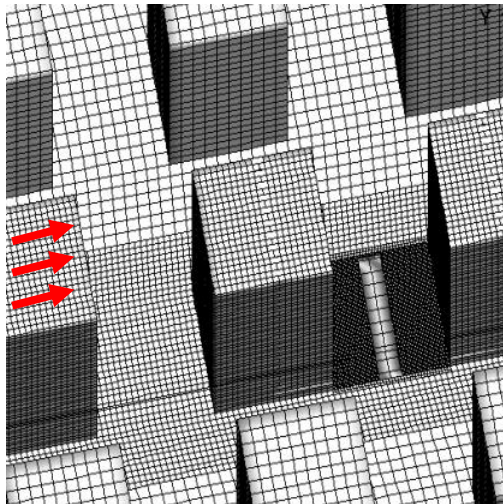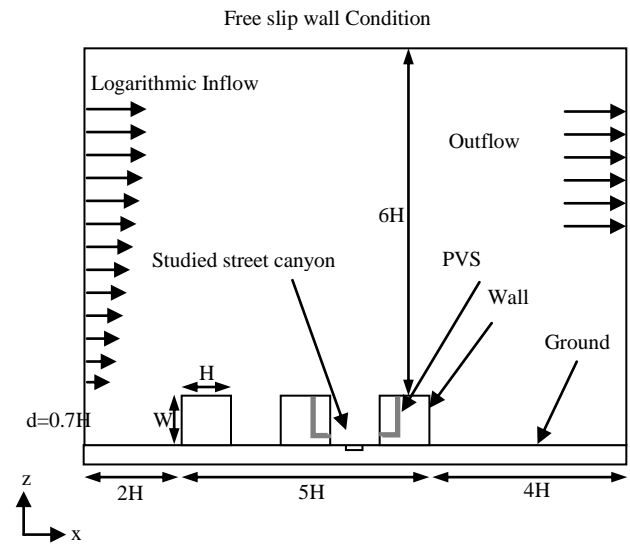
Figure 3.9 Simulation study domains (direction of prevailing wind is presented with red arrows)

Table 3.3 Boundary conditions, solution schemes, and model properties

Inflow boundary	Velocity: experimental logarithmic flow (Tominaga et al. 2008, Uehara et al., 2000) Temperature = constant Turbulent intensity = 10% Turbulent viscosity ratio = 10
Outflow boundary	Zero gradient assumption
Ground boundary	Logarithmic law with roughness length = 0.024 (m)
Top boundary	Free slip wall condition
Lateral boundary	Free slip wall condition
Walls and roof boundary	Logarithmic law for smooth wall
Bottom soil boundary	Constant temperature = 290 (K)
Lateral soil boundary	symmetry
Interior building boundary	Constant temperature = 298 (K)
Wall function condition	$30 < y^* < 300$
Enhanced wall treatment condition	$y^+ < 1$
Pollution mass fraction	0.01
Polltion release velocity	0.1 (m/s)
Pollution temperature:	Constant temperature = 310 (K)
Soil depth	5 (m)
Soil conductivity	Conductivity= 2 (W/mK) ,
Soil Cp	1840 (KJ/Kg K)
Soil density	2000 (Kg/m^3)
U value for roofs	0.1 (W/m^{2}K)
U value for walls	0.2 (W/m^{2}K)
Sunshine factor fo radiation model	0.5
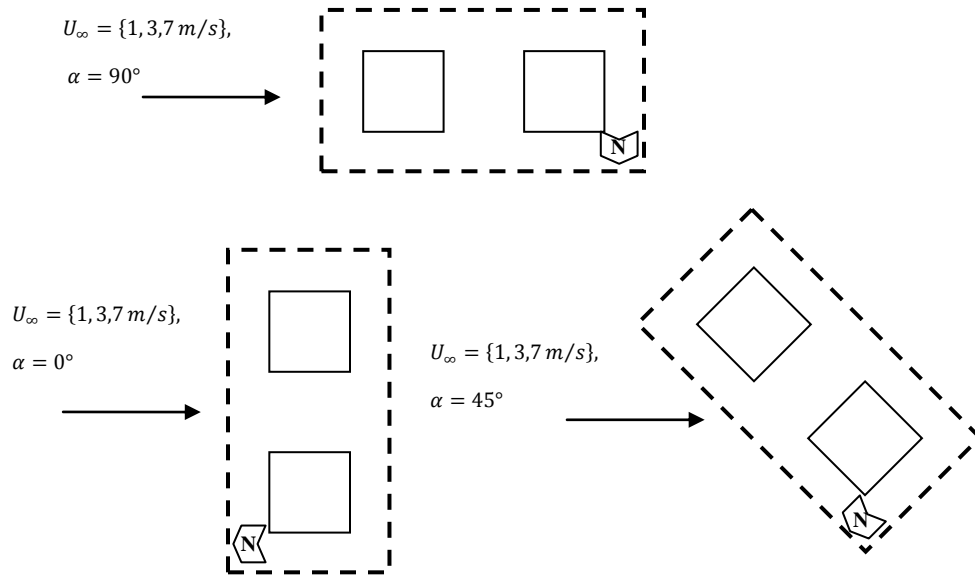
Figure 3.10 Top view of various wind velocities ($U_\infty = 1, 3, 7\ m/s$) and directions ($\alpha = 0, 45, 90\ °$) around the target street canyon (north -south)

3.6.3. Step 2: Defining Scenarios to Evaluate the Effect of Passive Strategies on

PCE

As discussed earlier, the aspect ratio, intersection of streets and stratification have significant impact on the streaming airflow through street canyons. Passive mitigation strategies are usually applied to adjust these parameters. In this study, the passive strategies, presented in table 2.1, are classified in two types: A and B. A-type strategies are related to modification of the buildings' design parameters. B-type strategies are attributed to techniques applied on the sidewalks and surface of the streets.

The PCE-algorithm, first investigates the possibility of changing the building design parameters in table 3.2. In this case study, aspect ratio and surface albedo of the buildings (A-type passive strategies) are the only parameters that can be modified under the restricted conditions. As illustrated in Table 3.4, the first three scenarios correspond to the variation of the aspect ratio (I and II) and the albedo of surfaces (II and III). Scenario IV (B-type passive strategy) is also defined to investigate the effect of higher-albedo pavement and road on PCE.

Table 3.4 Defined cases to evaluate the passive strategies on PCE

Passive Strategy	Scenario	Aspect ratio	Surface albedo	Street albedo
A-type	I	1	0.2	0.2
	II	2	0.2	0.2
	III	2	0.4	0.2
B-type	IV	2	0.2	0.4

The different surface temperatures of each building affect the airflow regime through street canyons. Alteration of the street material properties results in variation of its behavior in absorbing solar radiation and temperature. For example, studies show that a long street canyon one-circulation regime with AR=1 evolves into two counter-rotating

76

circulations (Mirzaei and Haghighat, 2010b) where the aspect ratio is two, as depicted in Figure 3.11. This means that the pollution dispersion correspondingly changes in magnitude and direction with the alteration of the aspect ratio.

Case I: Aspect Ratio = 1

Case II: Aspect Ratio = 2

Case III: Unstable Condition (Rb = -0.21)

Case IV: Stable Condition (Rb = 0.79)
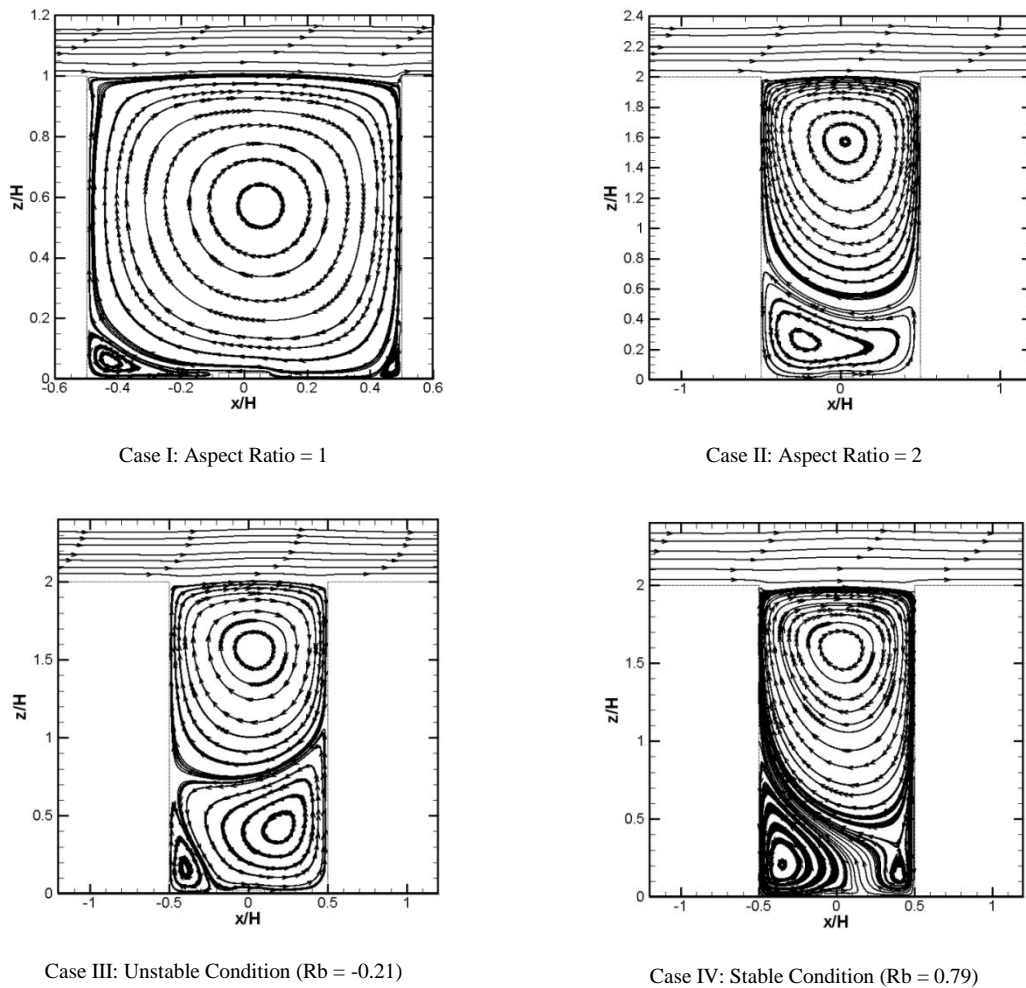
Figure 3.11 Streamline through street canyons with different characteristics

Also, it is evident that stratification drastically changes the velocity stream functions and pollution concentrations. Again, Figure 3.11 shows that the main circulation shrinks while the secondary circulation is enlarged when a street canyon is under unstable conditions (Rb=-0.21). This implies that buoyancy cooperates with the secondary circulations and empowers their rotation, which can consequently enhance the pollution removal from the pedestrian level. In a stable case of validation test (Rb=0.79), however, buoyancy opposes and shrinks the secondary circulation near the leeward sidewalk (Figure 3.11). In addition to the aspect ratio and stratification effect, the following section includes the effect of street intersections (3D effect) for building-scale scenarios of Table 3.4.

3.6.4. Step 3: Evaluating the Effect of the PVS on PCE

As demonstrated in Figure 3.3, four combinations of the PVS are eventually applied to an obtained scenario from step 2 in which PCE is not in an acceptable range. The final outcome of this step evaluates whether the active strategies are capable of enhancing PCE within the selected case study.

4. Chapter Four: Result and Discussion

4.1.   Domain Mesh and Geometry

In this study, the CFD model is simulated using FLUENT software (Fluent, 2008). The

corresponding meshes are also generated using a commercial package, GAMBIT

(GAMBIT, 2008). The CFD model was first validated with a dataset using wind tunnel

experiment in order to find the required dimension of Figure 3.4 (AIJ-case (C), Tominaga

et al. 2008). This test was conducted to an array of buildings with a similar arrangement

as Figure 3.7 (L=H=W=0.2m). Boundary conditions and solution schemes are presented

in Table 3.3. In the wind tunnel experiment, the wind velocity was measured at 63 points

located 2mm above the ground surface (Figure 4.1).
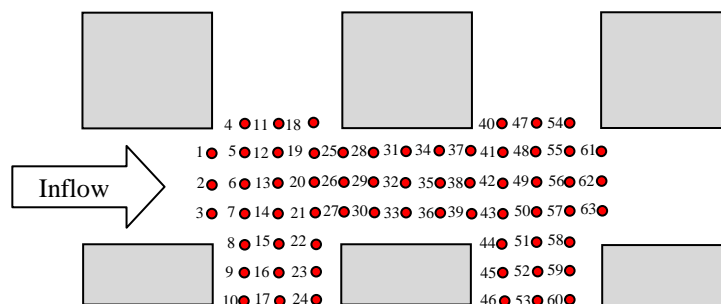
Figure 4.1 Half-domain measured points located 2mm above the ground (Top view)
(Tominaga et al. 2008)

Different mesh sizes were tested to find the proper dimension to simulate the study domain. These included 0.2H, 0.25H, and 0.3H. The result clearly demonstrates that the 0.25H mesh size is sufficient (less than 15% discrepancy) to model the case study (Figure 4.2). The reason that 0.2H mesh size is not better than 0.25H is related to the wall-function assumption (Launder and Spalding, 1974) which is discussed in previous chapter.
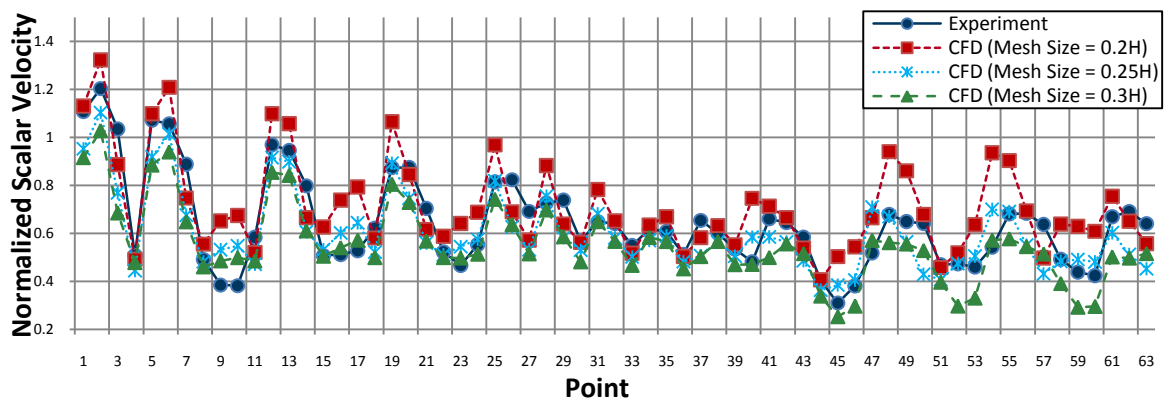
Figure 4.2 Comparison between measurement and CFD with different mesh size

It is also possible to conduct enhanced wall-treatment when more accuracy near ground is required: this drastically increases the computational cost. For example, less than 10% accuracy is obtained for the study domain generating about 10 times more meshes. The

effect of this limitation is reduced in PCE-algorithm simulations by refining meshes inside the studied street canyon. It should be noted that PCE-algorithm simulations are performed in real-scale (L=H=W=10m) unlike the mesh size test (L=H=W=0.2m) in which measurements are taken close to the viscous region (2mm above ground). Therefore, using the wall function with adapting meshes within the street canyon does not significantly affect the pedestrian region. This technique is demonstrated in Figures 3.9 and 4.9.

As illustrated in Figure 4.3, three cases were compared with fetch sizes (L_2) of 2H, 4H, and 10H. It is obvious from this figure that the results do not change significantly when the fetch length is increased more than 4H.
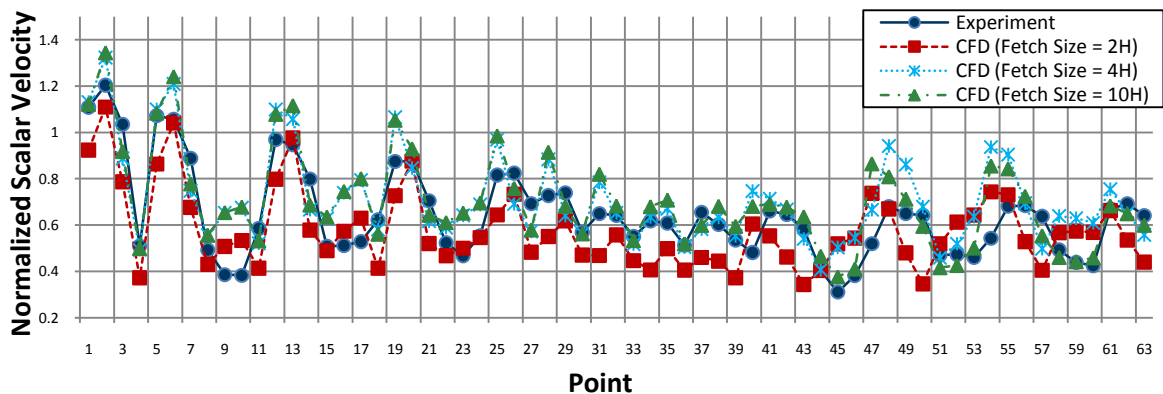
Figure 4.3 Comparison between measurement and CFD with different domain fetch

Also, as demonstrated in Figure 4.4, a height (L_5) of 5H provides almost the same result as the case where the height is 6H (wind tunnel height). This conclusion is corroborated by Tominaga et al. (2005): they suggested a vertical domain height of 3H or more. This conclusion is valid when thermal stratification does not exist. For simulation of thermal stratification, nonetheless, it is better to elevate the height to a suitable size.
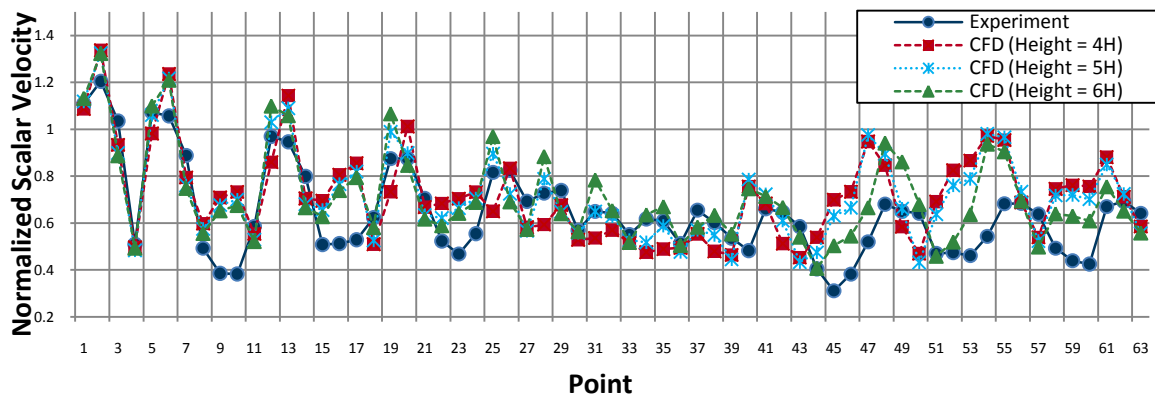
Figure 4.4 Comparison between measurement and CFD with different domain height

It was observed that the defined case study in section 3.6 is not significantly sensitive to L_1, L_3, and L_4. These parameters were set to 2H, 2H, and 2H, respectively. From results shown in Figures 4.2 through 4.4, it can be also concluded that a domain with a fetch size of (L_2) 4H, a height (L_5) of 5H, and a mesh size of 0.25H may reduce the computational

cost of the simulation. Therefore, the case (C) was again simulated with the obtained

mesh and length sizes (around 150,000 meshes in total). As shown in Figure 4.5, air

velocities are within an acceptable range and they are in fair agreements with those

obtained from wind tunnel measurements.
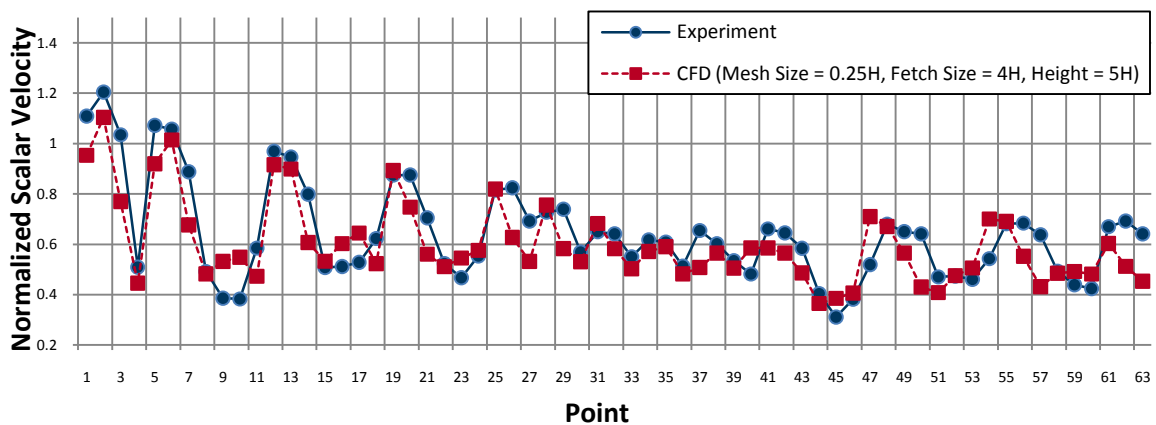
Figure 4.5 Comparison between measurement and CFD with suggested mesh size,
domain height and fetch length

4.2.   Validation of Velocity Field and Temperature Stratification

To show the thermal stratification within the street canyon, the simulation is validated

with the thermal wind tunnel experiment conducted by Uehara et al. (2000). The test was

performed at the National Institute for Environmental Studies of Japan (Ogawa et al.,

1981). Around three meters of homogeneous buildings consisted of 10mm cubes (H=W=L=100mm) placed 10mm and 5mm apart along the length and width of the tunnel, respectively. The quantities were measured in the street between the fifth and sixth rows of buildings. The turbulence was also modeled with a nine meters array of Styrofoam cuboids (2H=W=L=100mm). Furthermore, stratification was produced by changing the ground and air inflow temperature similar to Table 4.1.

First, it is necessary to mention that the airflow characteristics were represented by Reynolds ($Re_H = UH/\nu$) and bulk-Richardson ($Rb = gH(T_H - T_f)/(T_m U_H^2)$) numbers. Where U (m/s) is the upstream velocity at 7H, T_H (K) is the temperature at the top of the street canyon, T_f (K) is the ground temperature, T_m (K) is the mean air temperature, and U_H (m/s) is the mean wind speed at the top of the street canyon.

Table 4.1 Proposed case studies based on thermal wind tunnel experiment (Uehara et al., 2000)

Stability Condition	Bulk-Richardson Number	T_a = Inflow Temp. (K)	T_f = Ground Temp. (K)
Stable	0.89	351	294
Unstable	-0.18	293	352

The buildings were simulated together with a 3×3 array of buildings (H=W=L=100mm) similar to Figure 3.9. The ground and air temperature were also set in order to attain a

Bulk-Richardson number of -0.21 and 0.79 for unstable and stable stratification, respectively. These numbers are very close to the wind tunnel experiment situation (see Table 4.1).

Fetch length, height, and mesh size of the domain were chosen as 4H, 7H and 0.25H respectively, based on the test in the last section. Figure 4.6 illustrates generated meshes (around 150,000) for half of the domain due to the symmetry of this study.
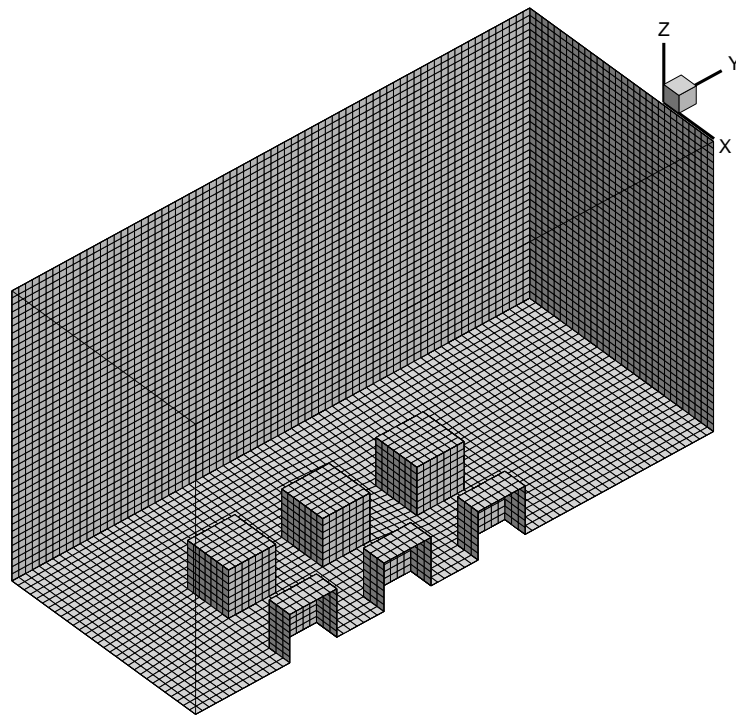
Figure 4.6 Domain and mesh size: fetch = 4H, height = 7H, mesh size = 0.25H
(H=W=L=100mm)

Figure 4.7 demonstrates that there is a good agreement between the model predictions and the experimental data except for minor discrepancies near the top-canyon surface

(z/H=1). This difference is mainly related to the weakness of the $k - \varepsilon$ turbulent model in capturing the airflow regime at the roof level (Tominaga et al., 2008). Here U_{700} is attributed to air velocity at a height of 0.7m from bottom of the target street canyon in the wind tunnel experiment.
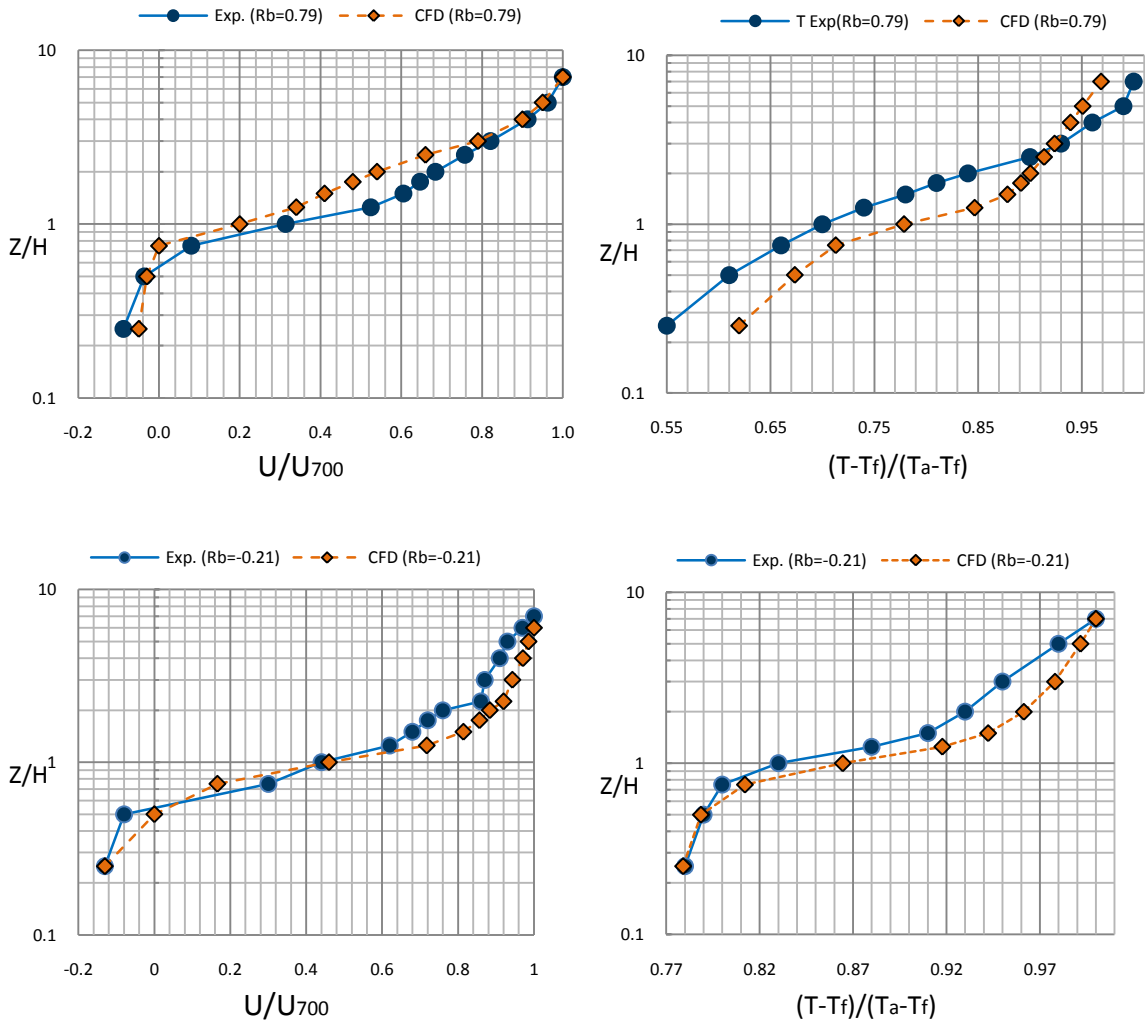
Figure 4.7 Comparison between measurement and CFD (Left) Velocity (Right) Temperature

4.3.   Validation of Pollution Dispersion

Another set of experimental data by Meroney et al., 1996 is used to validate pollution dispersion within street canyons. This test was carried out under isothermal conditions for an array of buildings (H=W= 60mm) with L/H>7. This implies that the street canyon was long enough to assume the geometry of a two-dimensional problem (see section 2.4).

Meroney et al. (1996) used two dimensionless numbers Re and $K = cULH/Q_{ethane}$ to characterize pollution dispersion. Where c is the ethane tracer concentration (in the range [0,1]), U is the inflow air velocity at 0.5m above the floor (5m/s), L is the line source length (0.9 m), and Q_{ethane} is the source strength when ethane was selected as the pollutant with a mass fraction of about 0.01 ($Q_{ethane} = 2.6 \times 10^{-7} \, m^3/s$ and $Q_{air} = 2.6 \times 10^{-5} \, m^3/s$). Here, again the arrangement of the array of buildings is created similar to the one in Figure 3.9. In order to obtain similarity within the Meroney et al. (1996) experiment (H=W=60mm) and study domain (H=W=100mm), the dimensionless numbers should be kept equal:

$Re_{H=60mm}$ (Meroney et al. 1996) $= Re_{H=100mm}$ (simulation domain)

$$\Rightarrow U_{Similation} = \frac{U_{Meroney} \; H_{Meroney}}{H_{Simulation}} \qquad (4.1)$$
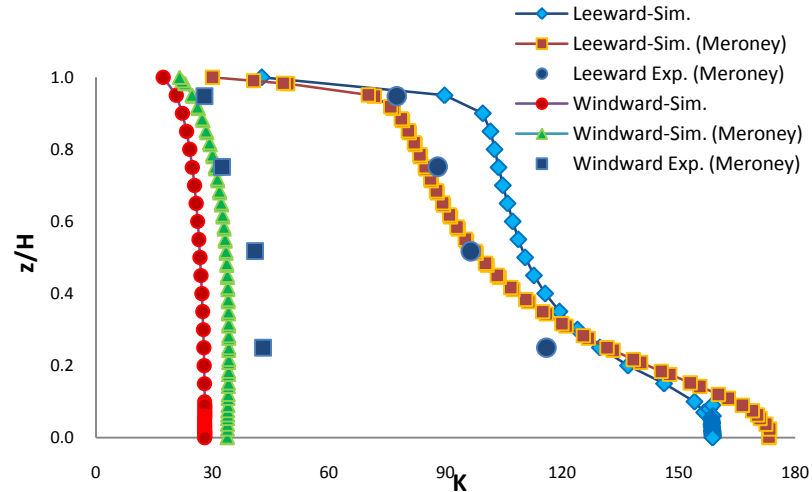
Figure 4.8 Comparison between Meroney et al. (1996) experiment case (H=W=60mm)
and simulation (H=W=100mm) domain size

Also, it can be concluded that K (Meroney et al., 1996) = K (simulation domain) will be

satisfied by preserving $Q_{Simulation} = Q_{Meroney}$. The pollution dispersion validation

adapted to the study domain is shown in Figure 4.8. An acceptable agreement is again

observed between the simulation results and the empirical results. Thus, it is evident that

the model can be validated using defined domain dimensions and boundary conditions.

This Figure also shows simulation results for the exact Meroney et al. (1996) test case

where U and H are 5m/s and 60mm, respectively.
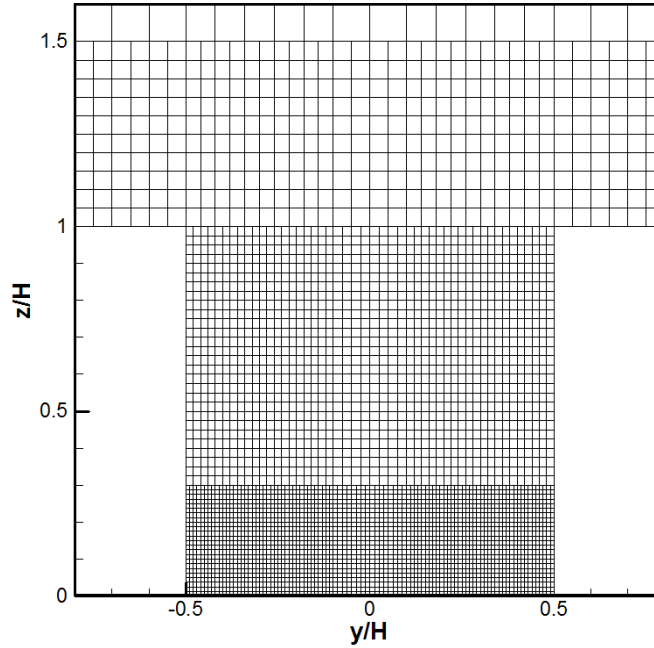
Figure 4.9 Structural meshes for pollution dispersion validation simulation domain

Since concentration of ethane compared to the air has a small magnitude and the proper mesh size is required to find its distribution inside the street canyon, another test has been performed to examine mass of ethane. In this test, the mesh size of the target street canyon is refined while the following equation is satisfied:

$$\frac{\dot{Q}_{top-canopy} + \dot{Q}_{PVS}}{\dot{Q}_{source}} = \frac{\dot{Q}_{outflow}}{\dot{Q}_{source}} = 1 \tag{4.2}$$

where $\dot{Q}_i$ (i= source, top-canopy surface, PVS and outflow) is the mass flow rate of ethane through different surfaces.

As depicted in Figure 4.9, meshes are refined until reaching less than 10 percent discrepancy in equation 4.2 (Cheng et al., 2008). It is noteworthy to mention that $\dot{Q}_{PVS}$ is zero when the PVS is not working.

4.4. Effect of Aspect Ratio on PCE

Most of the previous studies has been applied to long street canyons (L/H>7). This means that the studies were mostly limited to a 2-dimensional geometry. Thus, in addition to study the effect of aspect ratio, performing 3-dimensional CFD simulation includes the effect of streets' intersection in the short street canyons (L/H<3). Tables D.1 through D.4, present the results for mean air velocity, temperature, relative humidity, and pollution concentration inside the pedestrian plane which is defined as a three-meter height plane with one meter distance from the wall of the sidewalks. As demonstrated in Figure 3.9, L-S and R-S stands for left-sidewalk and right-sidewalk, respectively. The results are obtained after running nine sets of simulations for each scenario given in Table 3.4. It is worth again to be noted that the conclusions of this section cannot be expanded to all street canyons. This means that the results are unique to this specific case study. This is mainly due to the difference in heat fluxes (i.e. radiation, latent, sensible, advection, anthropogenic, storage, and conduction) presented in equations 2.1 and 2.2. The proposed

3-dimensional model in previous chapter helps to include the effect of these heat fluxes. For example, pre-simulation of soil and wall temperatures results in a non-uniform distribution over these surfaces. This provides more realistic heat fluxes for each surface to study PCE within street canyons.

Extracted from Figure 3.6, the frequency of occurrence for each prevailing wind magnitude and direction is demonstrated in Tables D.1 through D.4. For example, frequency of occurrence is 21% when wind angle and magnitude are 45 (degree) and 3 (m/s), respectively. Figures 4.10 through 4.12 show the frequency of occurrence summation (average on left and right sidewalks) for three indices calculated from Tables D.1 through D.4, including air quality (Appendix C.2), temperature-humidity (Appendix A.3), and wind comfort (Appendix B). In this study, AQI (for CO concentration) includes good-moderate (PPM<9.4), unhealthy-very unhealthy (9.5<PPM<30.4), and hazardous (30.5<PPM) situations. Moreover, THI contains warm range (22°C - 27°C) and very warm range (27°C - 32°C). Furthermore, WCI includes calm, light-air, and light-breeze conditions (Table B.1).

Figure 4.10 depicts when the aspect ratio changes, the AQI frequency of occurrence summation is almost the same for good-moderate situation. For example, the summation

of frequency of occurrence for 1m/s - 45degree (7%), 3m/s - 45degree (21%), 3m/s - 0degree (17%), and 7m/s - 0degree (17%) prevailing winds is 62% when aspect ratio is one (Table D.1). However, this implies that the increase in aspect ratio from AR=1 (case I) to AR=2 (case II) results in the AQI frequency of occurrence summation for unhealthy-very unhealthy situation being lower about 17%. As a result, almost the same percentage is elevated in hazardous situation when aspect ratio is increased form AR=1 to AR=2.
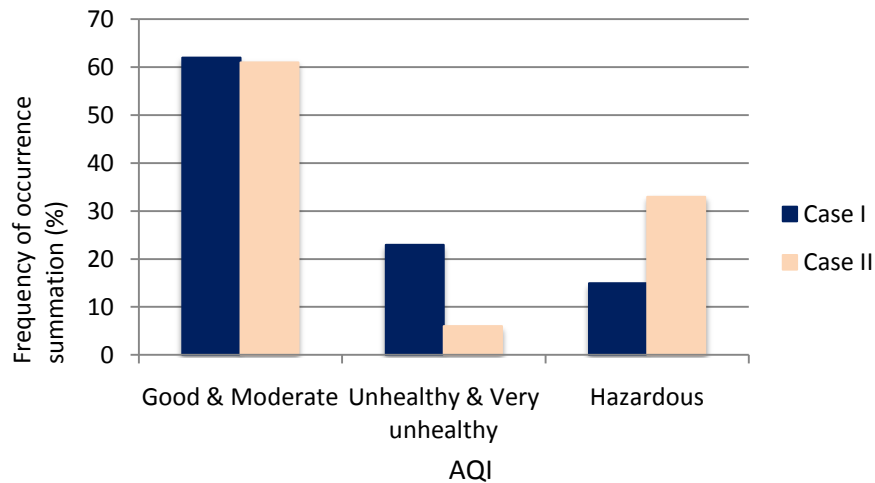
Figure 4.10 Air quality index (AQI) frequency of occurrence summation for AR=1 (case I) and AR=2 (case II)

As illustrated in Figure 4.11, for THIs of 27 and 28 (°C) both cases have approximately same frequency of occurrence summation. THI frequency of occurrence summation tends to be reduced about 20% from 30 (°C) to 29 (°C) when AR decreases from two to one. All THIs, nonetheless, lay in very warm range (27°C - 32°C) in which fatigue is possible for prolonged exposure (Steadman, 1979).
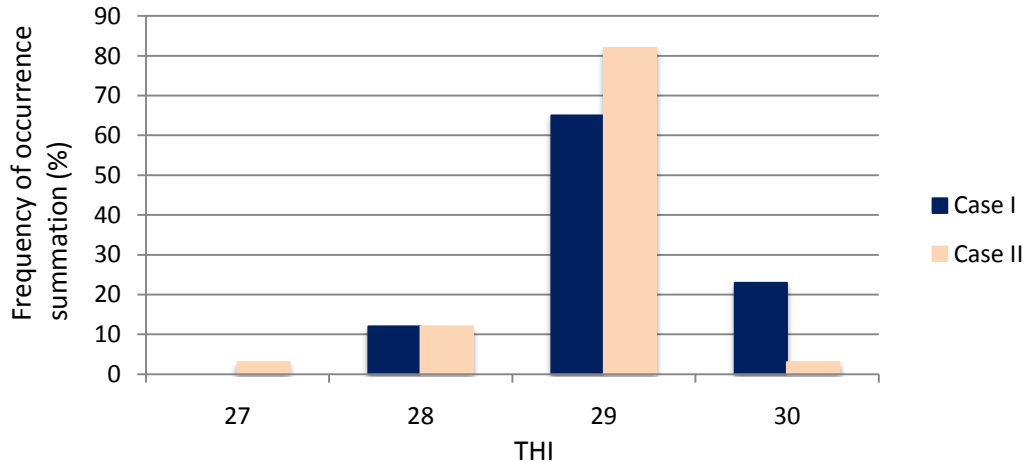
Figure 4.11 Temperature-humidity index (THI) frequency of occurrence summation for AR=1 (case I) and AR=2 (case II)

Furthermore, Figure 4.12 shows that increasing aspect ratio slightly decreases WCI inside the pedestrian plane. WCI frequency of occurrence summation for the calm condition is elevated 10% in AR=2 where the light-air condition is also reduced by the same amount. The light breeze frequency of occurrence summation has almost the same number in both aspect ratios (20%).
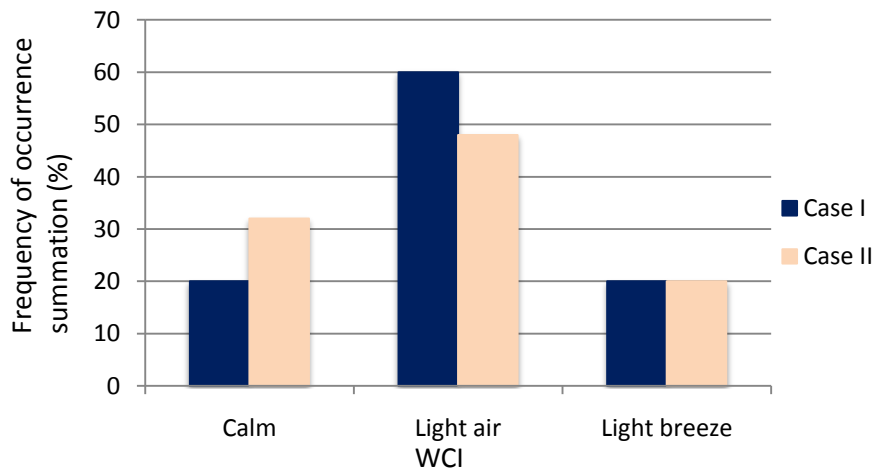
Figure 4.12 Wind comfort index (WCI) frequency of occurrence summation for AR=1 (case I) and AR=2 (case II)

Table 4.2 compares the acceptable range of three mentioned indices for various scenarios

of Table 3.4. In this study, the acceptable THI, WCI, and AQI are respectively defined

below 27 (°C), good-moderate situation, and above calm condition.

Table 4.2 Frequency of occurrence summation (%) for acceptable THI, WCI, and AQI in different scenarios

Scenario	I	II	III	IV
THI	0	0	0	0
WCI	20	20	3	3
AQI	62	61	49	34

It can be concluded that alteration of the aspect ratio from AR=1 (case I) to AR=2 (case

II) does not significantly contribute to a change in the frequency of occurrence

summation for the acceptable THI (0%), WCI (0%), and AQI (1%). In this study,

therefore, the aspect ratio is assumed to be selected AR=2 due to the economic benefit of

having more stories for the studied building.

4.5.   Effect of Thermal Stability on PCE

It is proven that the thermal stability plays a significant role in pollution dispersion. This

is mostly due to creation, weakening, or strengthening of small/large circulations within

street canyons. In most of the earlier investigations, uniform temperatures were usually

assigned to the walls and ground. However, the temperature of surfaces within a 3-

dimensional and real-size street canyon varies predominantly due to their variable

thermal storage and solar radiation absorption properties. Therefore, it is more realistic to

characterize airflow pattern based on the real distribution of temperature rather than using

a uniform temperature for each wall. Capturing temperature variation was one of the

advantages of the proposed simulation procedure that can be achieved by coupling

presented radiation and heat storage models in preceding chapter. Figure 4.13 shows non-

uniform contours of temperature for surfaces of the street canyon, including walls, roof,

street, and soil.

walls and roof   ground and soil
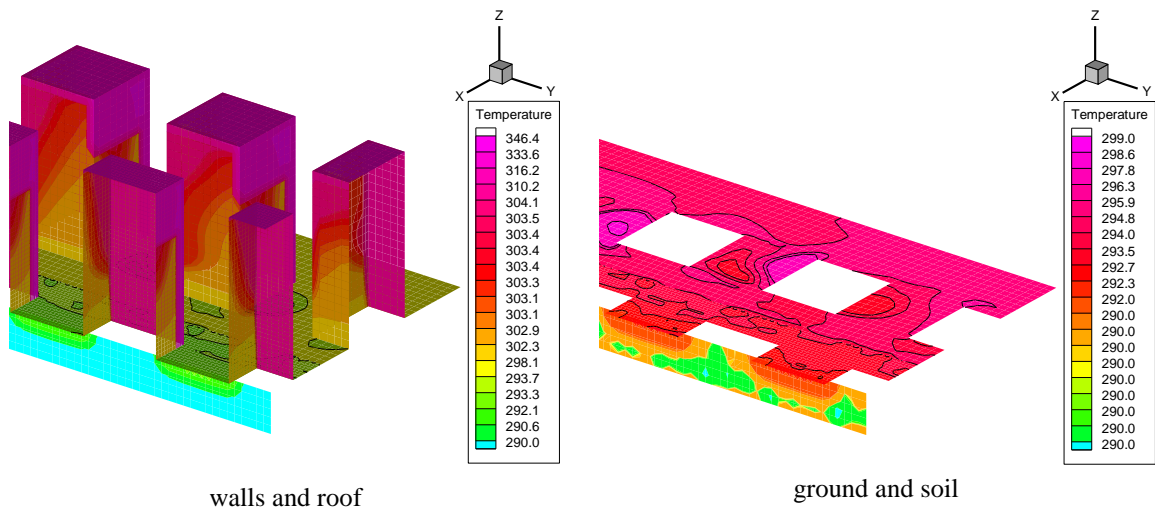
Figure 4.13 Non-uniform contours of temperature for surfaces of the studied street
canyons

The effect of changing walls and street albedo is investigated in the following sections.

The required data to calculate the PCE indices through the pedestrian plane is also

exhibited in Tables D.3 and D.4.

4.5.1. The Surface of Buildings

As previously stated, the passive strategies do not necessarily enhance PCE in studied street canyon (Table 4.2). This point is again confirmed in Figures 4.14 through 4.16 after applying higher-albedo material (an A-type passive strategy: scenario III) for the surface of building.

As depicted in Figure 4.14, the frequency of occurrence summation for the AQI in good-moderate and hazardous situations are respectively reduced about 13% and 9% in scenario III compared to scenario II. This means that the probability of having an unhealthy-very unhealthy situation is correspondingly increased by about 21%.
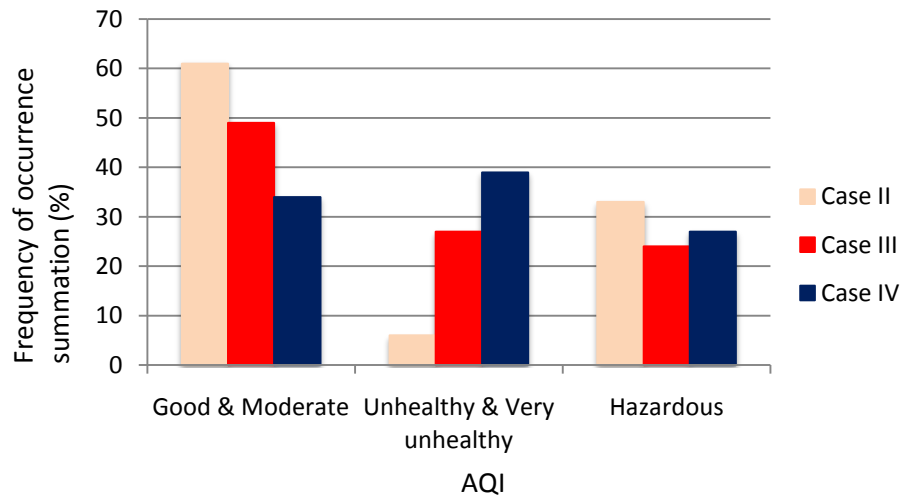
Figure 4.14 Air quality index (AQI) frequency of occurrence summation for AR=2 (case II) changing albedo of buildings' surface (case III) and changing albedo of road and pavement (case IV)

Again, there is not a considerable change in THI frequency of occurrence summation (Figure 4.15), as all numbers are within a very warm range (27°C - 32°C). This implies that the frequency of occurrence summations for 27 (°C), 28 (°C), 29 (°C), and 30 (°C) are 10%, 17%, 58%, and 15%, respectively.
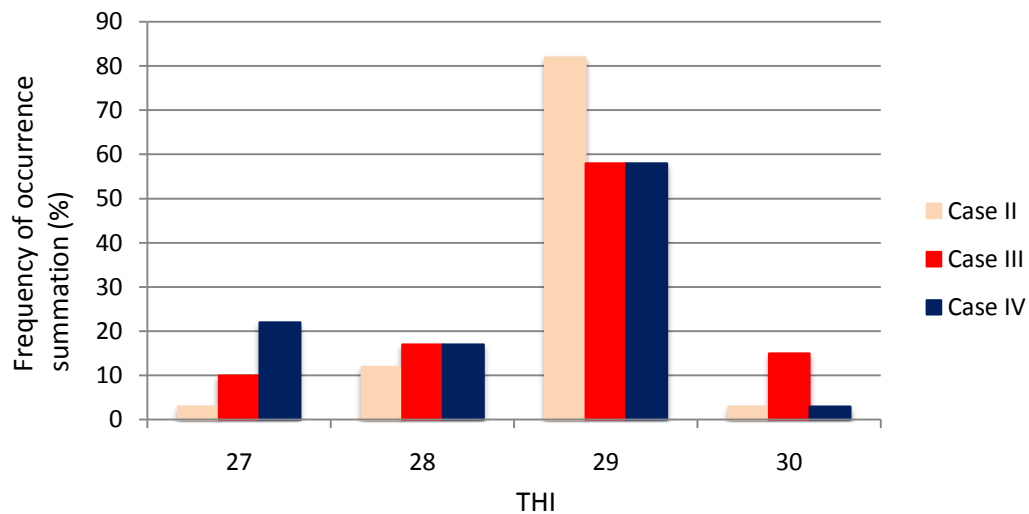
Figure 4.15 Temperature-humidity index (THI) frequency of occurrence summation for AR=2 (case II) albedo of buildings' surface (case III) and changing albedo of road and pavement (case IV)

As illustrated in Figure 4.16, WCI frequency of occurrence summation during calm and light-breeze conditions is furthermore reduced by about 12% and 17%, respectively. This means that the light-air condition is increased by about 29% when higher-albedo material is used for the surface of building.
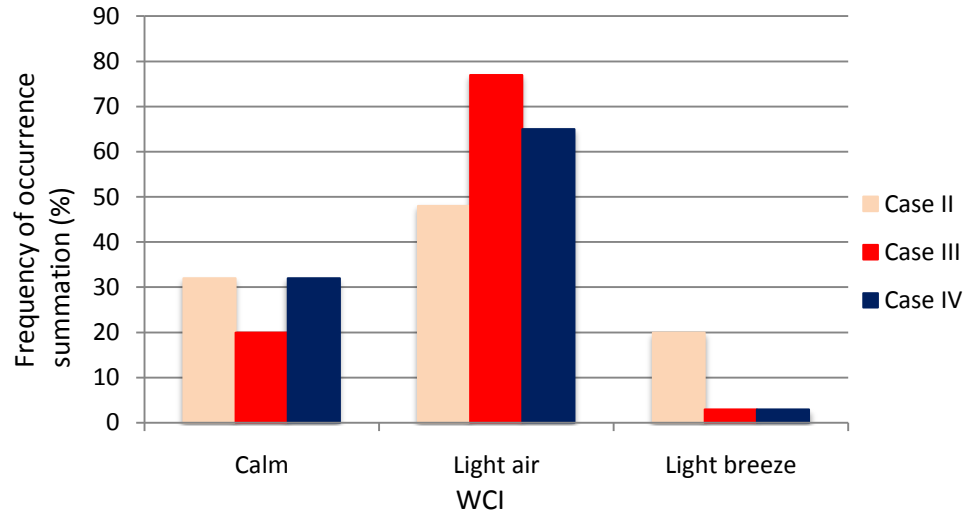
Figure 4.16 Wind comfort index (WCI) frequency of occurrence summation for AR=2 (case II) changing albedo of buildings' surface (case III) and changing albedo of road and pavement (case IV)

According to Table 4.2, the acceptable AQI and WCI are decreased by 12% and 17%, respectively. Acceptable THI also remains 0% for this scenario. The results of these indices, therefore, confirm that PCE of the studied street canyon is not improved and even worse by using more expensive higher-albedo materials for the exterior surface of buildings. In other words, since non-uniform distribution of walls and ground temperatures produces complex small and large circulations inside street canyons, the impacted circulations by changing surface materials may inversely affect PCE. Obviously, the influence of these circulations is more dominant on PCE when prevailing wind is relatively low.

4.5.2. Pavements and Roads

Alteration of pavement and road albedo from 0.2 to 0.4 with the replacement of these materials is classified as B-type passive strategies to enhance PCE (Table 3.4). Similar to the previous section, a considerable improvement in PCE is not achieved.

As shown in Figure 4.14, the AQI frequency of occurrence summation for the scenario IV for the good-moderate situation is in the lowest number (34%) compared to other scenarios. Also, the frequency of occurrence summation for the unhealthy-very unhealthy situation is decreased by 6% compared to the case of using ordinary construction material for the pavements and roads.

THIs are still within a very warm range (27°C - 32°C), even though the probability of having THI = 30 (°C) is reduced by 12% compared to case III, and THI = 27 (°C) is also increased by the same percentage (Figure 4.15).

Moreover, WCI in scenario IV for light breeze condition is similar to the scenario III (3%). In this case, however, calm condition is increased by about 12% compared to the scenario III. The summary of the scenario IV is again presented in Table 4.2. Thus, it is

not reasonable to apply B-type strategy for the defined case study in Montreal since acceptable AQI and WCI are reduced by 27% and 17% compared to case II, respectively.

4.6. Pollution Dispersion

Air quality index and pollution dispersion are two different concepts. AQI explains the effect of pollution on pedestrians walking through the target street canyon during a specific time. Released pollution within a street canyon, however, can be dispersed throughout the neighboring canyons. It is important, therefore, to investigate the effect of passive strategies on pollution dispersion.

Horizontal and vertical dispersion of the pollutant from the studied street canyon to neighboring canyons are shown in Figures 4.18 through 4.23. The pollutant concentration is normalized by concentration level at the released point (Figure 3.9).

4.6.1. Perpendicular Flow

When prevailing wind is perpendicular to the street canyon (frequency of occurrence summation is 18%) with AR=1, the one-circulation skimming flow forces the pollutant towards the leeward wall (Figure 4.18). As a result, normalized concentration near the leeward wall is considerably (about 4 to 5 times) higher than that of the windward

sidewalk. Increase in the prevailing wind velocity, nonetheless, significantly decreases concentration within the street canyon, and weakens the effect of thermal stability on airflow pattern.

As demonstrated in Figure 4.17a, when prevailing wind is increased (the higher Reynolds number), the stratification is weakened (the closer Bulk-Richardson number to zero). In other words, the effect of buoyancy forces is not significant when the effect of inertial forces is dominant. This causes a more symmetric dispersion for higher velocities. This is almost a valid rule for both aspect ratios (AR=1 and AR=2), and all wind velocities and directions. For example, the pollutant is more dispersed from left lateral surface compared to right one when U is 1 m/s (Figure 4.18a). However, it is equally dispersed from both lateral surfaces when U is 7 m/s (Figure 4.18c).

When the aspect ratio is two, a secondary weak circulation appears beneath the primary one which is near the top-canyon surface. The shape of the secondary circulation is highly sensitive to thermal stability. It is also much weaker than primary circulation and does not have considerable impact on the pollution dispersion at the pedestrian level. Therefore, as illustrated in Figure 4.19, the vertical distribution of pollution concentration is identical in both sidewalks.
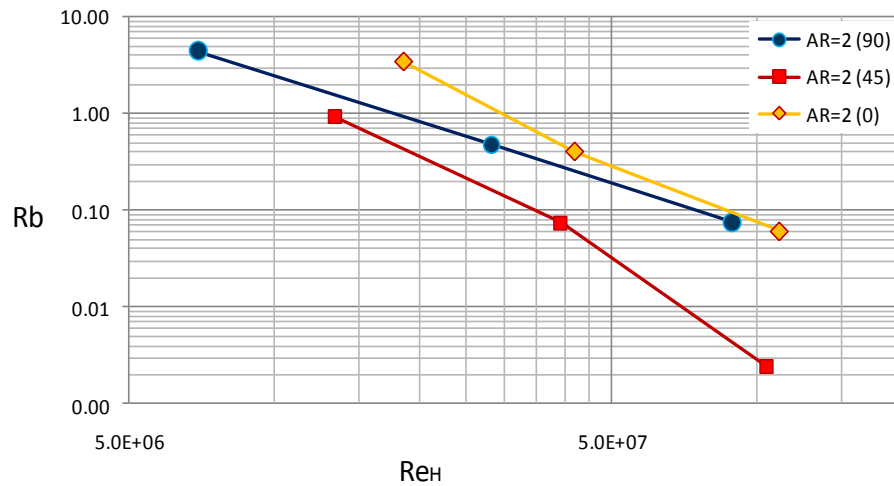
(a)
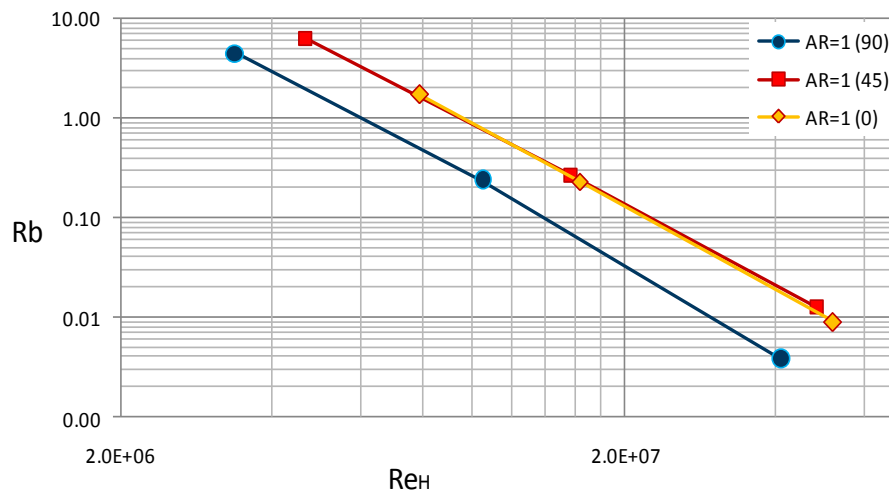
(b)

Figure 4.17 Bulk-Richardson number versus Reynolds number

Again, as shown in Figure 4.17b, higher velocity suppresses the effect of thermal stability, and produces more symmetric dispersions (e.g. Figure 4.19b: U = 3 m/s). Moreover, it results in a drastic decrease in overall concentration within the street canyon. The normalized concentration is between 20% and 50% when U = 1 m/s (Figure 4.19a), which is dropped to less than 1% when U is 7m/s (Figure 4.19c).
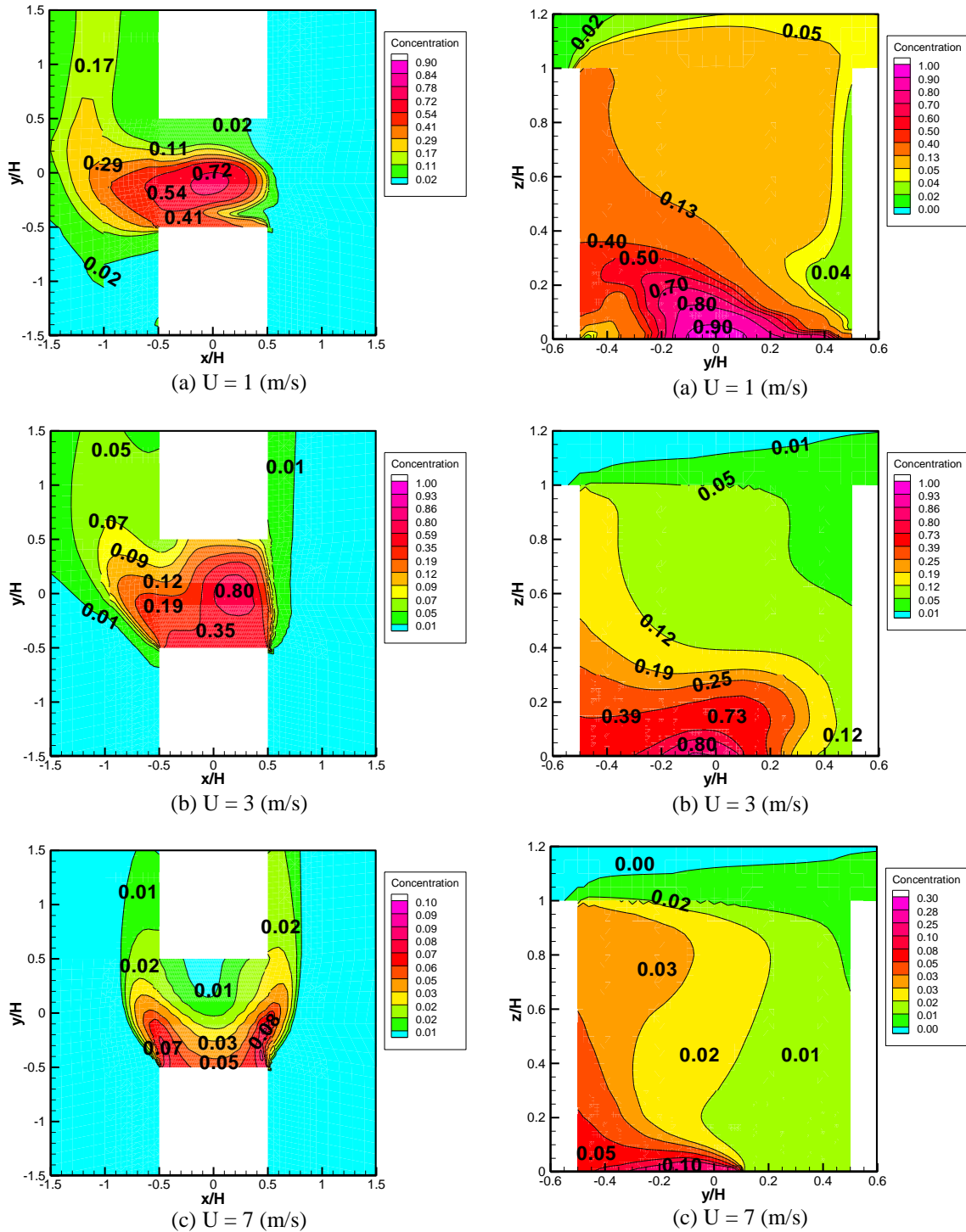
Figure 4.18 Normalized pollution concentration: wind direction = 90 (degree) and AR = 1 (Left) Horizontal section 1.5 above the ground (Right) Vertical section in middle of the studied street canyon
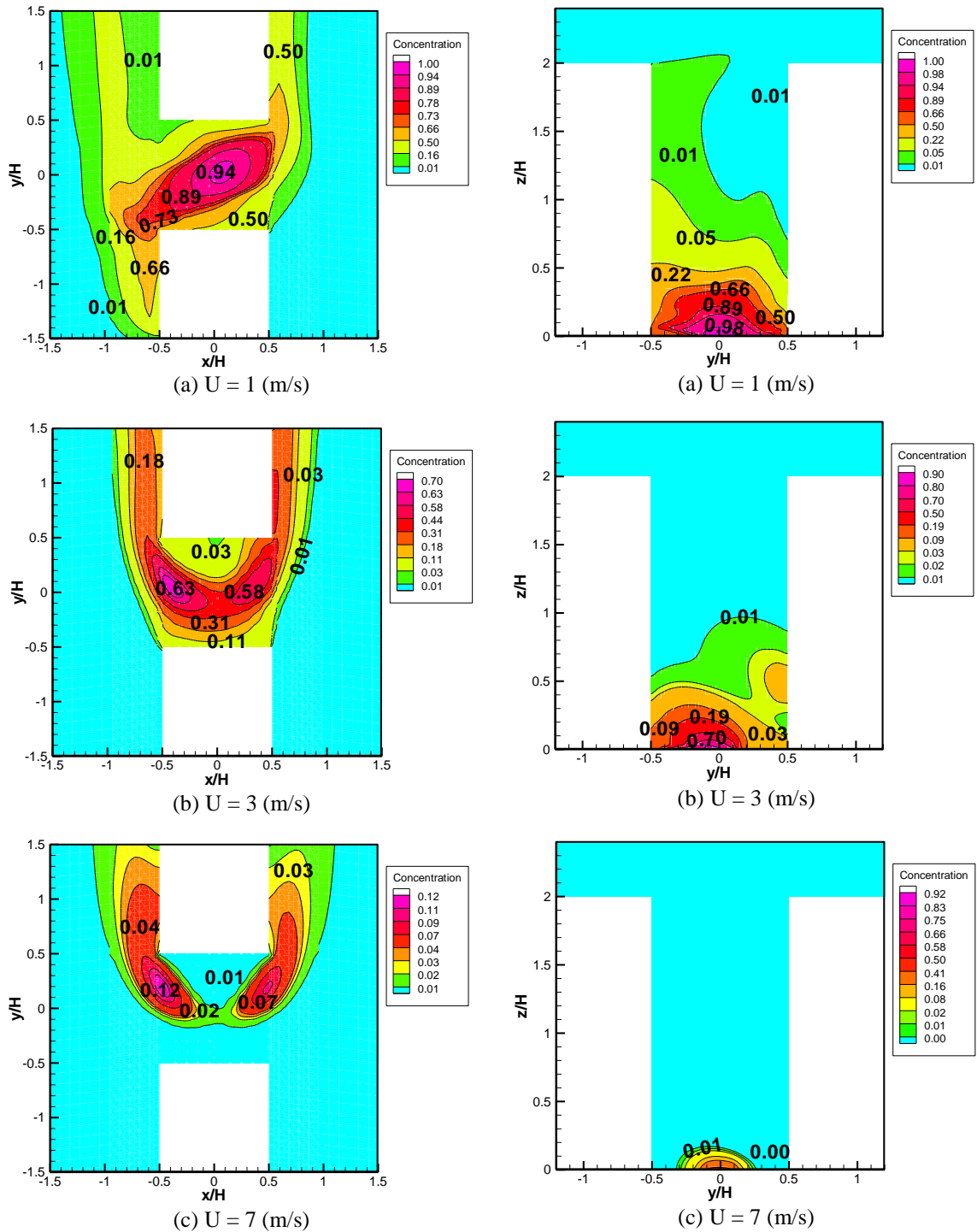
Figure 4.19 Normalized pollution concentration: wind direction = 90 (degree) and AR = 2 (Left) Horizontal section 1.5 above the ground (Right) Vertical section in middle of the studied street canyon

4.6.2. Parallel Flow

51 percent of prevailing wind is parallel with the street canyon orientation according to its frequency of occurrence summation (Table D.1). As illustrated in Figures 14.20 and 14.21, prevailing wind washes away most of the pollutant through the downstream when its direction is parallel with the street canyon. The dispersion begins from the center of the street canyon where pollutant source is located. This means that the concentration near the sidewalks is extremely low (below 10% of source concentration). At the lower air velocities (e.g. U = 1m/s), the pollutant is asymmetrically dispersed from the street canyon due to the effect of non-uniform temperature of the ground and walls on airflow (Figure 4.20a). Increase in the prevailing wind velocity, nonetheless, dominates thermal stability effect and consequently a symmetrical dispersion can be observed when U is 7 m/s (Figure 4.20c). As shown in Figure 14.21, the aspect ratio does not predominantly affect the concentration level. In other words, the concentration within the sidewalks is still very low. Additionally, concentration disperses more vertically when the buoyancy effect resulted by thermal stability is comparable with upstream flow (e.g. Figure 4.21a: U = 1 m/s). In general, the normalized concentration is extremely low within the street canyon except at locations close to the pollution source.
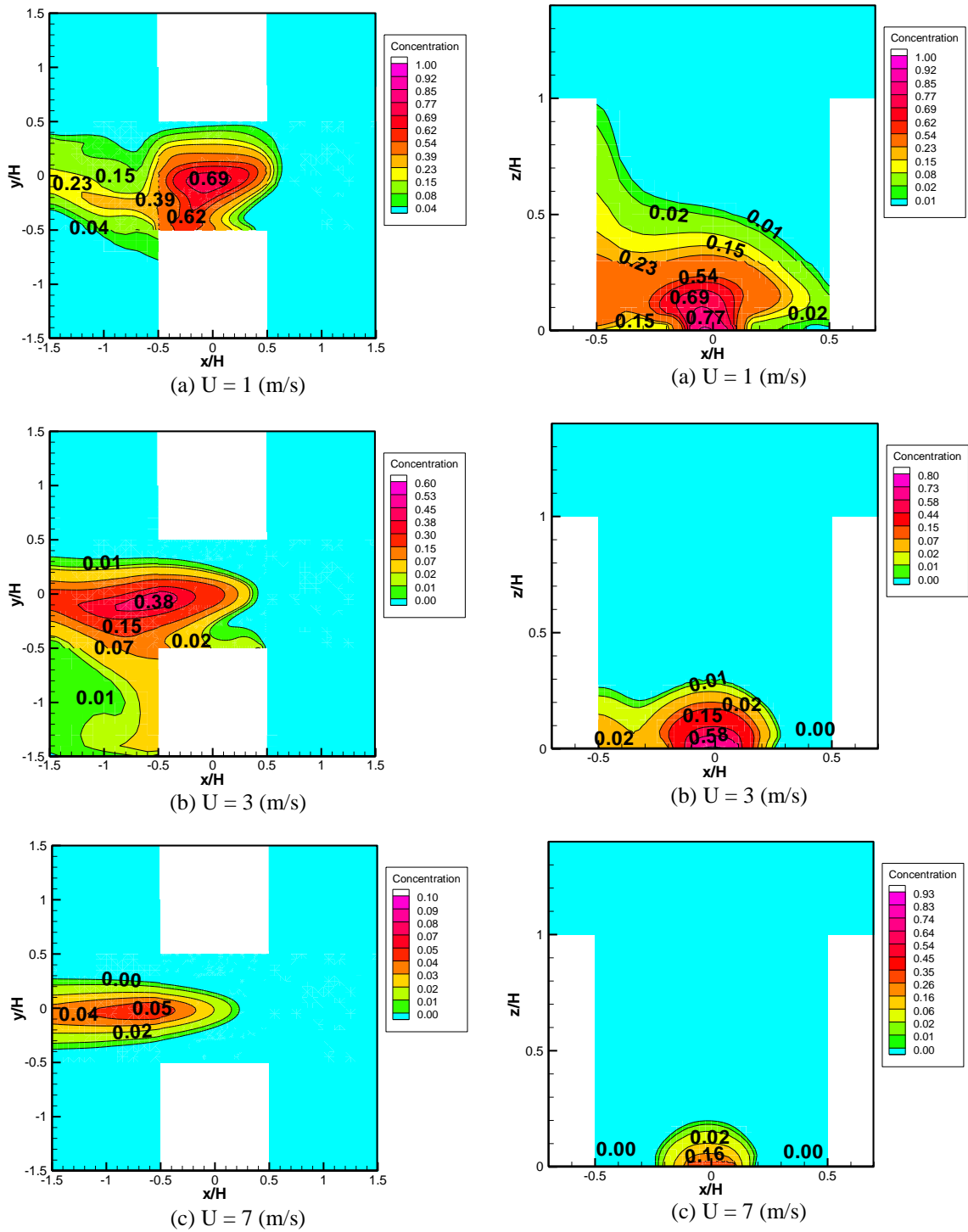
Figure 4.20 Normalized pollution concentration: wind direction = 0 (degree) and AR = 1
(Left) Horizontal section 1.5 above the ground (Right) Vertical section in middle of the
studied street canyon
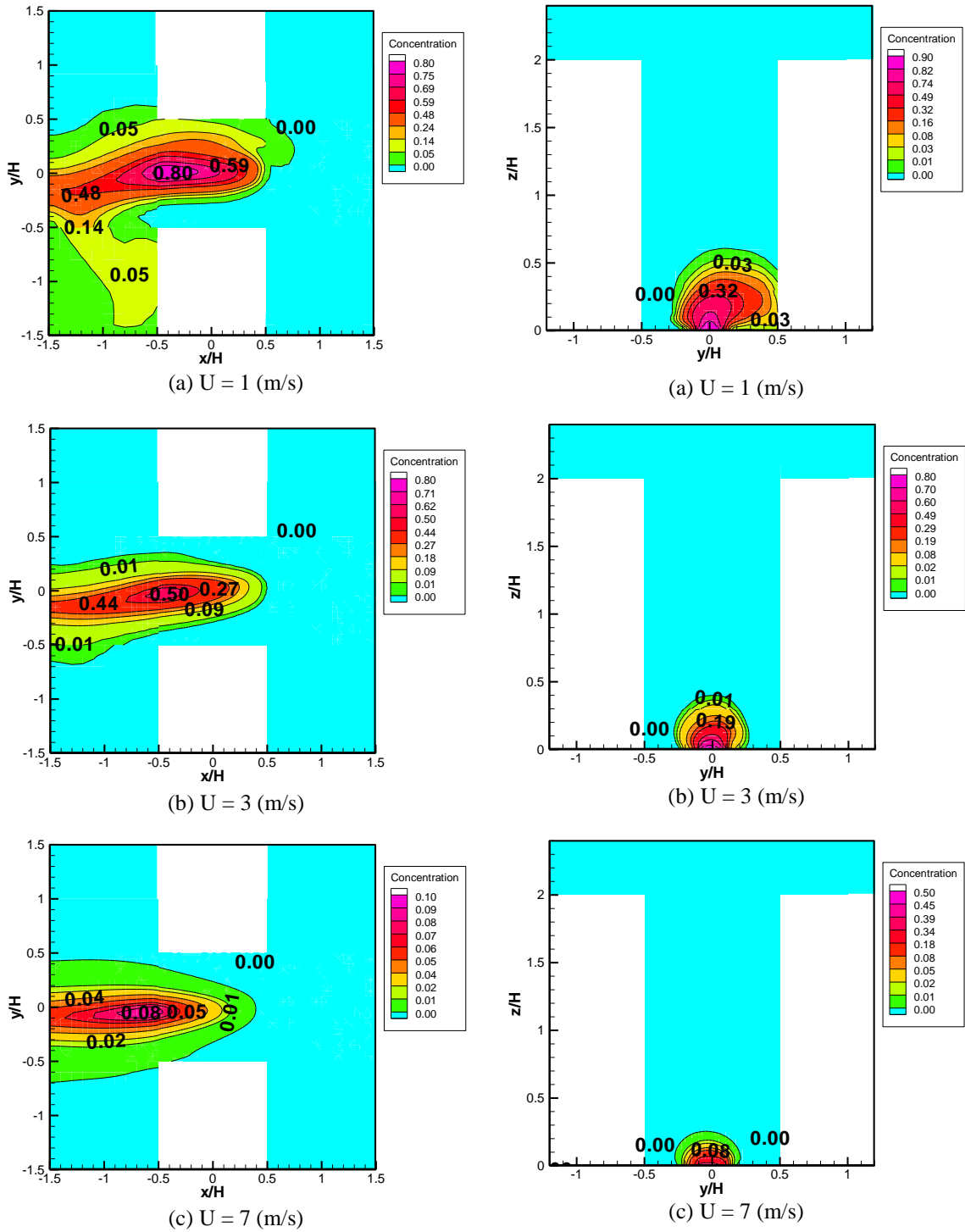
Figure 4.21 Normalized pollution concentration: wind direction = 0 (degree) and AR = 2 (Left) Horizontal section 1.5 above the ground (Right) Vertical section in middle of the studied street canyon

4.6.3. Inclined Flow

A very complex airflow pattern can be seen when the angle between the prevailing wind and the street canyon is 45 (degrees). The frequency of occurrence summation for this inclined angle is about 31 percent.

As demonstrated in Figure 14.22, pollution propagates slightly from the street canyon where AR is one. By increasing prevailing wind velocity, airflow assumes an asymmetrical formation with a tendency to horizontally disperse around the leeward building when vertical dispersion is decreased. Thus, the concentration level is again drastically reduced within street canyon excluding the vicinity of the pollutant source.

Opposite to AR=1, the dispersion is more accumulated in leeward side of street canyon when AR is two. Furthermore, when AR is two, both vertical and horizontal propagation is stronger than when AR=1 (Figure 14.23). Nonetheless, increase of wind velocity again results in an intensive decrease of vertical dispersion. For example, entire street canyon has a normalized concentration level above 1% when U is 1 m/s (Figure 14.23a). The concentration level, however, is reduced to below 1% for upper half of street canyon for higher wind velocities (e.g. U = 3, Figure 14.23b, or 7 m/s, Figure 14.23c).
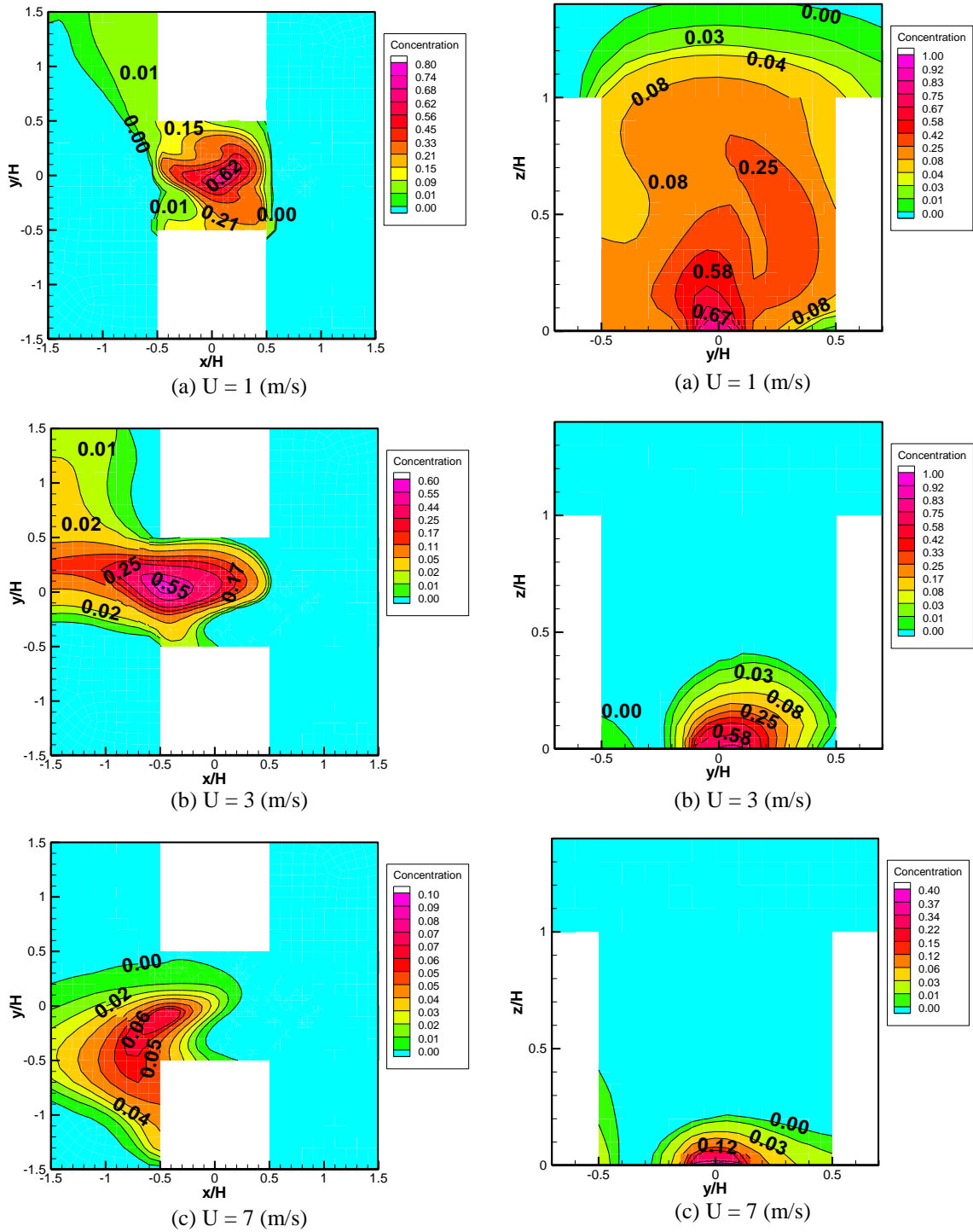
Figure 4.22 Normalized pollution concentration: wind direction = 45 (degree) and AR = 1 (Left) Horizontal section 1.5 above the ground (Right) Vertical section in middle of the studied street canyon
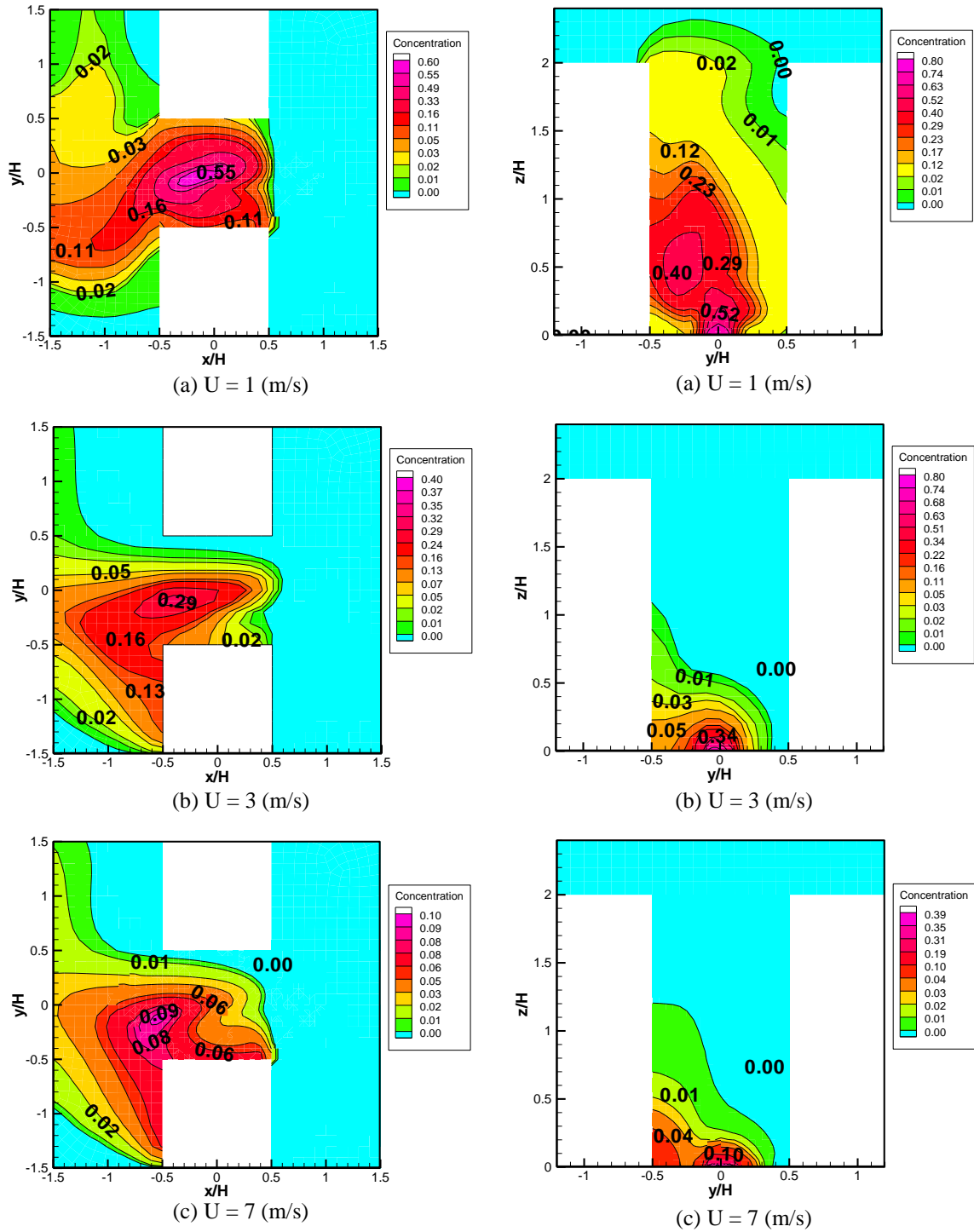
Figure 4.23 Normalized pollution concentration: wind direction = 45 (degree) and AR = 2 (Left) Horizontal section 1.5 above the ground (Right) Vertical section in middle of the studied street canyon

4.6.4. Thermal Stability

As discussed earlier, thermal stability has a considerable effect on the pollution dispersion when upstream airflow is low. The results of the preceding sections confirm the strong influence of thermal stability when prevailing wind velocity is 1 (m/s) and wind direction is 90 (degrees). In this case, as shown in Figure 4.17b, Bulk-Richardson number is in its highest value (Rb=4.1). This situation with a 3% frequency of occurrence summation (Table D.1) is chosen as a sample for further studies of thermal stability (AR=2).

Figure 4.24 compares pollution dispersion for scenarios II, III and IV. The asymmetric pattern of dispersion is influenced by non-uniform walls and ground temperature. The Bulk-Richardson number is calculated at 4.1, 4.2, and 3.9 for scenarios II, III and IV, respectively. The numbers are in stable range (positive) since the temperature of ground is less than that of airflow and surface of buildings. As expected, the greater Bulk-Richardson number, the higher pollution concentration inside pedestrian level can be observed. This implies that only a less stable condition is obtained by using higher-albedo materials for the ground. Moreover, decrease in concentration level is very low despite the implementation of more expensive materials.
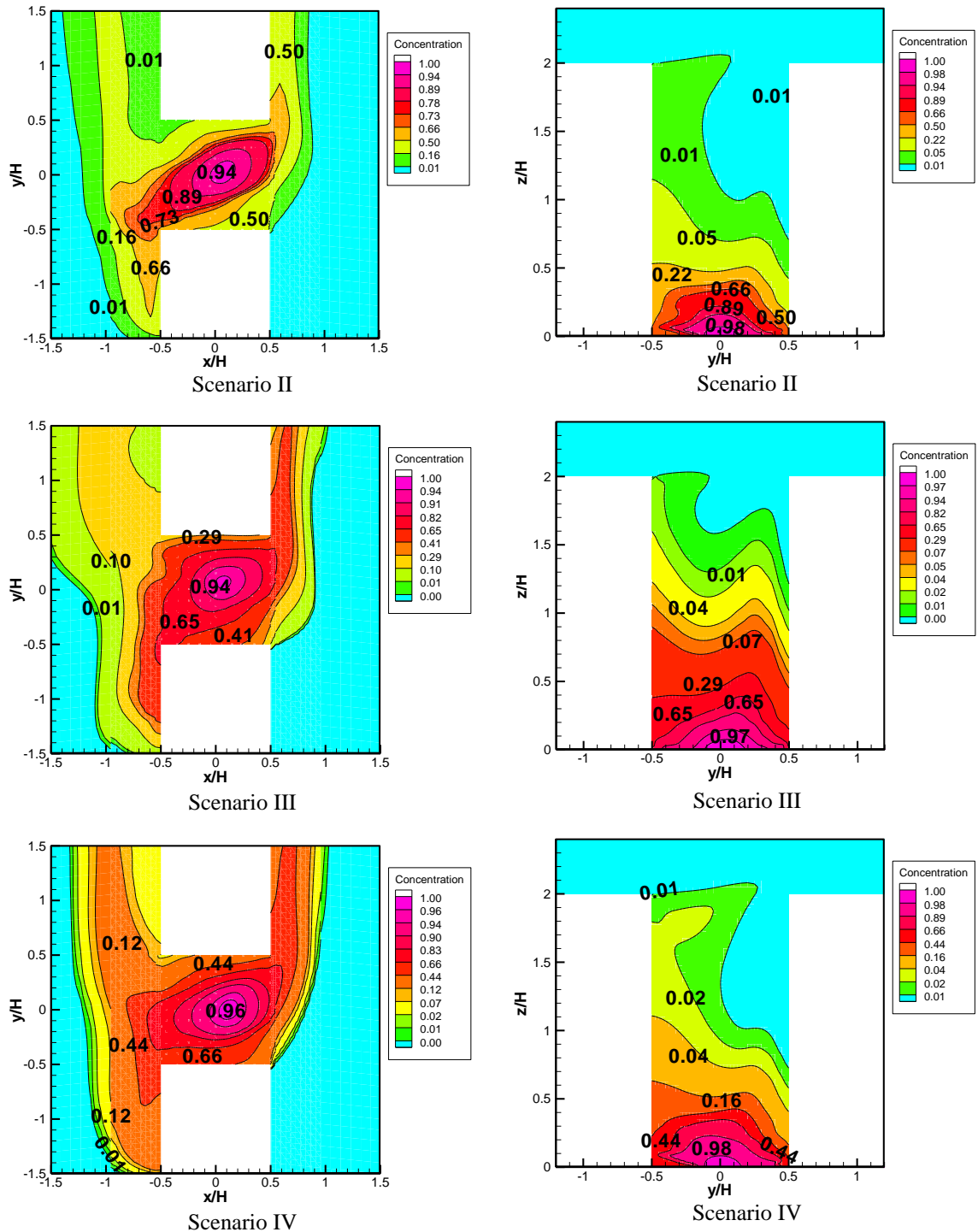
Figure 4.24 Normalized pollution concentration: AR = 2, wind direction = 90 (degree), and wind velocity = 1 (m/s) for different scenarios (Left) Horizontal section 1.5 above the ground (Right) Vertical section in middle of the studied street canyon

The results of this section again prove that using passive strategies is not always a solution to improve PCE since a noticeable change in the airflow pattern and pollution dispersion is not observed.

4.7. Effect of the PVS on Pollution Dispersion

The last part of the PCE-algorithm recommends the application of the PVS if PCE is not improved using passive technologies. As discussed in chapter 3, the performance of the proposed PVS is a function of fan pressure, ducting design, and ventilation strategy (Figure 3.3).

Here, rectangular ducts are installed in both adjacent walls of the street canyon. The area of ducts is 10 square meters across each wall with one meter above the sidewalk pavement. It is also assumed that the electrical fans have the ability to be employed as exhaust and/or supply fans. Different fan pressures are also examined to obtain a reasonable size and cost for the installed fan.

The worst frequency of occurrence selected from the previous section for the PCE indices is selected to study the effect of the PVS (Rb=4.1, U=1 m/s, and angle=90 degree). It is worth noting that the PCE improvement of other frequency of occurrences can be treated

with the same methodology. Tables D.5 through D.8 represent the PCE indices obtained

for the pedestrian plane after using the PVS combinations: (A), (B), (C), and (D). Five

fan pressures are also simulated for each combination, including 1, 10, 20, 50, and 100

(Pa). Selection of a proper type of PVS combination and fan pressure is discussed in the

following paragraphs.

4.7.1. Normalized CO Concentration

Normalized CO concentration and AQI for various fan pressures are depicted in Figure

4.25. The normalized concentration level and AQI are also shown with dash line when

the PVS is not installed.

Normalized CO concentration drops considerably in both sidewalks for all combinations

(Figure 3.3) as the fan pressure increases. The concentration is specifically below 1% by

implementation of the combination (B) with a fan pressure of more than 10 (Pa).

Furthermore, there is a correlation between increase in fan pressure and decrease in

normalized concentration in combination (A). Thus, it can be predicted that a fan with

pressure of 200 (pa) is required to reduce the normalized concentration below 1%. For

other combinations, it is necessary to apply fan pressures of greater than 20 (pa) in order

to keep the normalized concentration below 10%.
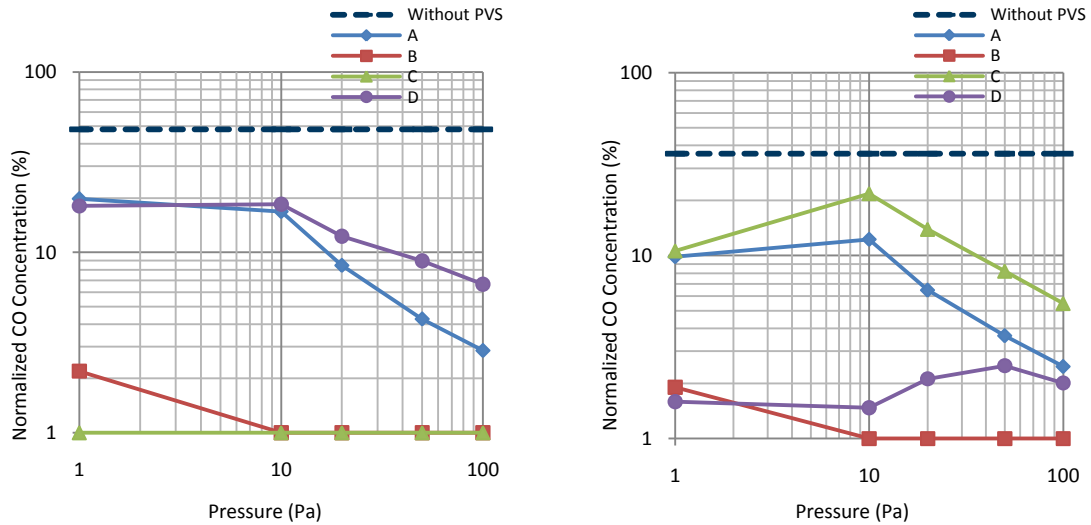
Figure 4.25 Normalized CO concentration within pedestrian plane for various PVS combinations (Left) left sidewalk (Right) right sidewalk

4.7.2. AQI

It should be noted that AQI is calculated based on the pollution concentration and air velocity within the pedestrian plane. Therefore, its behavior is not necessarily similar to the normalized concentration. As shown in Figure 4.26, AQI is elevated for combinations (A) and (D) in the left sidewalk and (A), (C), and (D) for the right sidewalk due to the increase in fan pressure. This means that increase in fan pressure produces higher air velocities which drastically affect on AQI. Combination (B) is nonetheless found to be a persistent strategy to decrease AQI. In other words, combination (B) keeps AQI in both sidewalks within a good-moderate situation when fan pressure is not greater than 10 (Pa).
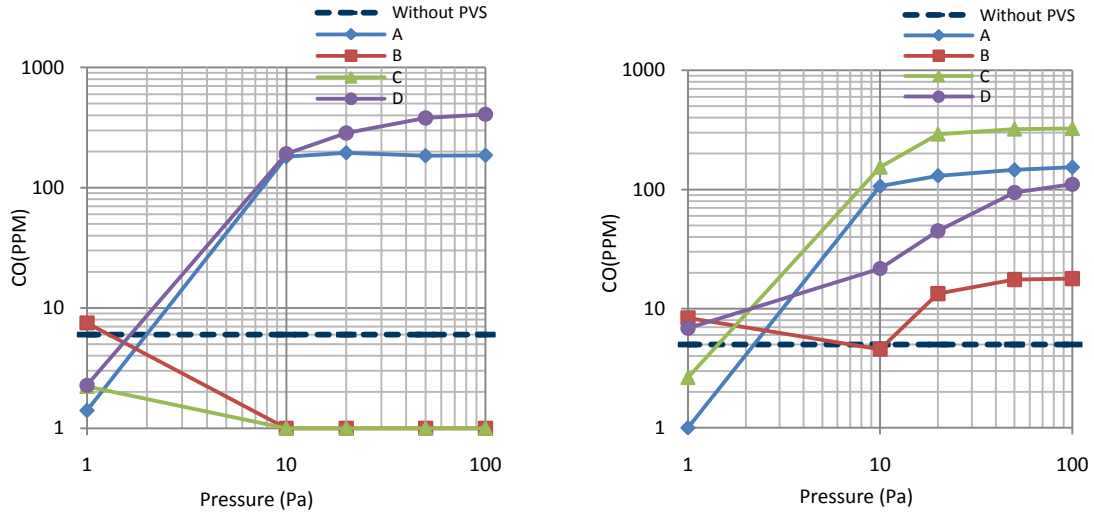
Figure 4.26 AQI within pedestrian plane for various PVS combinations (Left) left sidewalk (Right) right sidewalk

4.7.3. THI and WCI

It was observed that combinations (A) through (D) are not capable of enhancing the THI. This implies that the THI always falls in a very warm range (27°C - 32°C).

The WCI is also depicted in Figure 4.27. The trend of air velocity inside the pedestrian plane is consistently related to fan pressure. For combination (A), (C), and (D), applying a fan pressure greater than 20 (Pa) increases the WCI approximately to half of the light-air condition (0.5 m/s). Nonetheless, this pressure should be about 10 (Pa) for combination (B). It can be seen that a light-breeze condition for all combinations is only obtained when the fan pressure is greater than 70 (Pa).
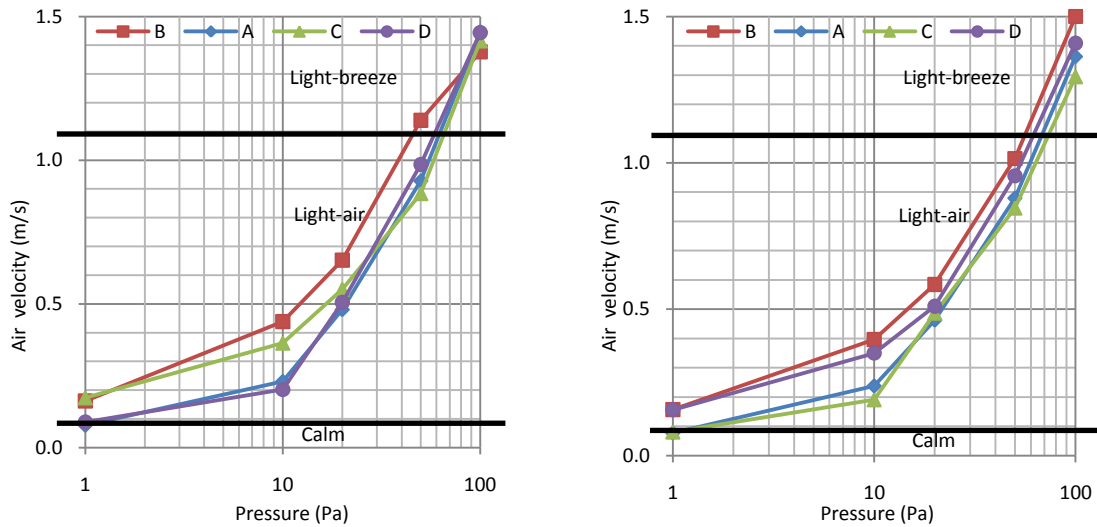
Figure 4.27 WCI within pedestrian plane for various PVS combinations (Left) left sidewalk (Right) right sidewalk

4.7.4. ACH and PCH

ACH and PCH are useful concepts to present the influence of the PVS combinations on air and pollutant movement within the street canyon. Since the fluctuation part of these concepts is still not developed for a 3-dimensional $k - \varepsilon$ model, the mean part is only calculated through the top and lateral surfaces of the pedestrian ventilation zone.

As shown in Figure 4.28, ACH and PCH are normalized with the natural condition of the street canyon while the PVS is not working. It is evident that combination (B) produces a large ACH from top and lateral surfaces. Conversely, combination (A) noticeably reduces ACH from the top surface while it remains almost constant from lateral surfaces. Also, combinations (C) and (D) change ACH only at fan pressures higher than 20 (Pa).
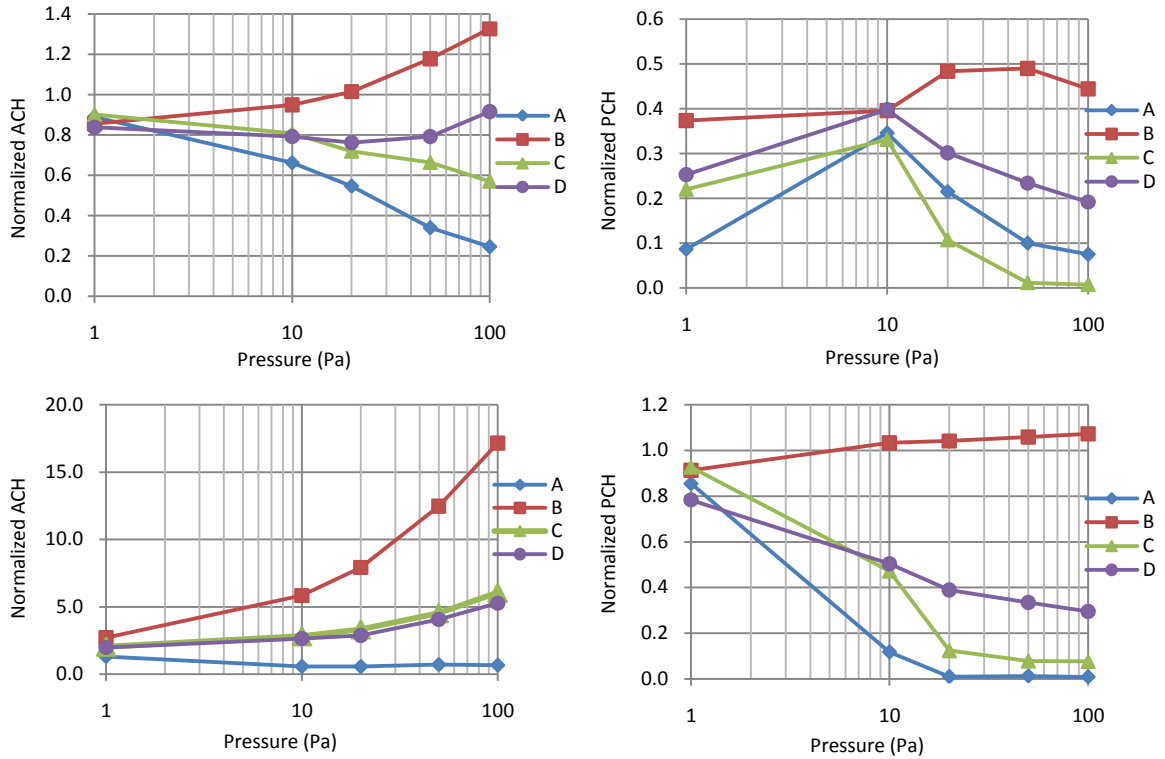
Figure 4.28 Normalized ACH and PCH (Top) top surface (Bottom) Lateral surfaces

For combinations (A), (C), and (D), a correlation between PCH reduction and fan pressure increase can be seen in Figure 4.28. The PCH reduction from lateral surfaces is much higher for combination (A). Compared to other cases, in combination (B), however, the pollutants are blown out of the street canyon from top and lateral surfaces, and a slight increase in PCH can be observed.

4.7.5. Fan Selection

Figures 4.25 through 4.28 provide proper information for a better selection of the required fan pressure. Here, fan pressure is chosen as 100 (Pa) in order to reduce the cost

and performance of the PVS combinations. This means that 100 (Pa) is an adequate fan pressure to improve the PCE indices.

Figures 4.29 and 4.30 compare pollution dispersion for different PVS combinations when fan pressure is fixed at 100 (Pa). These figures demonstrate how the PVS can produce an air shield above one sidewalk (C and D) or both sidewalks (B).

As demonstrated in Figure 4.29, implementation of combination (A) helps to significantly reduce pollution dispersion from lateral and top-canyon surfaces, but it results an increase in concentration level within the sidewalks due to the exhaust of the pollutants from the ducting system. As a subject of future study, this can be modified with changing the place of dampers close to the pollution source by using underground ducting system.

When a supplying strategy (B) is used, the pollution concentration level declines at the sidewalk level by more than 99%. Also, it can be seen in Figure 4.29 that most of the pollutants are dispersed through the lateral surfaces. Again, the dispersion is not symmetric due to the stratification resulted by non-uniform temperature distribution of the ground and walls.
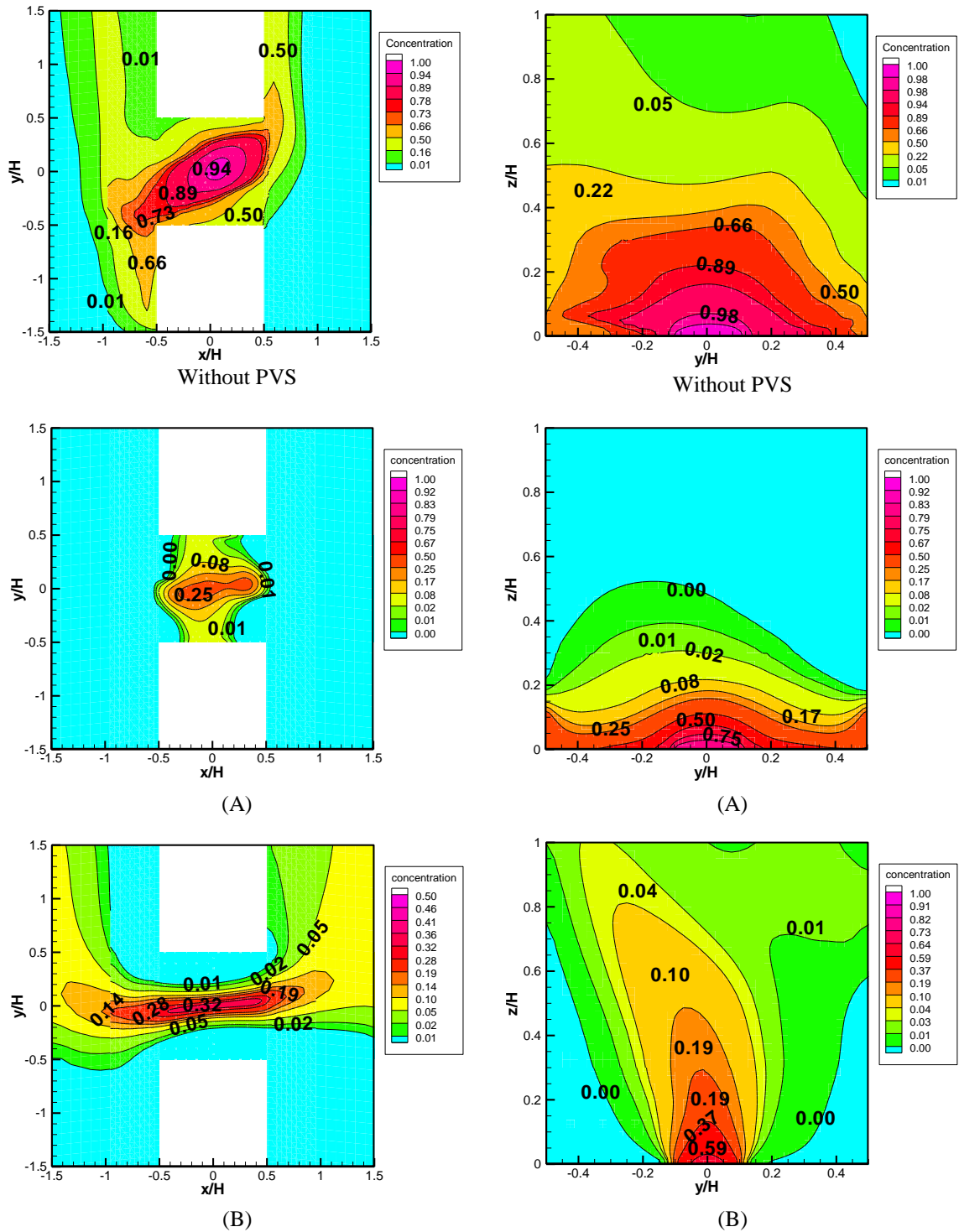
Figure 4.29 Normalized pollution concentration: AR = 2, wind direction = 0 (degree), wind velocity = 1 (m/s), and fan pressure = 100 (Pa) for various PVS strategies (Left) Horizontal section 1.5 above the ground (Right) Vertical section in middle of the studied street canyon
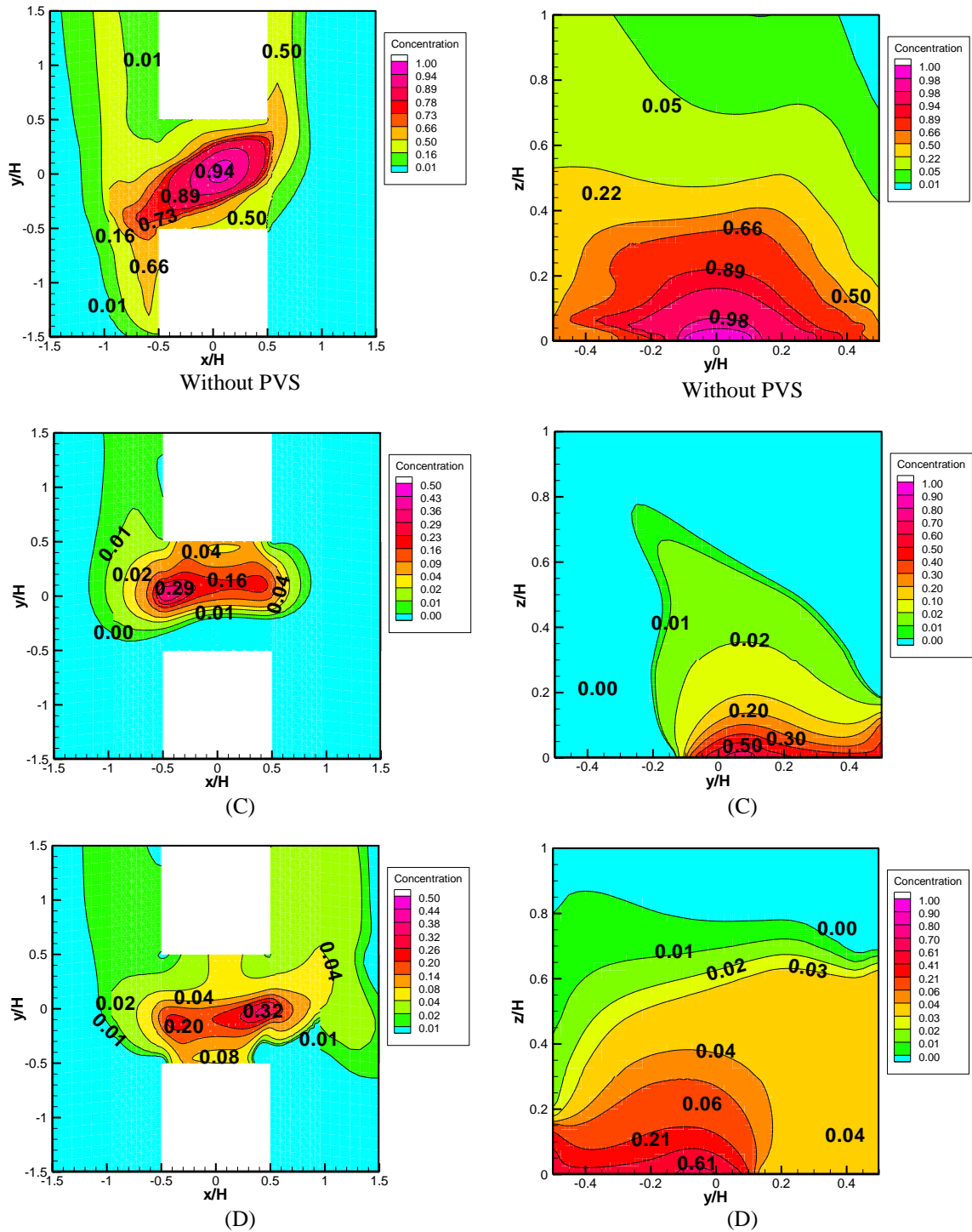
Figure 4.30 Normalized pollution concentration: AR = 2, wind direction = 0 (degree), wind velocity = 1 (m/s), and fan pressure = 100 (Pa) for various PVS strategies (Left) Horizontal section 1.5 above the ground (Right) Vertical section in middle of the studied street canyon

As illustrated in Figure 4.30, the advantage of using a washing flow mechanism (C or D) is to guide the pollution through the windward or leeward duct. Evidently, the strength of the washing flow is a function of fan pressure. The concentration level is always being low in one sidewalk (below 4%) and high in another. This implies that one sidewalk may be recommended to use by pedestrian in case of using combination (C) or (D).

Normalized CO concentration dispersion towards other street canyons is illustrated in Figures 4.31. To better exhibit the dispersion, only normalized concentration above 1% and below 20% is demonstrated.

The horizontal view shows almost similar contribution for combinations (B) and (D) on dispersing pollutant through the neighboring street canyons. However, combinations (A) and (C) show a good performance on controlling pollution dispersion through the top and lateral surfaces. Again, effect of solar radiation and heat storage through soil and walls causes non-uniform temperature differences in surfaces of street canyon. Thus, the pollution dispersion is affected by asymmetrical stratification when the influence of buoyancy is comparable with prevailing wind (Rb=4.1). The vertical view also magnifies the mechanism of each PVS combination in order to disperse the pollutants. Evidently, installing filters within the PVS can significantly reduce pollution concentration.
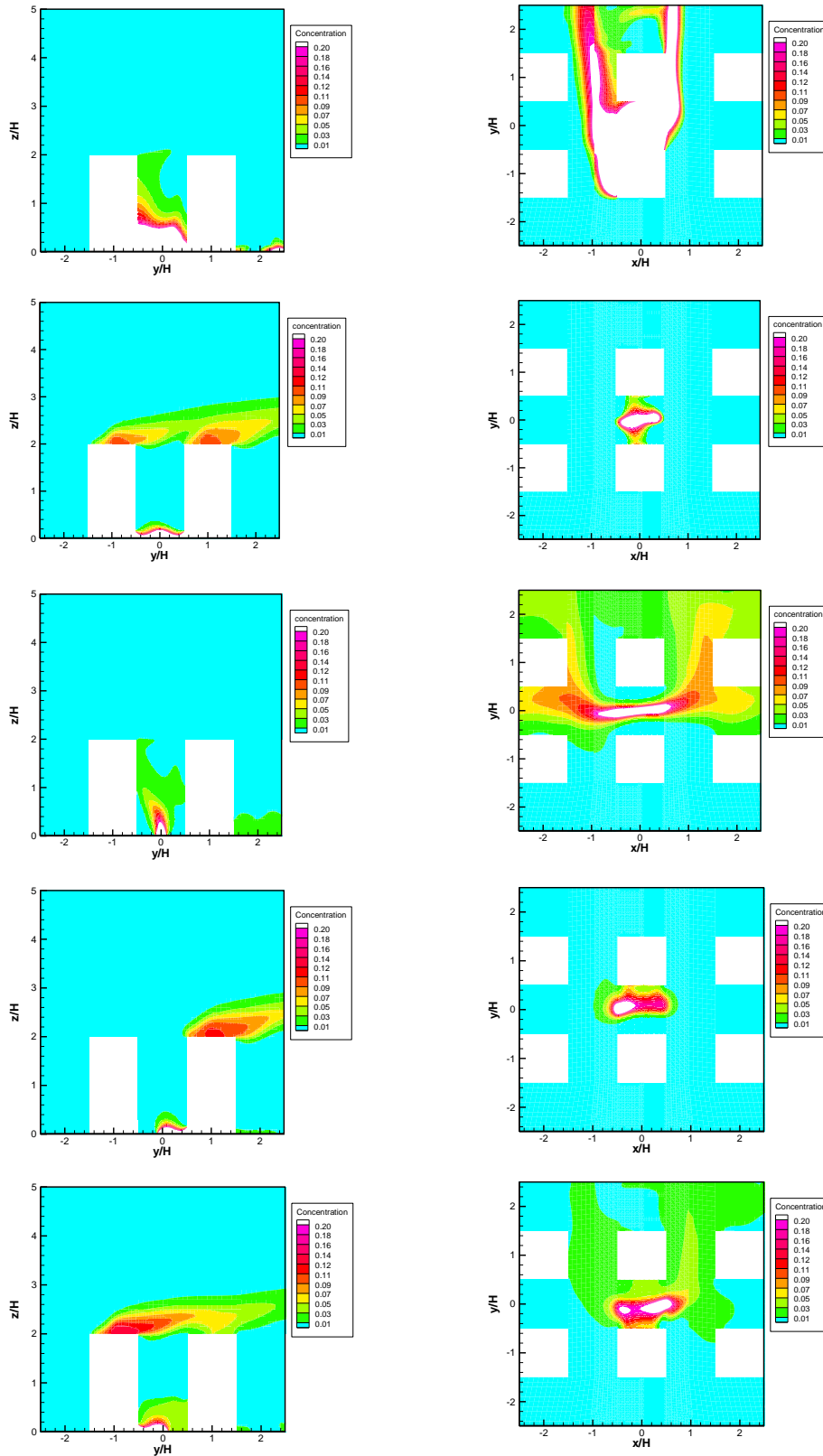
Figure 4.31 Normalized pollution concentration in (Left) a vertical section (Right) a horizontal section 1.5 above the ground for various PVS strategies

4.8.   Results Conclusion

It can be concluded that combination (C) with fan pressure = 100 (Pa) is an efficient alternative to enhance PCE for the worst case scenario. Table 4.3 summarized the PCE indices before and after using combination (C) of the PVS with fan pressure 100 (Pa). This means that the acceptable AQI, THI, and WCI for case II of Table 4.2 are now changed in left sidewalk by 3 (%), 0 (%), and 3 (%), respectively.

Dispersion through the neighboring street canyons is also remarkably reduced since normalized PCH from lateral and top surfaces is 0.1 and 0, respectively. Moreover, normalized CO concentration is decreased to below 1% and 5% within left and right sidewalks, respectively.

This methodology can be expanded to select a corresponding efficient combination for other frequency of occurrences in order to improve their PCE indices. Therefore, for this specific case study, it is predicted that 100% acceptable AQI and WCI will be achieved applying PVS combinations for different frequency of occurrences. It is, however, estimated that The THI will be not significantly improved.

Table 4.3 THI, WCI, AQI, CO concentration, ACH, and PCH before and after using the PVS when AR = 2, wind direction = 0 (degree), and wind velocity = 1 (m/s)

PVS Combination	Without PVS		(C) – Fan pressure = 100 (Pa)	
	L-S	R-S	L-S	R-S
THI (°C)	Very warm (29)	Very warm (29)	Very warm (30)	Very warm (30)
WCI (m/s)	Calm (0.1)	Calm (0.1)	Light breeze (1.4)	Light breeze (1.3)
AQI (PPM)	Unhealthy	Good	Good	Hazardous
Normalized CO concentration (%)	48	36	1	5
	Top surface	Lateral surfaces	Top surface	Lateral surfaces
Normalized ACH	1	1	0.6	6.1
Normalized PCH	1	1	0.0	0.1

5. Chapter Five: Conclusion and Remarks

Higher population density has altered the cities' old landscape with dense areas consisting of high-rise buildings. As a result, detrimental phenomena appeared inside modern cities that threatened the inhabitant's health and comfort. Among these phenomena, the Urban Heat Island (UHI) is known as the most harmful side effect of the urbanization which affects the outdoor environment

In addition to the reduction of wind velocity within the urban canopies, the accumulated pollution decreases the outdoor comfort and renders the pedestrian areas to hazardous level. Many cities recently started to apply mitigation protocols by increasing tree planting and vegetation inside urban areas. A few cities also promoted higher-albedo materials for urban surfaces. Moreover, guidelines are established by cities in order to design an appropriate street canyon and building layout to naturally ventilate urban areas. However, the UHI intensity varies in different street canyons and climates. Thus, the aforementioned mitigation technologies are not always practical or economical to reduce energy consumption and keep pedestrian comfort and exposure in the desired range.

In this study, the PCE-algorithm is proposed to integrate the advantages of passive and newly proposed pedestrian ventilation systems. This approach is also capable of

evaluating the possible advantages of passive mitigation strategies using a frequency of occurrence concept. This concept assesses the probability of having acceptable comfort indices within the street canyon. The PCE-algorithm algorithm first evaluates pedestrian comfort and exposure (PCE) around a building.

Two indices are considered as indicator of pedestrian comfort, including wind comfort index (WCI) and temperature-humidity index (THI). Moreover, air quality index (AQI) is applied as pedestrian air quality indicator. To assess PCE, the three aforementioned indices are calculated based on obtained air velocity, temperature, humidity, radiation intensity, and pollution concentration in an imaginary surface called pedestrian plane.

A computational fluid dynamics (CFD) model is developed to resolve airflow pattern inside the study domain. A radiation and soil model are also integrated within the CFD model to simulate the effect of heat storage. An RNG $k - \varepsilon$ model is used as turbulent scheme. Furthermore, several options are proposed in the PCE-algorithm to assign boundary conditions for the study domain.

To define proper dimension and mesh size for the study domain, two tests are proposed in the PCE-algorithm. Validation of the simulation with at least one experiment is also recommended in the PCE-algorithm.

The proposed algorithm is applied on an array of identical buildings located in Montreal. The studied street canyon is inside this array of buildings. Frequency of occurrence for wind direction and magnitude is also analyzed using Montreal weather data. As a result, nine sets of simulation are assumed with an associated frequency of occurrence.

Based on the design flexibility of the assumed case study, four scenarios are defined to investigate the influence of passive mitigation technologies, including alteration of aspect ratio, building surface material, and pavement and road properties. Surprisingly, these mitigation technologies do not have a considerable effect on WCI, THI, and AQI indices.

The PCE-algorithm therefore recommends using the pedestrian ventilation system due to the inefficient impact of passive mitigation technologies. Four options are possible for installing the PVS. Also, airflow rate of the PVS ducts can considerably change PCE. Thus, a procedure is proposed to select the proper airflow rate for the PVS combinations.

The most vulnerable situation is selected to study the effect of the PVS when velocity direction, magnitude, and occurrence frequency are 90 degrees, 1 m/s, and 3%, respectively. It is observed that the PVS is very effective to improve PCE. AQI in the left sidewalk is improved from unhealthy to good condition. WCI is also increased from 0.1

(m/s) to about 1.4 (m/s) in both sidewalks. Moreover, normalized ACH from lateral surfaces is elevated to six times its initial value.

Future Works

- It is possible to simultaneously calculate the energy consumption of a building by coupling a building energy simulation model with the proposed model. Instead of applying a defined interior boundary condition, the interactive building simulation coupled with the airflow model will provide released energy to the street canyon.

- Pedestrians are moving object, however, their impact on airflow filed and pollution dispersion is neglected. Adding pedestrian movement could be a subject of future research.

- Adaption of a general index to show PCE of the street canyon could be an invaluable subject of future research. For this purpose, current indices should be coupled with a human energy budget model considering psychological parameters.

- Long-wave radiation, vegetation, trees, and ponds are extremely important to the energy budget of a street canyon. Future PCE assessment models should contain these parameters.

- Alteration of building shape, changing the arrangement of the array of buildings, surface vegetation, tree planting, and shading with mobile objects are among other mitigation technologies. Their impact on PCE can be investigated in future studies.

- Similar to the role of an air conditioning system for indoor spaces, the PVS interactively controls PCE in outdoor spaces. Many novel ideas can improve this system, including enhancement of the ducting system through walls and the ground, adjustment of the PVS airflow rate, using other source of energy (e.g. solar radiation, waste energy from the air conditioner condenser, etc.) to provide stack effect, and using cool materials, water spray, and pergola inside the pedestrian zone.

- The Leadership in Energy and Environmental Design (LEED) is an internationally accepted benchmark for the design, construction and operation of high performance green buildings. However, using light-colored/high-albedo materials is the only recommended UHI mitigation technology in this program. Moreover, the impact of this technique is only considered on building energy. Therefore, it would be an interesting subject of future work to include the PCE inside the LEED by integration of proposed model.

Appendix A Thermal Comfort Indices

With indoor air studies, comfort is mostly limited to thermal comfort. Defined by American Society of Heating, Refrigerating and Air-Conditioning Engineers (ASHRAE) thermal comfort is a state in which the human mind is satisfied with the surrounding thermal environment (American Society for Heating Ventilating and air conditioning engineers, 2001). Thermal comfort is a function of different heat exchange mechanisms between a human body and the surrounding environment. These mechanisms also depend on various environmental and personal factors. Environmental factors include air temperature, air velocity, moisture, and mean radiant temperature. Personal factors also include clothing, activity level, health, psychology, sociology, and situational conditions. Furthermore, it is believed that the length of exposure to these conditions is a significant factor. Many regional and international studies have been conducted to develop a general thermal comfort index.

A.1. Mean Radiant Temperature

Mean radiant temperature (MRT) index is developed based on the Stefan-Boltzmann Law which represents the gained radiation heat by a human body when the surrounding object is assumed to be a blackbody with uniform temperature. MRT is generally measured with

a globe which is a dry-bulb thermometer. MRT can be considerably greater than ambient air temperature within the street canyon. Different approaches are also used to calculate MRT (Ali-Toudert and Mayer, 2006; Walton et al., 2007). For example Mochida et al., (2002) used the following formulation:

$$\theta_{MRT} = \theta_{globe} + 2.37\sqrt{\overline{U}}(\theta_{globe} - \theta_{air}) \tag{A.1}$$

where $\theta_{MRT}, \theta_{globe}$ and θ_{air} are MRT, globe, and air temperature, respectively. U is also wind velocity (m/s).

A.2. Wind Chill Index

Wind chill index (WCH) is developed to express the effect of wind velocity and temperature on exposed skin (Siple and Passel, 1945; Tseliou et al., 2010). For example, the following empirical equation can be used to estimate the wind chill index:

$$WCH = (10.45 + 10U^{0.5} - U)(33 - T_a) \tag{A.2}$$

where WCH (kcal/m^{2}h) is wind chill index, and T (°C) is the ambient air temperature.

A.3.   Temperature-Humidity Index

Adapted for outdoor spaces, the Temperature-Humidity index (THI) combines air temperature and moisture as shown below (Thom, 1959):

$$\text{THI} = T - (0.55 - 0.0055\text{RH}) \times (T - 14.5) \tag{A.3}$$

where RH is relative humidity (%).

A.4.   Thermal Sensation Models

Theses indices are developed by integrating thermal environmental factors and human body heat balance. Many thermal comfort models, including SET (Gagge et al., 1986) and PMV (Fanger, 1972), have been largely developed for indoor environment. These indices were later modified for outdoor spaces (e.g. PET by Mayer and Hoppe, 1987).

A.4.1. Effective Temperature

ET* stands for NEW Effective Temperature and represents the transient index for thermal comfort. This index includes radiative and latent heat exchanges. This model represents a 2-node model considering body core and skin as one node. The final mean temperature and wittedness of skin are associated with an effective temperature, solving

heat transfer between body core, skin and the environment for several time iterations. Also, in this model, the human body is assumed with two concentric core and skin cylinders. SET* stands for a relative form of the ET* compared to a standard person and environment.

A.4.2. PMV, DISC, and TSENS

The predicted mean vote index (PMV), the thermal discomfort index (DISC), and the thermal sensation index (TSENS) are steady-state thermal sensation models which describe a thermal strain assigning a vote for thermal discomfort by people. Scaling will finally interpret the outcome of these models. A positive number represents the warm side of the neutral comfort while a negative number shows the cool side. Also, PMV, DISC and TSENS are respectively known as seven, eleven, and eleven point indices.

A.4.3. PET

The physiologically equivalent temperature (PET) is based on human energy balance under typical indoor conditions (air temperature = MRT, RH = 50 %, and wind speed = 0.1 m/s). However, assuming the same perspiration rate and skin temperature as indoor conditions, PET is defined for outdoor spaces when the heat budget of the human body is

balanced. PET solves three sets of equations, including the heat balance for the human

body, the heat flow through the human body core to the skin surface, and the heat flow

from the human skin through the clothing surface.

Appendix B Wind Comfort Indices

Wind comfort indices (WCI) are mostly developed based on an acceptable range of wind

velocity for typical pedestrian activities (Hoppe, 2002; Soligo et al., 1998). As shown in

Table 2.2, Lawson and Penwarden (1975) have provided an extended ''Land Beaufort

Scale'' showing wind effects on people.

Table B.1 Extended Land-Beaufort scale (Lawson and Penwarden, 1975)

Beaufort Number	Wind Speed (m/s) at 1.75 (m) height	Description	Effect
0	0.0 – 0.1	Calm	-
1	0.2 – 1.0	Light air	No noticeable wind
2	1.1 – 2.3	Light breeze	Wind felt on face
3	2.4 – 3.8	Gentle breeze	Hair disturbed, clothing flaps, newspaper difficult to read
4	3.9 – 5.5	Moderate breeze	Raises dust and loose paper, hair disarranged
5	5.6 – 7.5	Fresh breeze	Force of wind felt on body, danger of stumbling when entering a windy zone
6	7.6 – 9.7	Strong breeze	Umbrellas used with difficulty, difficult to walk steadily, sideways wind force about equal to forwards walking force, wind noise on ears unpleasant
7	9.8 – 12.0	Near gale	Inconvenience felt when walking
8	12.1 – 14.5	Gale	Generally impedes progress, great
9	14.6 – 17.1	Strong gale	People blown over

Since the wind flow through the street canyon is a stochastic phenomenon, these indices are developed based on gust $(\widehat{U})$, mean $\overline{U}$ or the fluctuation part of the velocity (Soligo et al., 1998). Effective gust velocity is also defined as $\overline{U} + C\sigma$ where σ is the root-mean-square of velocity fluctuations and C is a constant (Blocken and Carmeliet, 2004). This number should be greater than a threshold number. Recently, indices present frequency of occurrence to reflect the safety and the level of comfort (Blocken and Carmeliet, 2004).

Appendix C Pollution Exposure

Since only limited studies have been conducted to develop pollution exposure indices to the outdoor space, many indoor air quality indices have been adapted. For example, purging flow rate (PFR), visitation frequently (VF), pollutant residence time (TP), air quality index (AQI), and air exchange rate (ACH) are developed indoor indices that are applied in outdoor problems (Bady et al., 2008; Liu et al., 2005).

C.1.   PFR, VF, and TP

PFR, VF, and TP represent the effect of geometry on ventilation efficiency from a domain. It is proven that aspect ratio is the most important and effective parameter on the ventilation efficiency. PFR can be defined for a certain domain as the required airflow to

remove or purge the pollutants. Therefore, PFR implies the capacity of an airflow regime to flush out the pollutants through the street canyon. VF index represents the trajectory of a pollution particle within a domain. This index shows a healthy situation when VF is relatively low. Average residence time is used as another indoor ventilation efficiency index in outdoor spaces (Bady et al., 2008). This index indicates the mean existence time of pollutants inside the domain.

C.2. Air Quality Index

Air quality Index (AQI) characterizes the quality of the air at a given location. AQI number is mostly obtained by converting pollution concentration using a certain function which varies by pollutant type (Mintz, 2009). This index represents the different range of concentration assigned to a descriptor and a color (e.g. red for hazardous situation).

C.3. Air and Pollution Exchange Rate

The air exchange rate (ACH) for a street canyon is defined as the number of air changes within the street canyon's volume. Unlike indoor spaces, the formulation of air exchange (ACH) and pollution exchange (PCH) in outdoor spaces is still a challenging issue due to the stochastic nature of the upstream flow in addition to the importance of thermal

turbulence in such problems. The rate of air removal from a street canyon was first proposed by Liu et al. (2005) using a LES model. They suggested that ACH_+ and ACH_- leaves and enters the street canyon carrying the pollutant and fresh air via the top-canyon surface. Evidently, ACH_+ and ACH_- are equal due to the continuity:

$$ACH_+ = \overline{ACH_+} + ACH_+' = \frac{1}{\lambda} \int_0^\lambda \int_\Gamma (w_+ + w_+')d\Gamma dt \qquad (C.1)$$

where $\overline{ACH_+}$ and ACH_+' are the mean and fluctuation components, respectively. w_+ and w_+' signify the positive components of the velocity in the z-direction, Γ is the top-canyon surface, and λ is the average time period.

ACH_+' represents the fluctuation part of the velocity and theoretically cannot be determined by the $k - \varepsilon$ model, although Li et al. (2005) adapted the following formulation for a $k - \varepsilon$ model assuming isotropic turbulence ($\acute{u}\acute{u} = \acute{v}\acute{v} = \acute{w}\acute{w}$) due to a high Reynolds flow. They also assumed equal air removal and entry through the top-canyon surface:

$$k = \left(\overline{\acute{u}\acute{u}} + \overline{\acute{v}\acute{v}} + \overline{\acute{w}\acute{w}}\right)/2 = 3\overline{\acute{w}\acute{w}}/2 \qquad (C.2)$$

$$ACH_+' = \frac{1}{\lambda} \int_0^\lambda \int_\Gamma w_+' d\Gamma dt = \frac{1}{2} \int_\Gamma \overline{\acute{w}\acute{w}}^{0.5} d\Gamma = \int_\Gamma \sqrt{\frac{k}{6}} d\Gamma \qquad (C.3)$$

The results obtained were shown to be surprisingly comparable with the LES results.

Recently, Cheng et al. (2008) modified this equation using the eddy-viscosity hypothesis and significantly improved the results:

$$\overline{\acute{w}\acute{w}} = -2\nu_t \left(\frac{\partial \overline{w}}{\partial z} \right) + \frac{2}{3} k \tag{C.4}$$

Hence, equation (C.3) can be rewritten as:

$$\text{ACH}'_+ = \int_\Gamma \left(\sqrt{-\frac{1}{2} \nu_t \left(\frac{\partial \overline{w}}{\partial z} \right) + \frac{1}{6} k} \right) d\Gamma \tag{C.5}$$

A similar approach is used to estimate PCH_+:

$$\text{PCH}_+ = \overline{\text{PCH}_+} + \text{PCH}'_+ = \frac{1}{\lambda} \int_0^\lambda \int_\Gamma (wc + \acute{w}\acute{c}) d\Gamma dt = \int_\Gamma (\overline{w}\overline{c} + \overline{\acute{w}\acute{c}}) d\Gamma \tag{C.6}$$

$$\overline{\acute{w}\acute{c}} = -D_t \frac{\partial \overline{c}}{\partial z} \tag{C.7}$$

where $D_t = \frac{\nu_t}{Sc_t}$ is eddy diffusivity of the pollutant, ν_t is eddy viscosity, and $Sc_t = 0.72$ is turbulent Schmidt number. Combining equations (C.6) and (C.7), the PCH_+ can be finally calculated by:

$$\text{PCH}_+ = \int_\Gamma (\overline{w}\overline{c} - D_t \frac{\partial \overline{c}}{\partial z}) d\Gamma \tag{C.8}$$

Appendix D Simulated Data

Table D.1 Simulated pedestrian comfort indicators inside the pedestrian plane (AR=1)

AR=1	Wind Velocity (m/s)	Wind Angle (degree)	Frequency of occurrence (%)	Air Temperature (K)		Air Velocity (m/s)		Air Relative Humidity (%)		CO concentration (PPM)	
				L-S	R-S	L-S	R-S	L-S	R-S	L-S	R-S
	1	90	3	306	306	0.1	0.1	47	57	29	7
		45	7	306	306	0.1	0.2	55	58	11	7
		0	17	306	306	0.1	0.1	48	63	26	0
	3	90	12	307	306	0.2	0.4	38	59	75	16
		45	21	306	306	0.2	0.4	64	65	2	2
		0	17	306	306	0.2	0.4	64	66	6	0
	7	90	3	307	307	0.9	1.2	58	62	119	20
		45	3	306	307	0.6	1.5	62	62	31	13
		0	17	306	306	1.3	1.8	64	64	0	0

Table D.2 Simulated pedestrian comfort indicators inside the pedestrian plane (AR=2)

AR=2	Wind Velocity (m/s)	Wind Angle (degree)	Frequency of occurrence (%)	Air Temperature (K)		Air Velocity (m/s)		Air Relative Humidity (%)		CO concentration (PPM)	
				L-S	R-S	L-S	R-S	L-S	R-S	L-S	R-S
	1	90	3	307	307	0.1	0.1	28	32	16	3
		45	7	306	306	0.2	0.3	55	62	2	9
		0	17	306	306	0.1	0.0	67	60	0	5
	3	90	12	306	306	0.1	0.1	56	57	23	42
		45	21	306	306	0.3	0.8	61	66	65	2
		0	17	305	305	0.6	0.1	68	67	0	0
	7	90	3	307	307	0.5	0.4	63	62	1	27
		45	3	306	306	0.6	2.1	60	64	44	2
		0	17	306	306	1.0	1.3	65	65	0	0

Table D.3 Simulated pedestrian comfort indicators inside the pedestrian plane (buildings' surfaces albedo = 0.4)

AR=2	Wind Velocity (m/s)	Wind Angle (degree)	Frequency of occurrence (%)	Air Temperature (K)		Air Velocity (m/s)		Air Relative Humidity (%)		CO concentration (PPM)	
				L-S	R-S	L-S	R-S	L-S	R-S	L-S	R-S
	1	90	3	307	307	0.0	0.1	30	31	2	18
		45	7	307	306	0.3	0.2	30	47	50	105
		0	17	305	307	0.1	0.1	68	35	1	93
	3	90	12	307	307	0.2	0.2	62	62	1	7
		45	21	306	306	0.4	0.5	64	67	28	0
		0	17	305	307	0.7	0.1	67	50	0	4
	7	90	3	307	307	0.5	0.5	63	63	1	11
		45	3	306	306	0.6	2.1	60	64	44	2
		0	17	306	306	0.5	1.0	65	65	0	0

Table D.4 Simulated pedestrian comfort indicators inside the pedestrian plane (street and pavement's surfaces albedo = 0.4)

AR=2	Wind Velocity (m/s)	Wind Angle (degree)	Frequency of occurrence (%)	Air Temperature (K)		Air Velocity (m/s)		Air Relative Humidity (%)		CO concentration (PPM)	
				L-S	R-S	L-S	R-S	L-S	R-S	L-S	R-S
	1	90	3	308	307	0.1	0.1	20	26	47	14
		45	7	308	306	0.1	0.2	13	59	55	35
		0	17	305	307	0.1	0.1	67	35	0	64
	3	90	12	308	308	0.1	0.1	26	20	1	27
		45	21	306	306	0.4	0.6	63	66	41	0
		0	17	305	306	0.7	0.1	67	51	0	2
	7	90	3	307	307	0.5	0.4	63	62	0	27
		45	3	306	306	0.6	2.1	61	64	41	2
		0	17	306	306	0.7	0.9	65	65	0	0

Table D.5 Calculated data within the pedestrian plane after applying the PVS; combination (A) with different fan powers

Fan Pressure (Pa)	Sidewalk	Air Velocity (m/s)	THI (degree)	CO (PPM)
Without PVS	L-S	0.1	27	6
	R-S	0.1	27	5
1	L-S	0.1	29	1
	R-S	0.1	29	1
10	L-S	0.2	29	181
	R-S	0.2	29	107
20	L-S	0.5	29	195
	R-S	0.5	29	130
50	L-S	0.9	29	184
	R-S	0.9	29	146
100	L-S	1.4	29	186
	R-S	1.4	29	154

Table D.6 Calculated data within the pedestrian plane after applying the PVS; combination (B) with different fan powers

Fan Pressure (Pa)	Sidewalk	Air Velocity (m/s)	THI (degree)	AQI (PPM)
Without PVS	L-S	0.1	27	6
	R-S	0.1	27	5
1	L-S	0.2	30	8
	R-S	0.2	30	8
10	L-S	0.4	30	1
	R-S	0.4	30	5
20	L-S	0.7	30	1
	R-S	0.6	30	13
50	L-S	1.1	30	1
	R-S	1.0	30	18
100	L-S	1.4	30	1
	R-S	1.5	30	18

Table D.7 Calculated data within the pedestrian plane after applying the PVS; combination (C) with different fan powers

Fan Pressure (Pa)	Sidewalk	Air Velocity (m/s)	THI (degree)	AQI (PPM)
Without PVS	L-S	0.1	27	6
	R-S	0.1	27	5
1	L-S	0.2	30	2
	R-S	0.1	29	3
10	L-S	0.4	30	1
	R-S	0.2	29	154
20	L-S	0.6	30	1
	R-S	0.5	29	291
50	L-S	0.9	30	1
	R-S	0.8	29	321
100	L-S	1.4	30	1
	R-S	1.3	30	324

Table D.8 Calculated data within the pedestrian plane after applying the PVS; combination (D) with different fan powers

Fan Pressure (Pa)	Sidewalk	Air Velocity (m/s)	THI (degree)	AQI (PPM)
Without PVS	L-S	0.1	27	6
	R-S	0.1	27	5
1	L-S	0.1	29	2
	R-S	0.2	30	7
10	L-S	0.2	28	191
	R-S	0.3	30	22
20	L-S	0.5	29	285
	R-S	0.5	30	45
50	L-S	1.0	29	381
	R-S	1.0	30	94
100	L-S	1.4	29	408
	R-S	1.4	30	111

References

Akbari H., Pomerantz M., Taha H. (2001) Cool surfaces and shade trees to reduce energy use and improve air quality in urban areas. Solar Energy 70:295-310.

Ali-Toudert F., Mayer H. (2006) Numerical study on the effects of aspect ratio and orientation of an urban street canyon on outdoor thermal comfort in hot and dry climate. Building and Environment 41:94-108.

American Society for Heating Ventilating and air conditioning engineers. (2001) ASHRAE Fundamentals Handbook New York.

Anthes R.A., Seaman N.L., Warner T.T. (1978) Developement of hydrodynamic models suitable for air polution and other mesometeorological studies. Mounthly Weather Review 106.

Arnfield A.J. (2003) Review two decades of urban climate research : a review of turbulence, exchanges of energy and water, and the urban heat island. International Journal of Climatology 23:1–26.

Bady M., Kato S., Huang H. (2008) Towards the application of indoor ventilation efficiency indices to evaluate the air quality of urban areas. Building and Environment 43:1991-2004.

Baik J.-J., Kim J.-J. (2002) On the escape of pollutants from urban street canyons. Atmospheric Environment 36:527-536.

Blocken B., Carmeliet J. (2004) Pedestrian wind environment around buildings: literature review and practical examples. Journal of thermal environment and building science 28:107-159.

CBCNews. (2006) Ontario hits record high for power use.

Cebeci T., Bradshaw P. (1977) Momentum Transfer in Boundary Layers. Hemisphere Publishing Corporation, New York.

Cermak J.E. (1984) Physical modeling of flow and dispersion over complex terrain. Boundary-Layer Meteorology 30:261-292.

Cermak J.E. (1996) Thermal effects on flow and dispersion over urban areas : capabilities for prediction by phisical modeling. Atmospheric Environment 30:393-401.

Chan A.T., So E.S.P., Samad S.C. (2001) Strategic guidelines for street canyon geometry to achieve sustainable street air quality. Atmospheric Environment 35:5681-5691.

Chandrasekhar S. (1960) Radiative Transfer Dover Publications Inc.

Chen F., Dudhia J. (2001) Coupling an advanced land-surface/hydrology model with the Penn State/NCAR MM5 modeling system. Part I: Model description and implementation. Monthly Weather Review 129:569–585.

Cheng W.C., Liu C.-H., Leung D.Y.C. (2008) Computational formulation for the evaluation of street canyon ventilation and pollutant removal performance. Atmospheric Environment 42:9041-9051.

Cheng W.C., Liu C.-H., Leung D.Y.C. (2009) On the correlation of air and pollutant exchange for street canyons in combined wind-buoyancy-driven flow. Atmospheric Environment 43:3682-3690.

Dudhia J., Bresch J.F. (2002) A global version of the PSU-NCAR Meso-scale model. Monthly Weather Review 130:2989-3007.

Environment-Canada. (Date Accessed: November, 2010) Hourly Data Report for August 01, 2006.

Fanger P.O. (1972) Thermal comfort. New York: McGraw Hill.

Flor F.S.d.l., Domınguez S.A. (2004) Modelling microclimate in urban environments and assessing its influence on the performance of surrounding buildings. Energy and Buildings 36:403–413.

Fluent. (2008) http://fluent.com/.

Gagge A.P., Fobelets A.P., Berglund L.G. (1986) A standard predictive index of human response to the thermal environment. ASHRAE Transactions 92:709-31.

GAMBIT. (2008) http://fluent.com/software/gambit/.

Goldreich Y. (2006) Ground and top of canopy layer urban heat island partitioning on an airborne image. Remote Sensing of Environment 104:247–255.

Gromke C., Buccolieri R., Di Sabatino S., Ruck B. (2008) Dispersion study in a street canyon with tree planting by means of wind tunnel and numerical investigations - Evaluation of CFD data with experimental data. Atmospheric Environment 42:8640-8650.

Hafner J., Kidder S.Q. (1999) Urban heat island modeling in conjunction with satellite-derived surface/soil parameters. Journal of Applied Meteorology 38:448-65.

Hefny M.M., Ooka R. (2009) CFD analysis of pollutant dispersion around buildings: Effect of cell geometry. Building and Environment 44:1699-1706.

Henkes R.A.W.M., Flugt F.F.v.d., Hoogendoorn C.J. (1991) Natural Convection Flow in a Square Cavity Calculated with Low-Reynolds-Number Turbulence Models. International Journal of Heat and Mass Transfer 34:1543-1557.

Hoppe P. (2002) Different aspects of assessing indoor and outdoor thermal comfort. Energy and Buildings 34:661-665.

Huang Y., Hu X., Zeng N. (2009) Impact of wedge-shaped roofs on airflow and pollutant dispersion inside urban street canyons. Building and Environment 44:2335-2347.

Hunter L.J., Johnson G.T., Watson I.D. (1992) An investigation of three-dimensional characteristics of flow regimes within the urban canyon. Atmospheric Environment. Part B. Urban Atmosphere 26:425-432.

Jeong S.J., Andrews M.J. (2002) Application of the k-[var epsilon] turbulence model to the high Reynolds number skimming flow field of an urban street canyon. Atmospheric Environment 36:1137-1145.

Kader B. (1981) Temperature and Concentration Profiles in Fully Turbulent Boundary Layers. International Journal of Heat and Mass Transfer 24:1541-1544.

Kanda M., Kawai T., Kanega M., Moriwaki R., Narita K., Hagishima A. (2005) A simple energy balance model for regular building arrays. Boundary-Layer Meteorology 116:423–443.

Kang Y.-S., Baik J.-J., Kim J.-J. (2008) Further studies of flow and reactive pollutant dispersion in a street canyon with bottom heating. Atmospheric Environment 42:4964-4975.

Kato S., Yamaguchi Y. (2005) Analysis of urban heat-island effect using ASTER and ETM+ Data: Separation of anthropogenic heat discharge and natural heat radiation from sensible heat flux. Remote Sensing of Environment 99:44–54.

Kim J.-J., Baik J.-J. (2001) Urban street-canyon flows with bottom heating. Atmospheric Environment 35:3395-3404.

Kim J.-J., Baik J.-J. (2003) Effects of inflow turbulence intensity on flow and pollutant dispersion in an urban street canyon. Journal of Wind Engineering and Industrial Aerodynamics 91:309-329.

Kolev I., Savov P., Kaprielov B., Parvanov O., Simeonov V. (2000) Lidar observation of the nocturnal boundary layer formation over Sofia Bulgarial. Atmospheric Environment 34:3223-3235.

Kondo A., Ueno M., Kaga A. (2001) The influence of urban canopy configuration on urban albedo. Boundary-Layer Meteorology 100:225–242.

Kondo H., Genchi Y., Kikegawa Y., Ohashi Y., Yoshikado H., Komiyama H. (2005) Developement of multi-layer urban canopy model for the analysis of energy consumption in a big city: structure of the urban canopy model and its basic performance. Boundary-Layer Meteorology 116:395–421.

Kubota T., Miura M., Tominaga Y., Mochida A. (2008) Wind tunnel tests on the relationship between building density and pedestrian-level wind velocity: Development of guidelines for realizing acceptable wind environment in residential neighborhoods. Building and Environment 43:1699–1708.

Kusaka H., Kondo H., Kikegawa Y., Kimura F. (2001) A simple single-layer urban

    canopy model for atmospheric models: comparison with multi-layer and slab

    models. Boundary-Layer Meteorology 101:329–358.

Launder B.E., Spalding D.B. (1972) Lectures in Mathematical Models of Turbulence

 Academic Press, London, England.

Launder B.E., Spalding D.B. (1974) Numerical computation of turbulent flows.

    Computer Methods in Applied Mechanics and Engineering 3:269-289.

Lawson T.V., Penwarden A.D. (1975) The Effects of Wind on People in the Vicinity of

    Buildings, 4th International Conference on Wind Effects on Buildings and

    Structures, Cambridge University Press. pp. 605-622.

Li X.-X., Liu C.-H., Leung D.Y.C. (2005) Development of a k-[epsilon] model for the

    determination of air exchange rates for street canyons. Atmospheric Environment

    39:7285-7296.

Li X.-X., Liu C.-H., Leung D.Y.C., Lam K.M. (2006) Recent progress in CFD modelling

    of wind field and pollutant transport in street canyons. Atmospheric Environment

    40:5640-5658.

Liu C.-H., Leung D.Y.C., Barth M.C. (2005) On the prediction of air and pollutant exchange rates in street canyons of different aspect ratios using large-eddy simulation. Atmospheric Environment 39:1567-1574.

Martilli A., Clappier A., Rotach M. (2002) An urban surface exchange parameterisation for mesoscale models. Boundary-Layer Meteorology 104:261–304.

Masson V. (2000) A phisically-based scheme for the urban energy budget in atmospheric models. Boundary-Layer Meteorology 94:357–397.

Mayer H., Hoppe P. (1987) Thermal comfort of man in different urban environments. Theoretical and Applied Climatology 38:43-9.

Memon R.A., Leung D.Y.C., Liu C.-H. (2009) Effects of building aspect ratio and wind speed on air temperatures in urban-like street canyons. Building and Environment In Press, Corrected Proof.

Meroney R.N., Pavageau M., Rafailidis S., Schatzmann M. (1996) Study of line source characteristics for 2-D physical modelling of pollutant dispersion in street canyons. Journal of Wind Engineering and Industrial Aerodynamics 62:37-56.

Mintz D. (2009) Technical Assistance Document for the Reporting of Daily Air Quality – the Air Quality Index (AQI), U.S. Environmental Protection Agency Office of Air Quality Planning and Standards.

Mirzaei P.A., Haghighat F. (2010a) A novel approach to enhance outdoor air quality: Pedestrian ventilation system. Building and Environment 45:1582-1593.

Mirzaei P.A., Haghighat F. (2010b) Pollution Removal Effectiveness of the Pedestrian Ventilation System. Journal of Wind Engineering & Industrial Aerodynamics Accepted Manuscript.

Mirzaei P.A., Haghighat F. (2010c) Approaches to study Urban Heat Island - Abilities and limitations. Building and Environment 45:2192-2201.

Mochida A., Yoshino H., Miyauchi S., Mitamura T. (2006) Total analysis of cooling effects of cross-ventilation affected by microclimate around a building. Solar Energy 80:371–382.

Mochida A., Tominaga Y., Yoshino H., Sasoki K., ohba M. (2002) Numerical study on thermal effects of cold and high-albedo surfaces covered with snow in outdoor environment. Journal of Asian Architecture and Building Engineering 1:175-182.

Mochida A., Murakami S., Ojima T., Kim S., Ooka R., Sugiyama H. (1997) CFD analysis of mesoscale climate in the Greater Tokyo area. Journal of Wind Engineering and Industrial Aerodynamics 67&68:459-477.

Murakami S. (2006) Environmental design of outdoor climate based on CFD. Fluid Dynamics Research 38:108–126.

Murena F., Favale G. (2007) Continuous monitoring of carbon monoxide in a deep street canyon. Atmospheric Environment 41:2620-2629.

Murena F., Favale G., Vardoulakis S., Solazzo E. (2009) Modelling dispersion of traffic pollution in a deep street canyon: Application of CFD and operational models. Atmospheric Environment 43:2303-2311.

Nazridoust K., Ahmadi G. (2006) Airflow and pollutant transport in street canyons. Journal of Wind Engineering and Industrial Aerodynamics 94:491-522.

Nikolopoulou M., Lykoudis S. (2006) Thermal comfort in outdoor urban spaces: Analysis across different European countries. Building and Environment 41:1455–1470.

Nunez M., Oke T.R. (1977) The energy balance of urban canyon. Journal of Applied Meteorology 16:11-19.

Ogawa Y., Diosey P.G., Uehara K., Ueda H. (1981) A wind tunnel for studying the effects of thermal stratification in the atmosphere. Atmospheric Environment 15:807-821.

Oke T.R. (1988) Street design and urban canopy layer climate. Energy and Buildings 11:103-113.

Oliveira Panao M.J.N., Goncalves H.J.P., Ferrao P.M.C. (2009) Numerical analysis of the street canyon thermal conductance to improve urban design and climate. Building and Environment 44:177-187.

Patz J.A., Campbell-Lendrum D., Holloway T., Foley J.A. (2005) Impact of regional climate change on human health. Nature 438:310-17.

Population Reference Bureau. (2005) 2005 World Population Data Sheet.

Poreh M. (1996) Investigation of heat islands using small scale models. Atmospheric Environment 30:467-474.

Rafailidis S. (1997) Influence of building areal density and roof shape on the wind characteristics above a town. Boundary-Layer Meteorology 85:255–271.

Reisner J., Rasmussen R.J., Bruintjes R.T. (1998) Explicit forecasting of super cooled liquid water in winter storms using the MM5 mesoscale model. Quarterly Journal of the Royal Meteorological Society 124:1071-1107.

Saitoh T.S., Shimada T., Hoshi H. (1996) Modeling and simulation of the tokyo urban heat island. Atmospheric Environment 30:3431-3442.

Sarrat C., Lemonsu A., Masson V., Guedalia D. (2006) Impact of urban heat island on regional atmospheric pollution. Atmospheric Environment 40:1743–1758.

Sasaki K., Mochida A., Yoshino H., Watanabe H., Yoshida T. (2008) A new method to select appropriate countermeasures against heat-island effects according to the regional characteristics of heat balance mechanism. Journal of Wind Engineering and Industrial Aerodynamics 96:1629–1639.

Schultz P. (1995) An explicit cloud physics parameterization for operational numerical weather prediction. Monthly Weather Review 123:3331-3343.

ScienceDaily. (2006) Hot Summer Topic: Economist Explains Why Heat Waves Spur Electricity Blackouts, Massachusetts Institute Of Technology.

Sini J.-F., Anquetin S., Mestayer P.G. (1996) Pollutant dispersion and thermal effects in urban street canyons. Atmospheric Environment 30:2659-2677.

Siple P.A., Passel C.F. (1945) Measurements of dry atmospheric cooling in subfreezing temperatures. Proceedings of the American Philosophical Society 89:177-99.

Skamarock W.C., Klemp J.B., Dudhia J., Gill D.O., Baker D.M., Wan W., Powers J.G. (2005) A description of the advanced research WRF version2. NCAR Technical Note.

Soligo M.J., Irwin P.A., Williams C.J., Schuyler G.D. (1998) A comprehensive assessment of pedestrian comfort including thermal effects. Journal of Wind Engineering and Industrial Aerodynamics 77-78:753-766.

Soulhac L., Garbero V., Salizzoni P., Mejean P., Perkins R.J. (2009) Flow and dispersion in street intersections. Atmospheric Environment 43:2981-2996.

Steadman R.G. (1979) The Assessment of Sultriness. Part I: A Temperature-Humidity Index Based on Human Physiology and Clothing Science. Journal of Applied Meteorology18:861-873.

Taha H. (1997) Urban climates and heat islands: albedo, evapotranspiration, and anthropogenic heat. Energy and Buildings 25:99-103.

Takahashi K., Yoshida H., Tanaka Y., Aotake N., Wang F. (2004) Measurement of thermal environment in Kyoto city and its prediction by CFD simulation. Energy and Buildings 36:771–779.

Tao W.K., Simpson J. (1993) The goddard cumulus ensemble model. Part I: model description. Terrestrial, Atmospheric and Oceanic Sciences 4:35-72.

Thom E.C. (1959) The discomfort index. Weatherwise 12:57-60.

Tominaga Y., Yoshie R., Mochida A., Kataoka H., Harimoto K., Nozu T. (2005) Cross comparisons of CFD prediction for wind environment at pedestrian level around buildings. part 2 : comparison of results for flowfield around building complex in actual urban area, The Sixth Asia-Pacific Conference on Wind Emgineering, Korea.

Tominaga Y., Mochida A., Yoshie R., Kataoka H., Nozu T., Yoshikawa M., Shirasawa T. (2008) AIJ guidelines for practical applications of CFD to pedestrian wind environment around buildings. Journal of Wind Engineering and Industrial Aerodynamics 96:1749–1761.

Tong H., Walton A., Sang J., Chan J.C.L. (2005) Numerical simulation of the urban boundary layer over the complex terrain of Hong Kong. Atmospheric Environment 39:3549–3563.

Tseliou A., Tsiros I.X., Lykoudis S., Nikolopoulou M. (2010) An evaluation of three biometeorological indices for human thermal comfort in urban outdoor areas under real climatic conditions. Building and Environment 45:1346-1352.

Uehara K., Murakami S., Oikawa S., Wakamatsu S. (2000) Wind tunnel experiments on how thermal stratification affects flow in and above urban street canyons. Atmospheric Environment 34:1553-1562.

Voogt J.A., Oke T.R. (2003) Thermal remote sensing of urban climates. Remote Sensing of Environment 86:370–384.

Walton D., Dravitzki V., Donn M. (2007) The relative influence of wind, sunlight and temperature on user comfort in urban outdoor spaces. Building and Environment 42:3166-3175.

White F., Christoph G. (1971) A Simple New Analysis of Compressible Turbulent

Skin Friction Under Arbitrary Conditions. Technical Report AFFDL-TR-70-133.

Xie X., Huang Z., Wang J. (2006) The impact of urban street layout on local atmospheric

environment. Building and Environment 41:1352-1363.

Xie X., Liu C.-H., Leung D.Y.C. (2007) Impact of building facades and ground heating

on wind flow and pollutant transport in street canyons. Atmospheric Environment

41:9030–9049.

Xiu A., Pleim J.E. (2001) Development of a land surface model part I: Application in a

mesoscale meteorology model. Journal of Applied Meteorology 40:192-209.

Yakhot V., Orszag S.A., Thangam S., Gatski T.B., Speziale C.G. (1992) Development of

turbulence models for shear flows by a double expansion technique. Physics of

Fluids 4:1510-1520.

Yamada T. (2004) Merging CFD and atmospheric modeling capabilities to simulate

airflows and dispersion in urban areas. Computational Fluid Dynamics Journal

13(2):329-341.

Yamada T., Bunker S. (1987) Developement of nested grid, seccond moment turbulence

closure model and application to the 1982 ASCOT brush creek data simulation.

Journal of Applied Meteorology 27:562-578.